Academy of Sciences of the Czech Republic
Institute of Molecular Genetics, v.v.i.
Department of Molecular Virology

Charles University in Prague
Faculty of Science
Molecular and Cellular Biology, Genetics and Virology

Molecular mechanisms of apoptosis induced by photodynamic activation in cancer cells

PhD Thesis

Irena Moserová

Supervisor: Jarmila Králová, PhD

Prague 2012

Statement of authorship

I certify that the thesis represents valid work elaborated under the supervision of Jarmila Králová, PhD and that neither this manuscript nor one with substantially similar content under my authorship has been submitted in support of an application for any other academic degree.

Prague,..…….

Irena Moserová, M.Sc.

Statement of co-authors

I certify that Irena Moserová substantially contributed to preparation of the papers used as a basis of this thesis.

Prague, ……..

Jarmila Králová, PhD

Acknowledgements

I would like to express my sincere thanks to my supervisor Jarmila Králová, PhD for the scientific and financial support throughout my PhD studies, to all the friends and colleagues from the department of Molecular Virology for their help and goodwill, and to the collaborators and co-authors of our publications as well.
Special thanks also to my family and friends for great support.

Abstract

Photodynamic therapy (PDT) is a treatment modality for cancer. It combines selective accumulation of chemical compounds, called photosensitizers (PS), with light to irreversibly damage cancer cells via oxidative stress. The main goal of this thesis was to study photosensitizers represented by a unique group of newly synthesized porphyrin derivatives with glycol chain substitution. Glycol-functionalized porphyrins containing one to four low molecular weight glycol chains that are linked via ether bonds to the meta-phenyl positions of meso-tetraphenylporphyrin (mTPP(EG)1-4) were compared with fluorinated (pTPPF(EG)4) and nonfluorinated (TPP(EG)4) derivatives having glycol chains in para-phenyl positions. The cellular uptake and photodynamic activity was significantly dependent on terminal groups of the glycol substituent. Hydroxy glycol porphyrins, in contrast with methoxy glycol porphyrins, exhibited efficient intracellular transport and high induction of apoptosis in tumor cell lines in vitro. After initial testing effective prototype hydroxy ethylene glycol derivatives were selected and analyzed in detail. Para derivatives pTPP(EG)4 and pTPPF(EG)4 accumulated mainly in lysosomes whereas meta derivatives mTPP(EG)1-4 in the endoplasmic reticulum (ER). Position of ethylene glycol chain on the porphyrin ring affected not only intracellular localization but also PDT efficacy demonstrated by permanent ablation of human breast carcinoma (MDA-MB-231) in nude mice following treatment with meta derivatives. After photoactivation, both types of derivatives induced death of tumor cells via reactive oxygen species (ROS). Para derivatives pTPP(EG)4 and pTPPF(EG)4 activated the p38 MAP kinase cascade, which in turn induced the mitochondrial apoptotic pathway. In contrast, meta porphyrin derivative mTPP(EG)4 induced dramatic changes in Ca^{2+} homeostasis manifested by Ca^{2+} rise in the cytoplasm, activation of calpains and stress caspase-12 or caspase-4. ER stress developed into unfolded protein response. Immediately after irradiation the PERK pathway was activated through phosphorylation of PERK, eIF2α and induction of transcription factors ATF4 and CHOP, which regulate stress response genes. PERK knockdown and PERK deficiency protected cells against mTPP(EG)4-mediated apoptosis, confirming the causative role of the PERK pathway.

Analysis of the cell-death mechanism revealed that mTPP(EG)4 represent a novel nonmitochondrially localized photosensitizer that has a profound ability to induce apoptosis in tumor cells and exhibits a superior PDT efficacy in elimination of experimental tumors in comparison to clinically used photosensitizer Foscan. The presented work thus suggests an interesting avenue for further development of photosensitizers aiming at their future clinical application.

Abstrakt

Fotodynamická terapie (PDT) je terapeutický prostředek používaný při léčbě nádorů. Tato metoda je založena na aplikaci fotosenzitivní látky, která se hromadí v nádorových buňkách a po ozáření světlem způsobuje jejich usmrcení. Hlavním cílem této disertační práce bylo studium nových fotosenzitivních látek - porfyrinů s glykolovou substitucí. Porfyriny obsahující jeden až čtyři nízkomolekulární glykolové řetězce vázané éterovou vazbou v pozici meta na meso-tetrafenylporfyrin (mTPP(EG)1-4) byly porovnány s fluorinovanými (pTPPF(EG)4) a nefluorinovanými (pTPP(EG)4) deriváty majícími glykolový řetězec v para pozici. Vstup do buněk a fotodynamická aktivita byly výrazně závislé na koncových skupinách glykolových substituentů. Porfyriny s hydroxyglykolovou substitucí, na rozdíl od porfyrinů s methoxyglykolovou substitucí, byly účinněji transportovány do buněk a způsobovaly hojně apoptózu v nádorových buňkách *in vitro*. Po počátečním otestování byly vybrány a detailně analyzovány prototypy hydroxy etylenglykolových derivátů. Para deriváty pTPP(EG)4 a pTPPF(EG)4 se akumulují především v lysozomech, zatímco meta deriváty mTPP(EG)1-4 v endoplazmatickém retikulu (ER). Pozice etylenglykolového řetězce na porfyrinovém kruhu má vliv nejen na nitrobuněčnou lokalizaci ale i na účinnost fotodynamické terapie *in vivo*. PDT zprostředkovaná meta deriváty vedla u NuNu myší k úplnému vymizení nádorů (lidský karcinom prsu MDA-MB-231). Po fotoaktivaci oba typy derivátů indukují smrt nádorových buněk pomocí reaktivních druhů kyslíku (reactive oxygen species, ROS). Para deriváty pTPP(EG)4 a pTPPF(EG)4 aktivují p38 MAP kinázovou signální kaskádu, která následně spustí mitochondriální apoptickou dráhu. Na rozdíl od para derivátů, meta derivát porfyrinu mTPP(EG)4 vyvolává dramatické změny homeostázy Ca^{2+} projevující se zvýšenou hladinou Ca^{2+} v cytoplazmě, aktivací kalpainů a stresových kaspáz -12 nebo -4. Stres endoplazmatického retikula vede k rozvoji tzv. unfolded protein respose (UPR), jejíž součástí je PERK signální dráha aktivovaná fosforylací PERK, eIF2α. Následně jsou indukovány transkripční faktory ATF4 a CHOP, které regulují geny odpovídající na stresové podněty. Úlohu PERK dráhy v mTPP(EG)4-zprostředkované buněčné smrti potvrzují pokusy, kdy vyřazení (knockdown) genu PERK nebo jeho utlumení chrání buňky před apoptózou.

Výsledky získané analýzou mechanismu buněčné smrti navozené PDT jasně dokládají, že mTPP(EG)4 představuje nový fotosensitizér s lokalizací mimo mitochondrie, který má schopnost velmi účinně aktivovat apoptózu v rakovinných buňkách. Navíc je při odstranění experimentálních nádorů výrazně účinnější než klinicky používaný Foscan. Předkládaná práce tak ukazuje zajímavý způsob, jak dále vyvíjet fotosensitizéry pro budoucí použití v klinické praxi.

This thesis is based on the following papers:

Kralova J, Briza T, **Moserova I**, Dolensky B, Vasek P, Pouckova P, Kejik Z. Glycol porphyrin derivatives as potent photodynamic inducers of apoptosis in tumor cells. *J. Med. Chem.* 2008**,** *51,* 5964–5973 (IF=5.207)

Moserova I, Kralova J. Role of ER stress response in photodynamic therapy: ROS generated in different subcellular compartments trigger diverse cell death pathways. *PLoS ONE* 2012, *7,* e32972 (IF=4.411)

The above papers are included in full in this PhD thesis. For the complete list of my published articles, see List of papers.

LIST OF ABBREVIATIONS

ADP	adenosine diphosphate
AIF	apoptosis inducing factor
ALA	5-aminolevulinic acid
AlPc	aluminum phthalocyanine
AlPcS2	bisulfonated aluminium phthalocyanine
Ambra-1	activating molecule in Beclin-1-regulated autophagy
AMD	age-related macular degeneration
Apaf-1	apoptotic protease-activating factor 1
APF	3’-p-(aminophenyl) fluorescein probe
ATF4	activating transcription factor 4
ATF6	activating transcription factor 6
ATG	autophagy-related gene
ATP	adenosine-5'-triphosphate
Bad	Bcl-2-associated death promoter
Bak	Bcl-2 homologous antagonist/killer
BAPTA	1,2-bis(o-aminophenoxy)ethane-N,N,N',N'-tetraacetic acid
Bax	Bcl-2–associated X protein
Bcl-2	B-cell lymphoma 2
Bcl-w	Bcl-2-like protein 2
Bcl-XL	B-cell lymphoma-extra large
Bid	BH3 interacting domain death
Bif-1	Bax interacting factor 1
Bip	binding immunoglobulin protein
BH	Bcl-2 homology domain
BPD	benzoporphyrin derivatives
Capn4/Capns1	calpain 4/calpain small subunit 1
Ce6/PVP	chlorine e6-polyvinypyrrolidone
CHOP	C/EBP-homologous protein-10
CIS	carcinoma in situ
CMLS	confocal laser scanning microscopy
CMXRos	chloromethyl-X-rosamine
CPO	capronyloxy-tetrakis methyloxyethyl porphycene
DAMPs	damage-associated molecular patterns
DISC	death-inducing signaling complex
DMSO	dimethyl sulfoxide
DNA	deoxyribonucleic acid
DR	death receptors
ECL	enhanced chemiluminiscence
EDTA	ethylenediaminetetraacetic acid
EG	ethylene glycol
eIF2α	α subunit of eukaryotic initiatin factor 2
endoG	endonuclease G
EPR	enhanced permeability and retention effect
ER	endoplasmic reticulum
ERK	extracellular signal regulated kinase
FACS	fluorescent activated cell sorting
FasL	Fas ligand

FIP200	focal adhesion kinase family interacting protein of 200 kD
FITC	fluorescein isothiocyanate
GADD153	growth arrest and DNA damage induced gene-153
GAPDH	glyceraldehydes-3-phosphate dehydrogenase
GRP78	glucose regulated protein 78 kD
HMGB1	high-mobility group protein B1
HPD	hematoporphyrin derivative, photofrin
HPPH	2 devinyl pyropheophorbide-a
HrtA2	high temperature requirement protein A 2
HSP	heat shock protein
IAP	inhibitors of apoptosis
IC	inhibitory concentration
IL	interleukin
IMS	inter-mitochondrial membrane space
IRE1	inositol requiring enzyme 1
JNK/SAPK	Jun N-terminal kinases/stress activated protein kinases
KO	knockout
LC3	microtubule-associated protein light chain 3
LD	light dose
LDL	low-density lipoprotein
LED	light-emitting diode
LS11	talaporphin sodium
LuTex	lutetium texaphyrin
MACE	mono-(L)-aspartylchlorin-e6
MAPK	mitogen-activated protein kinase
Mcl-1	myeloid cell leukemia sequence 1
MEF	mouse embryonic fibroblast
MKK3/6	mitogen-activated protein kinase kinase 3/6
M-MLV	Moloney murine leukemia virus
MMP	mitochondrial membrane permeabilization
MSU	monosodium urate
mTHPC	m-tetrahydroxyphenylchlorin, Temoporfin, Foscan
mTOR	mammalian target of rapamycin
NAC	N-acetyl-L-cysteine
Na pyruv	sodium pyruvate
Npe6	mono-L-aspartyl chlorin e6
OMM	outer mitochondrial membrane
PARP-1	poly (ADP-ribose) polymerase 1
Pc4	phthalocyanine
PDT	photodynamic therapy
PE	phosphatidylethanolamine
PEG	polyethylene glycol
PEGME	polyethylene glycol methyl ether
PERK	pancreatic ER kinase (PKR)-like ER kinase
PI	propidium iodide
PI3KC3	phosphatidylinositol 3-kinase class 3
PI3P	phosphatidylinositol-3-phosphate
PMSF	phenylmethylsulfonyl fluoride
PPME	pyropheophorbide-a methyl ester
PS	photosensitizer

RIP1	receptor interacting protein 1
RNA	ribonucleic acid
ROS	reactive oxygen species
RT-PCR	real time-polymerase chain reaction
Ru360	ruthenium amino binuclear complex
S1P	site 1 protease
S2P	site 2 protease
SERCA 2	sarco/endoplasmic reticulum Ca^{2+} ATPase
siRNA	small interfering RNA
Smac/DIABLO	second mitochondria-derived activator of caspase/ direct IAP binding protein with a low pI
SnEt2	tin ethyl etiopurin
TG	thapsigargin
TNF-α	tumor necrosis factor α
TNF-RI	tumor necrosis factor receptor-I
TPPS2a	meso-tetraphenyl porphyrin disulphonate
TRAIL	TNF-related apoptosis-inducing ligand
ULK	UNC-51-like kinase
UPR	unfolded protein response
UV	ultraviolet
UVRAG	UV radiation resistance-associated gene
Vps34	vacuolar protein sorting 34
WT	wild type
XBP1	X-box binding protein 1
Zn-BC-AM	Zn(II) benzochlorin analog

CONTENTS

1 INTRODUCTION

1.1 Photodynamic therapy

Photodynamic therapy (PDT) is a promising type of cancer therapy based on the selective accumulation of photosensitizer (PS) (a synthetic or natural compound excitable by light) inside the tumor and irradiation of tumor by light. PDT consists of three essential components: photosensitizer, light and oxygen (21, 22). None of these is individually toxic, but together they initiate a photochemical reaction that culminates in the generation of reactive oxygen species (ROS). The latter can rapidly cause significant toxicity leading to cell death via apoptosis or other major cell death subroutines (e.g. necrosis, autophagic cell death) (9, 62, 95).

1.1.1 History of PDT

The history of modern PDT goes back to the attempts of ancient Egyptians to treat skin diseases with light-absorbing compounds. Six-thousand-year old annals tell us that ancient Egyptian applied vegetable substances to produce photoreaction in tissues. The substances were employed in the treatment of depigmented skin lesion (vitiligo). These lesions used to be regarded as manifestation of leprosy. Egyptians utilized natural photosensitizers psoralens. They are contained in many plants such as parsnip or parsley. Egyptians made a powder of these plants and applied it to the skin with following exposure of the person to bright sunlight. Photomedical procedures were also described in ancient Indian and Buddhist books. The 1903 Nobel Prize was awarded to Niels Finsen for his work on phototherapy. Finsen discovered that light treatment could control skin manifestations of tuberculosis, a very common ailment at the time (28). German physician Friedrich Mayer-Betz performed the first study with what was first called photoradiation therapy with porphyrins in 1913 in humans. The clinical use of PDT for cancer dates to the late 1970s. In 1978, Dougherty et al. reported the first large series of patients successfully treated with PDT using a mixture of hematoporphyrin derivatives (HPD, Photofrin) (23). Since this early work, there have been over 200 clinical trials for PDT. Clinically applied photosensitizers are summarized in Table 1.1.

1.1.2 Advantages and limitations of PDT

Therapy has only localized effects as the photosensitizer is selectively absorbed at a greater rate by target tissues, can be performed in outpatient or day-care settings, is more economical than radiation and surgical therapy for cancer patients, shows faster post-op healing with no long-term side effects, is less invasive and can be repeated many times at the same site if needed, unlike radiation.

Light needed to activate the photosensitizer cannot penetrate more than 1 cm of tissue depth using standard laser and low-powered light-emitting diode (LED) technology, and hence is less effective in the treatment of large tumors and metastasis. It may leave many people very sensitive to light post therapy and cannot be used in people allergic to photosensitizers.

PDT mostly produces superficial effects. Due to the limited light penetration through tissues, the depth of tumor destruction ranges from a few millimeters to up to 1 centimeter. This apparent disadvantage can be favorably exploited in the treatment of superficial diseases, such as premalignant conditions (mucous dysplasia, actinic keratosis), carcinoma in situ (CIS), or superficial tumors (such as malignant pleural mesothelioma (36) or intraperitoneal disseminated carcinomatosis (35, 40). Moreover, PDT can be used supplemental to surgery, to irradiate the tumor bed, and to increase the probability of long-term local disease control.

1.2 Photosensitizer

A photosensitizer is defined as a drug or chemical compound which upon absorption of light induces a chemical or physical alteration of another chemical entity. When taken up by cancer cells and exposed to light of specific wavelengths, the drug becomes active and initiates processes leading to cancer cell death.

1.2.1 Ideal photosensitizer

There are several important aspects characterizing an ideal photosensitizer. First of all it should be a single pure compound with guaranteed quality control analysis, low manufacturing costs and good stability in storage. Further, it should have photo- and biological stability and strong absorption at wavelength 600-800 nm (red to deep red), as the absorption of photons with wavelengths longer than 800 nm does not provide enough energy to excite oxygen to its singlet state and to form a substantial yield of

reactive oxygen species and with shorter wavelength it has low tissue penetration (22). Clearance of PS from normal tissues (body) should be relatively rapid to minimize phototoxic side effects. PS should not display toxicity in the absence of light (dark toxicity) but effectively generate ROS, effectively penetrate tissue and be soluble in biological media. Moreover, it should display selectivity to tumor cells and exclusive accumulation within tumor tissue. Despite some partial successes, a continuous search for better photosensitizers with required properties is still in progress.

The mechanisms involved in the preferential distribution of sensitizers in tumors are not fully understood. Many hypotheses have been proposed to account for the tumor-localizing properties in PDT (22). These include leaky microvasculature due to fast formation of neovasculature, and poor lymphatic drainage known as the enhanced permeability and retention effect (EPR) (52). Some of the most effective compounds bind preferentially to low-density lipoprotein (LDL), suggesting that upregulated LDL receptors found on tumor cells could be important (57).

1.2.2 Classification of photosensitizers

Photosensitizers are a wide group of different types of molecules and their nomenclature is not always clear. Tables 1.1 and 1.2 contain the list of most often used PSs together with their name, abbreviation/trade name and chemical classification.

Photosensitizers are generally grouped under three generations. First generation PS to be clinically employed for cancer therapy represented a water-soluble mixture of porphyrins called hematoporphyrin derivatives (HPD). A purified form of this mixture – porfimer sodium – later became known as Photofrin. Numerous photosensitizers of second generation have been developed to alleviate certain problems associated with the first generation molecules such as prolonged skin photosensitization and suboptimal tissue penetration. The second generation of photosensitizers represents chemically pure compounds which compared with the first generation absorbs light at a higher wavelength and cause significantly less skin photosensitization after treatment. The second generation includes 5-aminolevulinic acid (ALA), Verteporfin (BPD), Temoporfin (Foscan, mTHPC, m-tetrahydroxyphenylchlorin) and Talaporphin sodium (LS11). Foscan (mTHPC) is the most potent amongst them. ALA is a biosynthetic precursor of the PS protoporphyrin IX. The third generation of photosensitizers includes

currently available drugs that are modified by targeting with monoclonal antibodies or liposomes for selective accumulation within tumor tissue (53).

Table 1.1 Clinically applied photosensitizers. Adapted from Agostinis et al. (1).

PHOTOSENSITIZER	STRUCTURE	WAVELENGTH, nm	APPROVED	TRIALS	CANCER TYPES
Porfimer sodium (Photofrin) (HPD)	Porphyrin	630	Worldwide		Lung, esophagus, bile duct, bladder, brain, ovarian
ALA	Porphyrin precursor	635	Worldwide		Skin, bladder, brain, esophagus
ALA esters	Porphyrin precursor	635	Europe		Skin, bladder
Temoporfin (Foscan) (mTHPC)	Chlorin	652	Europe	United States	Head and neck, lung, brain, skin, bile duct
Verteporfin	Chlorin	690	Worldwide (AMD)	United Kingdom	Ophthalmic, pancreatic, skin
HPPH	Chlorin	665		United States	Head and neck, esophagus, lung
SnEt2 (Purlytin)	Chlorin	660		United States	Skin, breast
Talaporfin (LS11, MACE, NPe6)	Chlorin	660		United States	Liver, colon, brain
Ce6-PVP (Fotolon), Ce6 derivatives (Radachlorin, Photodithazine)	Chlorin	660		Belarus, Russia	Nasopharyngeal, sarcoma, brain
Silicon phthalocyanine (Pc4)	Phthalocyanine	675		United States	Cutaneous T-cell lymphoma
Padoporfin (TOOKAD)	Bacteriochlorin	762		United States	Prostate
Motexafin lutetium (Lutex)	Texaphyrin	732		United States	Breast

Abbreviations: ALA, 5-aminolevulinic acid; AMD, age-related macular degeneration; Ce6/PVP, chlorine e6-polyvinypyrrolidone; HPD, hematoporphyrin derivative; HPPH, 2-devinyl pyropheophorbide-a; MACE, mono-(L)-aspartylchlorin-e6; mTHPC, m-tetrahydroxyphenylchlorin; nm indicates nanometers; SnEt2, tin ethyl etiopurin.

Table 1.2 Photosensitizers - their nomenclature and chemical identity.

Photosensitizer	Abbreviation/Trade name	Chemical class
5-aminolevulinic acid	ALA/Levulan	Porphyrin
Protoporphyrin IX	PpIX	Porphyrin
13,17-bis(1-carboxypropionyl) carbamoylethyl-8-etheny-2-hydroxy-3-ydroxyiminoethylidene-2,7,12,18-tetraethyl porphyrin sodium	ATX-s10	Porphyrin
Lutenium texaphyrin	LuTex	Porphyrin
Porfimer sodium	HPD/Photofrin	Porphyrin-oligomer
Meso-tetraphenylporphyrin disulphonate	TPPS2a	Porphyrin
N-aspertylchlorin e6	Npe6	Chlorin
Tin etiopurpurin	SnET2/Purlytin	Chlorin
Talaporfin sodium	LS11	Chlorin
Meta-tetrahydroxyphenylchlorin	mTHPC, Foscan, Temoporfin	Chlorin
Verteporfin	BPD/Visudyne	Chlorin
Zn(II) benzochlorin analog	Zn-BC-AM	Chlorin
Aluminium phthalocyanine	AlPc	Phthalocyanine
Bisulfonated aluminium phthalocyanine	AlPcS2	Phthalocyanine
Silicon phthalocyanine	Pc4	Phthalocyanine
9-capronyloxytetrakis (methoxyethyl)porphycene	CPO	Porphycene
MitoTracker Red	CMXRos	Chloromethyl-X-Rosamine
Pyropheophorbide-a methylester	PPME	Chlorophyll-a derivative
Hypericin	Hyp	Phenantroperylenequinone
Rose Bengal	RB	Tetraiodo-fluorescein

Suitable PSs are porphyrins (67) because they are not toxic. Porphyrins have diverse functions in nature and can take on an amazing variety of roles in the world, which is why they are widely utilized and researched. The basic structure of a chlorophyll molecule, hemoglobin, cytochromes and vitamin B12 is a porphyrin ring, coordinated to a central atom. In all these molecules the structure is very similar; in heme the central atom is iron whereas in chlorophyll it is magnesium.

Porphyrins have a high selectivity for cancer cells and absorb light in the visible range of the spectrum, which is caused by the polyconjugated aromatic system. A limitation, however, is their high hydrophobicity. The problem of the low solubility and the low cellular uptake of the porphyrin core can be solved by addition of a hydrophilic substituent (e.g. hydroxyl, sugar, amino borate, sulfate, phosphonate, cyclodextrin, peptide and PEG). Many water-soluble porphyrins showed strong affinities for cancer cells and high anticancer effects. Substitution of the PS core can also be used for the modulation of the photophysical properties and adjustment of chemical characteristics of the macrocycle. For example, these substituents can direct self-assembly (17) and target the PSs to therapeutically important objects (cancer cells (117), mitochondria (118), DNA (122)) or modulate their electronic properties such as absorption and emission (65). Two types of these groups can be distinguished: ionic and nonionic. The electrical charge mediates recognition of important cancer receptors such as sialic acid. Some nonionic hydrophilic groups such as PEG and PEGME can have an affinity for the cell membrane and can therefore be used for the facilitation of membrane entry (134).

1.2.3 PS absorption and light penetration

PDT requires a source of light that activates the photosensitizer by the exposure to low-power visible light at a specific wavelength. Blue light penetrates least efficiently through tissues, whereas red and infrared radiations penetrate more deeply. The region between 600 and 1200 nm is often called the optical window of the tissue. Consequently, most PSs are activated by red light between 630 and 700 nm, corresponding to a light penetration depth from 0.5 cm (at ~ 630 nm) to 1.5 cm (at ~ 700 nm). However, light up to only approximately 800 nm can generate singlet oxygen ($^1O_2$), because longer wavelengths have insufficient energy to initiate a photodynamic reaction (Figure 1.1).

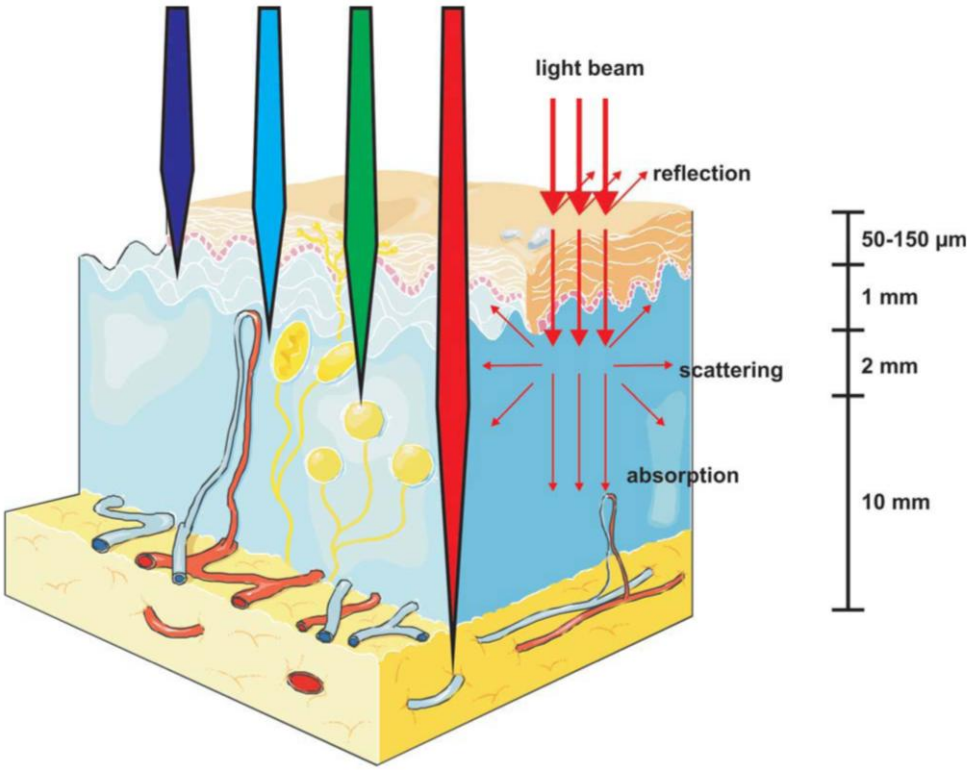

Figure 1.1 Light propagation through the tissues. Adapted from Agostinis et al. (1).

1.2.4 PDT mechanism of action - photophysics and photochemistry

Photosensitizer in ground state has two electrons with opposite spins located in an energetically most favorable molecular orbital. Absorption of light leads to a transfer of one electron to a higher energy orbital. This excited PS is very unstable and emits the excess energy as fluorescence and/or heat. Alternatively, an excited PS may undergo an intersystem crossing to form a more stable triple state with inverted spin of one electron. The PS in triplet state can either decay radiationlessly to the ground state or transfer its energy to molecular oxygen (O_2), which is unique in being a triplet in its ground state. This step leads to the formation of singlet oxygen ($^1O_2$), and the reaction is referred to as a Type II process. A Type I process can also occur whereby the PS reacts directly with an organic molecule in a cellular microenvironment, acquiring a hydrogen atom or electron to form a radical. Subsequent autooxidation of the reduced PS produces a superoxide anion radical ($^{\bullet}O_2^-$). Dismutation or one electron reduction of O_2 yields hydrogen peroxide (H_2O_2), which in turn can undergo one-electron reduction to a powerful and virtually indiscriminate oxidant hydroxyl radical ($^{\bullet}OH$). Reactive oxygen species (ROS) generation via Type II chemistry is mechanistically much simpler than

via Type I, and most PSs are believed to operate via a Type II rather than Type I mechanism.

As shown in Figure 1.2, both reactions can occur simultaneously and the ratio between them depends on the photosensitizer and the nature of the substrate molecules.

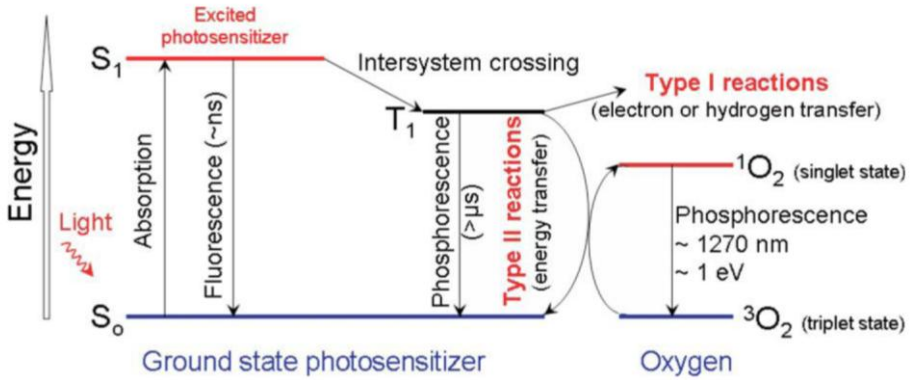

Figure 1.2 Modified Jablonski energy diagram. Adapted from Agostinis et al. (1).

1.2.5 Intracellular localization PSs

It is generally accepted that the intracellular localization of photosensitizes coincides with the primary site of photodamage (85). This is because the photogenerated singlet oxygen has a very short life and very limited diffusion in biological systems (half-life, <0.04 μsec; radius of action, <0.02 μm), indicating that primary molecular targets of the photodynamic process must reside within a few nanometers from the dye (84).

Effective photosensitizers localize in the mitochondria, endoplasmic reticulum (ER), Golgi apparatus, lysosomes and plasma membrane, or might have multiple targets. Generally it has been demonstrated that oxidative stress induced by photoactive compounds localizing to the mitochondria (Verteporfin, Pc4, AlPc, CMXRos, ATX-s10 etc.) (7, 50, 58, 63, 81, 82, 124, 125, 142) or the ER (Hypericin, Foscan, CPO, PPME) (41, 58, 59, 79, 80, 121) promotes apoptosis, while PDT with photosensitizers targeting either the plasma membrane or lysosomes predispose cells to necrosis-like phenotype (Photofrin, Npe6, LuTex) (48, 61, 105, 136). It must be noted that PDT-mediated apoptotic/necrotic outcome is influenced by the cell type, identity and concentration of photosensitizer as well as light doses used in the PDT protocol when the type of cell death switches from apoptosis to necrosis with the increase of intensity of the insult.

1.3 Molecular mechanism of cell death in PDT

1.3.1 Three major forms of the programmed cell death

PDT can evoke the three main cell death pathways: apoptosis, necrosis, and autophagy-associated cell death (Figure 1.3). For therapy, apoptosis, which is an ordered regulated process, is preferable to necrosis characterized by uncontrolled bursting of cells followed by an inflammatory reaction (126). Many factors influence the type of cell death caused by PDT (3, 60, 95).

1.3.1.1 Apoptosis

Apoptosis is a form of programmed cell death in response to key physiological cues and intracellular damage. Apoptosis is morphologically characterized by chromatin condensation, cleavage of chromosomal DNA into internucleosomal fragments, cell shrinkage, membrane blebbing and formation of apoptotic bodies without plasma membrane breakdown. Typically, apoptotic cells release „Find me“ and „Eat me“ signals required for the clearance of the remaining corpses by phagocytic cells. Apoptosis can be distinguished from necrotic cell death by the distinct absence of an associated inflammatory response.

1.3.1.2 Necrosis

Necrosis is morphologically characterized by vacuolization of the cytoplasm, swelling and breakdown of the plasma membrane resulting in an inflammatory reaction due to the release of cellular contents and pro-inflammatory molecules. Necrosis is thought to be the end result of a bio-energetic catastrophe resulting from ATP depletion to a level incompatible with cell survival (25). However, although necrosis has long been described as a passive and unorganized way to die, recent evidence suggests that necrotic cell death can be actively propagated as part of a signal transduction pathway. For instance, the engagement of TNF and Fas receptors in certain cell lines triggers necrosis through the activation of RIP1 (receptor interacting protein 1) kinase, under conditions of caspase inhibition (46, 129). Moreover, RIP1 has been suggested to be a key element of the JNK-mediated necrotic cascade activated by poly(ADP) polymerase-1 (PARP-1) following oxidative stress injury (139). These observations thus indicate

that in certain circumstances necrotic cell death may rely on the activation of an intracellular program in response to specific cues (27).

A shift from apoptotic to necrotic cell death using a particular dye can be usually instigated by increasing the intensity of the PDT dose (e.g. by increasing the light dose or concentration of the dye). This generates massive induction of ROS leading to an immediate bioenergetics catastrophe, drastic drop in ATP levels and general metabolic inhibition.

Necrosis is the major cell death morphology induced by PDT with compounds localized to the plasma membrane (11, 26, 48). This is likely due to a rapid loss of plasma membrane integrity, incapability to maintain ion fluxes across the plasma membrane and fast depletion of intracellular ATP, following photosensitization as shown in studies using Photofrin (48) or Zn-BC-AM (26).

1.3.1.3 Autophagy

Autophagy is a lysosomal degradative pathway that provides energy through self-digestion under conditions of starvation. During oxidative stress, autophagy serves as a defense mechanism to clear oxidatively damaged proteins and organelles (18). Autophagy is characterized by massive vacuolization of the cytoplasm. Autophagic cytoplasmic degradation requires formation of a double membrane structure called the autophagosome, which sequesters cytoplasmic components as well as organelles and traffics them to lysosomes.

Several types of autophagy have been described, including chaperone-mediated autophagy (found in mammalian cells alone and degrading cytosolic proteins selectively), microautophagy (lysosomes directly engulf cytosolic constituents through invagination of the lysosomal membrane) and macroautophagy. Macroautophagy (hereafter referred to as autophagy) typically occurs in severe stress conditions and is therefore the best characterized. Autophagy functions by de novo formation of specialized vacuoles, the autophagosomes, in which the proteins are sequestered before being targeted to the lysosomes. So far, 30 autophagy-related (*Atg*) genes have been identified in yeast, and several mammalian homologs have been isolated and functionally characterized (138).

The classical signaling pathway of autophagy acts through mTOR (mammalian target of rapamycin), a protein kinase that is important in controlling translation, cell-cycle

progression and in negative regulation of autophagy. When mTOR is inhibited in response to starvation or treatment with rapamycin, the ULK-Atg13-FIP200 (ULK = UNC-51-like kinase, FIP200 = focal adhesion kinase family interacting protein of 200 kD) complex is activated, which leads to induction of autophagosome formation (54). The synthesis of autophagic vacuoles requires vesicle nucleation, which is initiated by the assembly of another complex, the PI3KC3 (Vps34)-complex (PI3KC3 – phosphatidylinositol 3-kinase class 3, Vps34 – vacuolar protein sorting 34). Within this complex Beclin-1 (Atg6) serves as a platform for binding PI3KC3 (Vps34), UV radiation resistance-associated gene (UVRAG), Bax interacting factor 1 (Bif-1) and activating molecule in Beclin-1-regulated autophagy (Ambra-1), all of which positively regulate PI3KC3 activity (98). Interestingly, Bcl-2 (B-cell lymphoma 2) represses autophagy by binding Beclin-1 and thereby abrogating autophagic signaling (99). During starvation Bcl-2 becomes phosphorylated, which releases Beclin-1 and stimulates autophagy (132). Activation of the PI3KC3 (Vps34)-complex finally results in the generation of PI3P (phosphatidylinositol-3-phosphate). Consequently, other Atg proteins that mediate vesicle membrane elongation are recruited. Two ubiquitin-like conjugation systems are implicated in this process. During a first conjugation step, an Atg12 – Atg5 – Atg16(L) multimer complex that could be involved in vesicle curvature is formed (83). During a second conjugation step, LC3 (microtubule-associated protein light chain 3) (Atg8) is lipidated by binding to phosphatidylethanolamine (PE). In contrast to the cytoplasmic localization of LC3, LC3-PE (mostly referred to as LC3-II) specifically binds to the autophagic membranes, and for that reason it is generally used as an autophagic marker. Finally, the autophasome fuses with a lysosome, releasing its autophagic content into the lysosomal lumen for degradation by hydrolases.

Recent studies with diverse cancer cells and photosensitizers show that both autophagy and apoptosis are frequent outcomes of PDT (9, 62, 104). Autophagy can be activated by various stress signals relevant to cancer therapy, including oxidative stress (1, 18).

The role of autophagy in PDT-induced cell death is not yet clear. There are several ways how autophagy can participate in the photodynamic process. Autophagy can be activated by PSs that localize in lysosomes (NPe6), ER (Hypericin and CPO), mitochondria (Foscan), or both ER and mitochondria (Pc4). (104). Autophagy can be stimulated by PDT (104). However, the dynamics between autophagy and apoptosis in PDT is dependent on the cell type, nature of the PS, and light dose.

An example of the simultaneous induction of autophagy and apoptosis has been reported for murine leukemia L1210 cells after PDT with porphycene CPO (62). PDT induction of autophagy with Hypericin was demonstrated in murine embryonic fibroblasts lacking the proapoptotic effectors Bax and Bak following ER damage (10).
From several PDT studies it is clear that Bcl-2 proteins, known as central regulators of apoptosis, are targets of PSs action also involved in autophagy induction and autophagosome formation (11, 58, 63, 99, 142). One of the mechanisms is the stimulation of beclin-1-dependent Bcl-2 regulation (99).

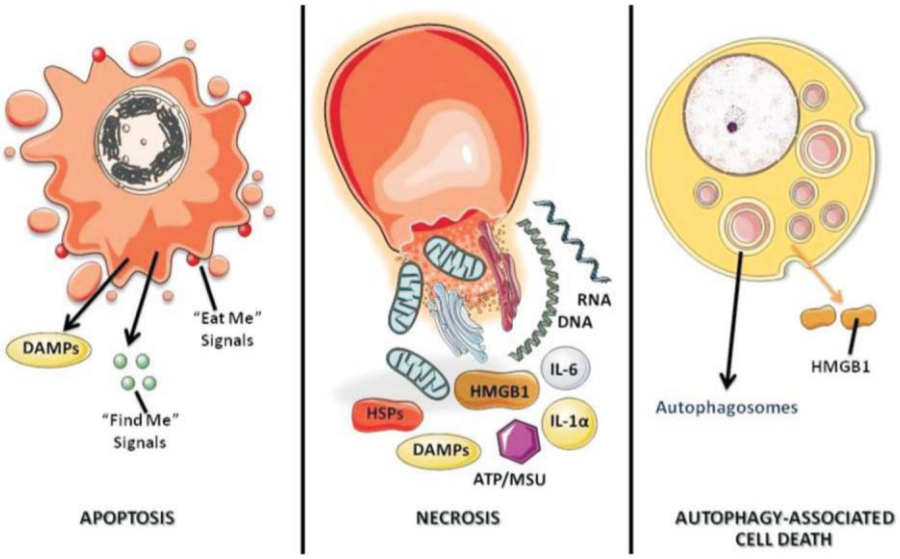

Figure 1.3 Major forms of the cell death. Adapted from Agostinis et al. (1).
DAMPs indicates damage-associated molecular patterns; HSPs, heat shock proteins; HMGB1, high-mobility group protein B1; IL, interleukin; ATP/MSU, adenosine triphosphate/monosodium urate.

1.3.2 Regulatory pathways in photodynamic therapy-induced apoptosis

Apoptotic cell death is unquestionably the best studied form of programmed cell death and is considered to have the most widespread physiological, pathological and therapeutic role. Apoptosis is generally the major cell death modality in cells responding to PDT. At the biochemical level, apoptosis entails the activation of caspases, a highly conserved family of cysteine-dependent aspartate-specific proteases, of which 11 members have been identified in humans. All caspases are activated in response to an apoptotic signal by proximity-induced dimerization at a multimeric

protein complex (initiator caspases) or by limited proteolysis by an upstream caspase (effector caspases). It is generally accepted that once activated, the effector caspases are responsible for most of the stereotypic morphological and biochemical changes observed during apoptosis by cleaving a restricted subset of vital substrates.

1.3.2.1 Apoptotic cell death (extrinsic and intrinsic pathway)

The apoptotic caspases act in two main converging pathways, called extrinsic and intrinsic, in which initiator caspases-8/-10 and -9 directly activate the effector procaspases-3 and -7.

The **extrinsic pathway (death receptor-mediated apoptosis)** is triggered by binding death ligands (e.g.FasL, TNF-α, TRAIL) to their cell surface death receptors (DR) (e.g. Fas, TNF-RI, TRAIL receptor). This induces DR clustering and formation of the death-inducing signaling complex (DISC), the oligomeric platform which recruits the initiator procaspases-8 and -10 and results in their dimerization-induced activation. Caspases-8/-10 in turn cleave and activate the effector caspases-3 and -7, which leads to apoptosis (Figure 1.4) (reviewed in (11, 70)).

The **intrinsic pathway (mitochondria-mediated apoptosis)** plays a central role in apoptotic cell death. Death signals function directly or indirectly on the mitochondria. Mitochondria are life-essential organelles for the production of metabolic energy in the form of ATP. Overlapping signaling pathways activated by cell insults converge on mitochondria to induce permeabilization of the mitochondrial membranes (MMP). MMP results in the release of several apoptogenic proteins stored in the inter-mitochondrial membrane space (IMS) into the cytosol. IMS proteins identified so far to have a prominent role in apoptosis include activators of caspases such as cytochrome c, Omi/HrtA2 (Omi stress-regulated endoprotease/High temperature requirement protein A 2) and Smac/DIABLO (second mitochondria-derived activator of caspase/direct IAP binding protein with a low pI), as well as apoptosis-inducing factor (AIF) and endonuclease G (endoG), which acts in a caspase-independent fashion (127). The binding of cytosolic cytochrome c to Apaf-1 (apoptotic protease-activating factor 1) in the presence of ATP or dATP leads to the recruitment and activation of procaspase-9 resulting in the formation of a heptameric complex called apoptosome. Once free in cytosol, Omi/HrtA2 and Smac/DIABLO antagonize the activity of endogenous inhibitors of caspases (IAPs), thereby promoting caspase activation (24, 39, 114).

Meanwhile, AIF and EndoG translocate to the nucleus where they mediate chromatin condensation and large-scale DNA fragmentation, independently from caspase signaling (73, 115).

The caspase-8-mediated cleavage of the cytosolic proapoptotic Bcl-2 family member Bid (BH3 interacting domain death) provides a molecular link between the extrinsic and intrinsic apoptotic pathways (Figure 1.4) (reviewed in (11, 70)).

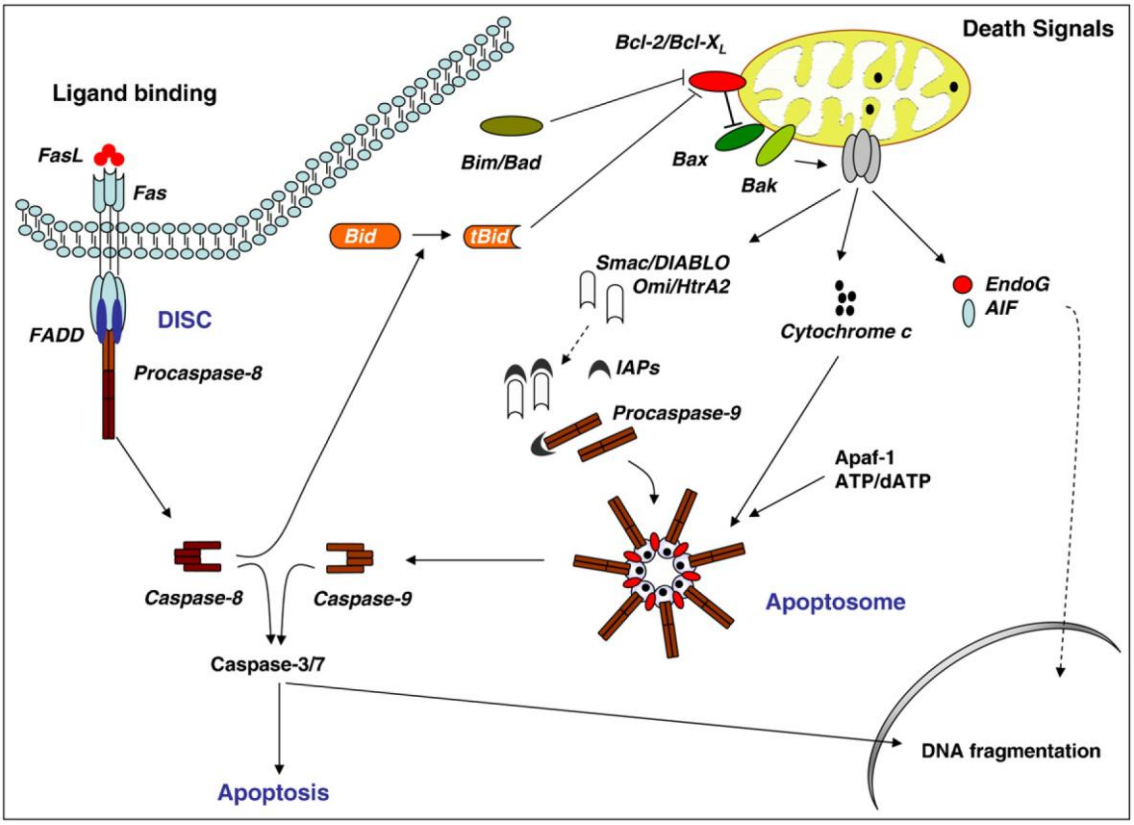

Figure 1.4 Apoptosis can be triggered in a cell through either the extrinsic pathway or the intrinsic pathway. Adapted from Buytaert et al. (11).

1.3.2.2 Bcl-2 family members in PDT

The Bcl-2 family of proteins constitutes a critical control point in apoptosis residing immediately upstream of irreversible cellular damage, where the family members control the release of apoptogenic factors from mitochondria. At present, more than 30 proteins of this family have been identified; they contain one of four Bcl-2 homology domains (BH1 to BH4). Antiapoptotic Bcl-2 proteins (e.g. Bcl-2, Bcl-XL, Bcl-w)

contain all four BH domain and reside at the cytoplasmic side of cellular membranes of the mitochondria, ER and nucleus; proapoptotic Bcl-2 proteins can be subdivided into the BH123 multidomain, e.g. Bax (Bcl-2–associated X protein), Bak (Bcl-2 homologous antagonist/killer), and BH3-only proteins, e.g. Bid, Bad (Bcl-2-associated death promoter) (16).

Importantly, many of these proteins function at the level of mitochondria, and translocation of proapoptotic members from the cytosol to mitochondria is a key initiating event in apoptosis. Antiapoptotic Bcl-2 proteins potently inhibit apoptosis in response to many but not all cytotoxic insults. Bcl-2 and several other pro-survival molecules associate with the mitochondria outer membrane and the endoplasmic reticulum/nuclear membrane and maintain their integrity (72). They can prevent cytochrome c release and subsequent caspase-9 activation. They probably also regulate the activation of several other caspases, independently of mitochondrial damage (15).

Proapoptotic Bax is a cytosolic monomer that, upon apoptotic stimuli, changes conformation and integrates in the outer mitochondrial membrane (OMM) where it oligomerizes (33), whereas Bak is associated with the OMM (4, 32, 33). Multidomain Bax and Bak proteins, once activated, undergo a conformational change (taking place in the cytosol for Bax, or at the mitochondrial membrane for Bak) that triggers their oligomerization/activation and formation of supramolecular pores mediating MMP.

Proapoptotic Bcl-2 family member Bid provides a molecular link between the extrinsic and intrinsic apoptotic pathways. This cell death pathway is controlled by Bcl-2 family proteins (16).

Both propapototic and antiapoptoic Bcl-2 family members are implicated in PDT-induced apoptosis (3, 11, 97). The antiapoptotic Bcl-2 protein, whose photodamage leads to the release of cytochrome c from mitochondria, activation of caspase-3 and initiation of the apoptotic program, was identified as a molecular target for several mitochondria and ER localized PSs, namely Pc4 (141), Foscan (79) and CPO (59). However, overexpression of Bcl-2 has also been shown to enhance the apoptotic response to PDT (63). This may be due to the selective destruction of Bcl-2 and increased levels of Bax following PDT, suggesting that the balance between proapoptotic and antiapoptotic Bcl-2 family members plays an important role in PDT-induced apoptotic death. The relocation of Bax from the cytosol to the mitochondria has

been reported in different PDT paradigms to occur with kinetics matching the release of cytochrome c (9, 30).

1.3.2.3 The role of ER stress in apoptotic cell death after PDT

The endoplasmic reticulum plays an important role in the maintenance of intracellular calcium homeostasis, protein synthesis, posttranslational modification, and proper folding of proteins as well as their sorting and trafficking. Many stimuli, including alterations in calcium homeostasis and accumulation of unfolded proteins in ER, can cause stress (86, 103). ER stress initiates apoptosis through at least two different mechanisms, namely Ca^{2+} signaling and the unfolded protein response (UPR) (37, 89, 90, 103).

1.3.2.3.1 Effect of PDT on the calcium homeostasis

Oxidative damage to the ER following PDT can result in dramatic changes in calcium homeostasis. In addition, the release of Ca^{2+} from the ER may cause activation of calpains, central players in the conversion of Ca^{2+} signals from ER to the caspase-12 activation. It can lead to caspase-9/caspase-3/7 activation and apoptosis in a cytochrome c and Apaf-1-independent manner. Caspase-12, specifically found on the cytosolic face of the ER membrane, is considered a key caspase involved in the apoptosis in response to ER stress (71). An alternative to caspase-12 in human is caspase-4, which is involved in ER stress-induced cell death pathway (45). Both murine caspase-12 and human caspase-4 are localized to the ER and cleaved specifically by ER stress (45, 47, 88, 89).

1.3.2.3.2 Activation of the UPR in response to PDT-mediated ER

Apart from Ca^{2+} storage and signaling, the main function of the ER is folding, modifying and sorting the newly synthesized proteins. Disturbances in any of these functions can lead to ER stress. Ca^{2+} overload and depletion of the ER Ca^{2+} pool are insults leading to ER stress, changes in protein folding and subsequent activation of the unfolded protein response. Generally, ER stress is sensed by three integral stress receptors including the pancreatic ER kinase (PKR)-like ER kinase (PERK), activating transcription factor 6 (ATF6) and inositol requiring enzyme 1 (IRE1) (107). These ER transmembrane proteins are kept at inactive state through the direct association of their luminal domain with the ER chaperone Bip/GRP78 (glucose regulated protein 78 kD). However, upon accumulation of unfolded proteins, GRP78 dissociates from these

molecules, which leads to their activation. PERK phosphorylates the α subunit of eukaryotic initiation factor 2 (eIF2α) to promote translation of activating transcription factor 4 (ATF4) (76), which subsequently upregulates expression of the proapoptotic protein CHOP (C/EBP-homologous protein-10 also known as GADD153) (38, 77). IRE1 induces unconventional splicing of XBP1 mRNA (X-box binding protein 1) translating into a functional transcription factor to up-regulate gene expression for ER quality control (13, 144). ATF6 activation involves regulated intramembrane proteolysis. The protein translocates to the Golgi, where it is proteolytically cleaved by the sequential actions of site 1 protease (S1P) and site 2 protease (S2P) (87). The main pathways activated by ER stress are illustrated in Figure 1.5.

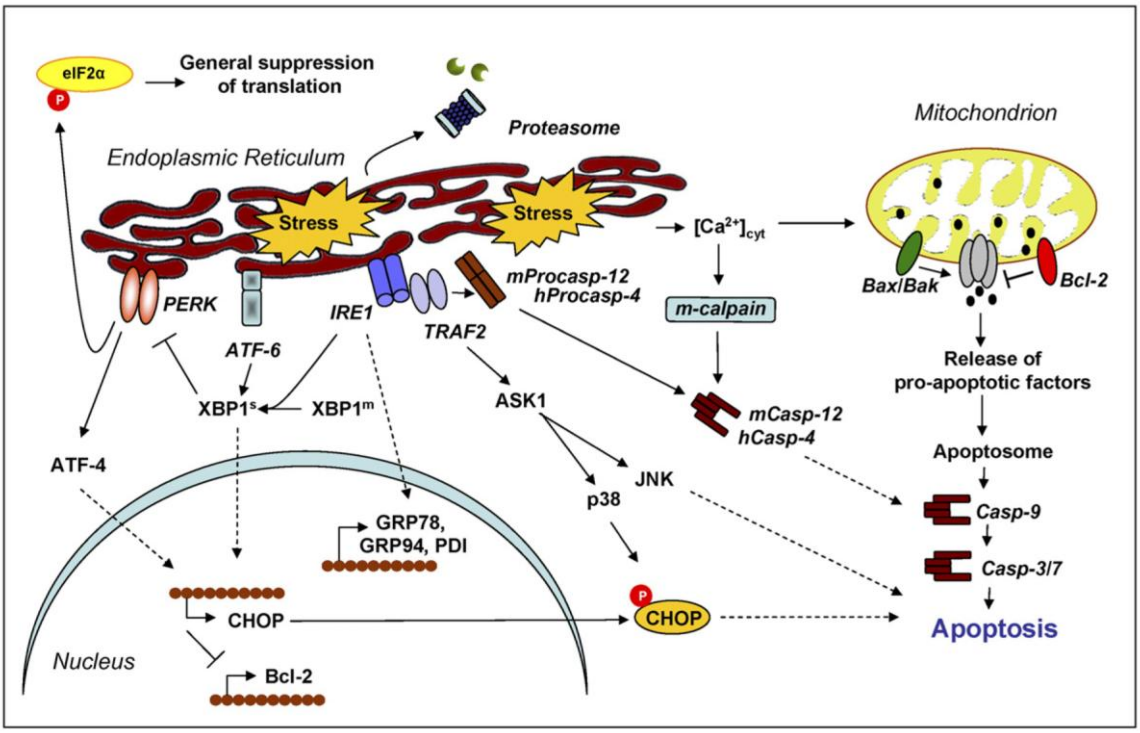

Figure 1.5 UPR signaling pathways. Adapted from Buytaert et al. (11).

1.3.2.4 Role of MAPKs in PDT

As mentioned before, in recent times, various types of photosensitizers have been developed and evaluated for their efficacy in tumor eradication. It is now clear that the target of PDT is not restricted to a single cellular component or a single signaling pathway. Multiple intracellular components and signaling pathways have been implicated in PDT-induced cell death (11).

Oxidative stress activates multiple signaling pathways including mitogen-activated protein kinase (MAPK). The mitogen-activated protein kinases represent a group of serine/threonine protein kinases which are activated by dual phosphorylation on tyrosine and threonine residues. In this family three MAPKs have been characterized: the extracellular signal-regulated kinases (ERKs), the Jun N-terminal kinases/stress-activated protein kinases (JNK/SAPK), and the p38 MAPK. JNK and p38 MAPK were shown to be key mediators of stress signals (43) and are often associated with apoptosis (14). The exact roles of JNK and or p38 MAPK in PDT-induced apoptosis remain highly ambiguous. However, activation of MAPKs was observed following photoactivation of Verteporfin (120), 5-aminolevulinate (64), Hypericin (5), Pc4 (140) and Photofrin (123).

In the case of Pc4, Rose Bengal and PORF-TEG (in the thesis also called pTPPF(EG)4, alternative nomenclature shown in Table 3.1), the activation of p38 was shown to be directly connected with apoptosis (69, 140, 147). However, in Hypericin- and Photofrin-mediated apoptosis, JNK and p38 MAPK were rather implicated in cellular resistance against the PDT stress (5, 123).

2 AIMS OF THE THESIS

Extensive research over the past years demonstrated that photosensitizers used in PDT vary widely in their activity depending on their chemical structure, subcellular localization and cellular context. Therefore, understanding of the structure/activity relationships seems to be a critical issue in the development toward an ideal photosensitizer. On the other hand, even closely related structures with similar localization might exhibit different PDT efficacy. To bring deeper insight into this topic, we set up the main goal of this thesis to investigate a unique group of newly synthesized glycol-porphyrin derivatives representing very similar molecules differing in some cases only in the glycol chain being in either the meta-phenyl or the para-phenyl position. The present study was undertaken to determine subcellular localization of the derivatives, and overall PDT efficacy *in vitro* and *in vivo*. In selected prototypes we studied the modality of the cell response and the commitment events leading to cell death by comparing the signaling pathways induced in two tumor cell lines of different origin.

The specific aims are as follows:

1. To identify promising photosensitizers in a group of newly synthesized compounds (generated at the Institute of Chemical Technology) with improved properties in comparison to clinically used Foscan

2. To determine how the changes in molecular structure of photosensitizers affect their cellular uptake

3. To characterize cellular trafficking and specific compartment localization of new photosensitizers

4. To analyze and determine the mechanism of cell death induced by photosensitizers in cancer cells following light exposure

5. To reveal the major signaling pathways responsible for cell death induction

6. To confirm the photodynamic efficacy of selected photosensitizers *in vivo*

3 MATERIAL AND METHODS

3.1 Synthesis of the porphyrins

Synthesis and elemental analysis of porphyrin derivatives used in the studies were performed at the Institute of Chemical Technology (Prague) and were described in the paper published in J. Med. Chem. (68). All 12 derivatives are listed in Table 3.1 together with their numbering, abbreviation and chemical identity.

Briefly, two of meso-tetrasubstituted porphyrins were prepared and tested. The first type, which comprised symmetrical nonfluorinated derivatives **2-5** (Scheme 3.1) or asymmetrical nonfluorinated porphyrins **10-12** (Scheme 3.3), consists of the porphyrins that were substituted by monoethylenene glycol chains. The glycol units that were used for the substitution of the porphyrins were composed of two types of monoethyleneglycol chains: one with the terminal hydroxy group (**2**, **4**, **6**, **10**-**12**) and the other with the terminal methoxy group (**3**, **5**, and **7**). The glycol chains were anchored at para or meta positions of meso-phenyl groups (Schemes 3.1 and 3.3).

The second type of meso-tetrasubstituted porphyrins, which is represented by fluorinated derivatives **6-8** (Scheme 3.2), was prepared by the substitution in para positions of meso-pentafluorophenyl groups with either monoethylene glycol or monopropylene glycol chains (Scheme 3.2). Porphyrin derivative **9** with side chains connected to porphyrin fluorophenyl groups via a nitrogen atom was also prepared.

Table 3.1 Porphyrin derivatives used in the experiments and alternative nomenclature.

Derivative	Abbreviation	Alternative label	Chemical identity
1a	**mTHPP**		m-tetrahydroxyphenylporphyrin
1b	**pTHPP**		p-tetrahydroxyphenylporphyrin
2	**mTPP(EG)4**		5,10,15,20-Tetrakis-[3-(*O*-ethyleneglycol)phenyl]-21,23H-porphyrin
3	**mTPP(EGME)4**		5,10,15,20-Tetrakis-[3-(ethyleneglycolmonomethoxyether)phenyl]-21,23H-porphyrin
4	**pTPP(EG)4**		5,10,15,20-Tetrakis-[4-(ethyleneglycol)phenyl]-21,23H-porphyrin
5	**pTPP(EGME)4**		5,10,15,20-Tetrakis-[4-(ethyleneglycolmonomethoxyether)phenyl]-21,23H-porphyrin
6	**pTPPF(EG)4**	**PORF-TEG**	5,10,15,20-Tetrakis-[4-(ethyleneglycol)tetrafluorophenyl]-21,23H porphyrin
7	**pTPPF(EGME)4**		5,10,15,20-Tetrakis-(4-(ethyleneglycolmonomethoxyether)tetrafluorophenyl)-21,23H-porphyrin
8	**pTPPF(DEG)4**		5,10,15,20-Tetrakis-[4-(diethyleneglycol)tetrafluorophenyl]-21,23H-porphyrin
9	**pTPPF(ETA)4**		5,10,15,20-Tetrakis-[4-(*N*-ethanolamine)tetrafluorophenyl]-21,23H-porphyrin
10	**mTPP(EG)1**		5-[3-(ethyleneglycol)phenyl]-10,15,20-Tris-(3-hydroxyphenyl)-21,23H-porphyrin
11	**mTPP(EG)2**		5,10-Bis-[3-(ethyleneglycol)phenyl]-15,20-Bis-(3-hydroxyphenyl)-21,23H-porphyrin
12	**mTPP(EG)3**		5,10,15-Tris-[3-(ethyleneglycol)phenyl]-20-(3-hydroxyphenyl)-21,23H-porphyrin
	mTHPC	**Foscan**	m-tetrahydroxyphenylchlorin

m=meta, **p**=para

Scheme 3.1 Syntheses of symmetrical nonfluorinated porphyrins 2-5.

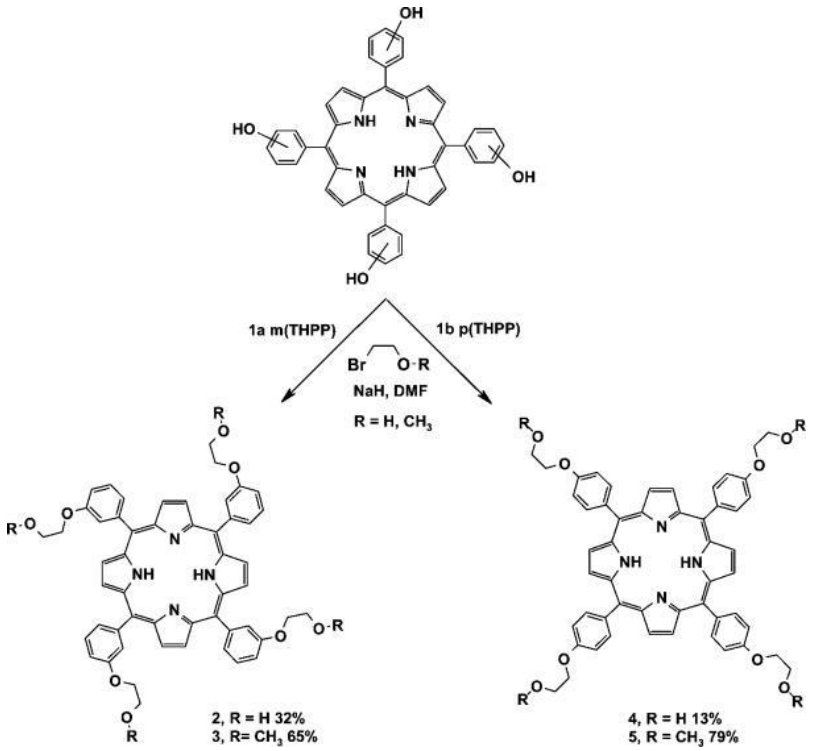

Scheme 3.2 Syntheses of symmetrical fluorinated porphyrins 6-9.

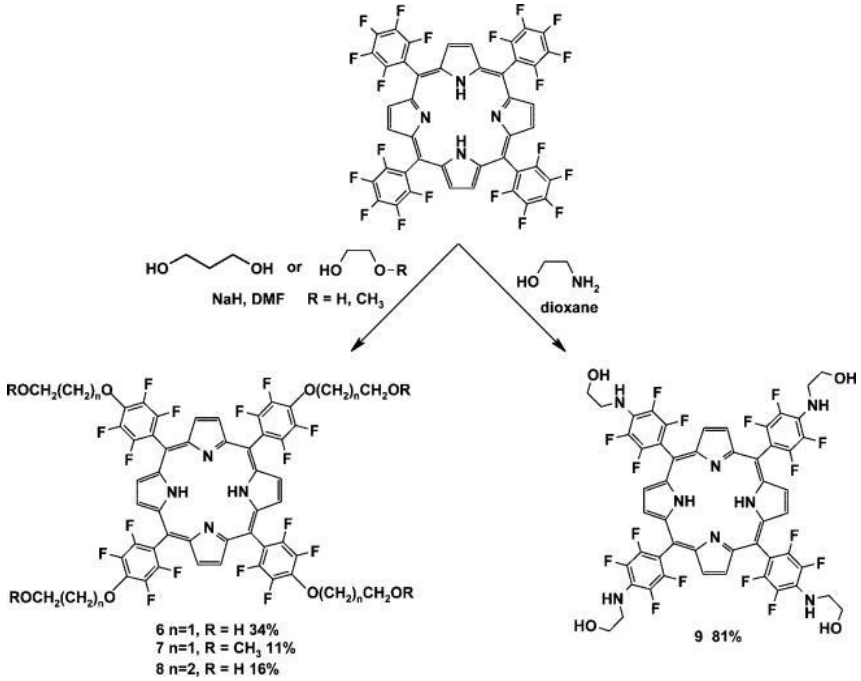

Scheme 3.3 Syntheses of asymmetrical nonfluorinated porphyrins 10-12.

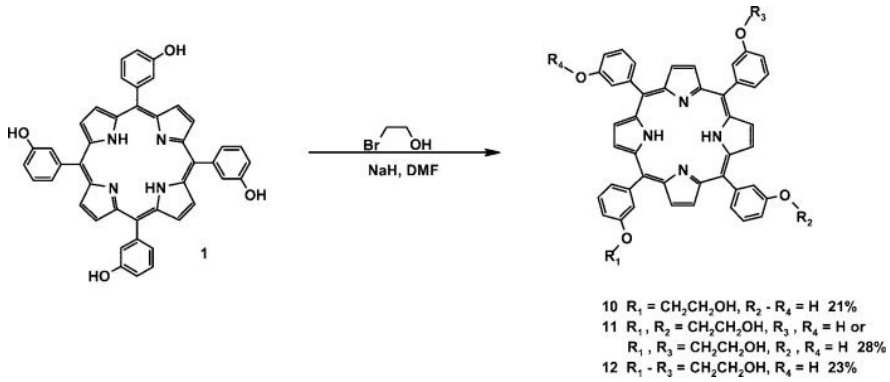

3.2 Antibodies

Antibodies recognizing phospho-MKK3/MKK6 (Ser189/207), phospho-p38 MAPK (Thr180/Tyr182), phospho-SAPK/JNK (Thr183/Tyr185), phospho-PERK (Thr980), phospho-eIF2α (Ser51), phospho-c-Jun (Ser73), MKK3 kinase, p38 MAPK, SAPK/JNK, PERK, eIF2α, Bcl-2, CHOP, caspases-3, -8, -9 and -12 were from Cell Signaling Technology Inc. (Beverly, MA, USA), ATF4 from ProteinTech Group Inc. (Chicago, IL, USA), caspase-4 from MBL International Corporation (Woburn, MA, USA), fodrin from Enzo Life Sciences (Farmingdale, NY, USA), Mcl-1 (S-19), CREB-2 (ATF4), c-Jun from Santa Cruz Biotechnology (Santa Cruz, CA, USA), cytochrome c, PARP from BD Bioscience Pharmingen (San Diego, CA, USA) and actin from Sigma Aldrich (St Louis, MO, USA). GAPDH antibody was from GeneTex (Irvine, CA, USA). Antibody against m-calpain was kindly provided by Dr. Peter Greer and used as described previously (108). Secondary anti-rabbit and anti-mouse antibodies conjugated with horseradish peroxidase, fluorescence secondary antibody Cy3 anti mouse were purchased from Jackson ImmunoResearchLaboratories (Bar Harbor, ME, USA).

3.3 Inhibitors

Kinase inhibitors JNK II (SP600125) and p38 (PD 169316) were purchased from Calbiochem (San Diego, CA, USA), caspase inhibitor Z-VAD-FMK was from Alexis (Lausen, Switzerland), ROS scavengers L-histidine, trolox (6-Hydroxy-2,5,7,8-tetramethylchromane-2-carboxylic acid), NAC (N-Acetyl-L-cysteine), tiron (4,5-dihydroxy-1,3-benzene disulfonic acid), DMSO (dimethyl sulfoxide) and thapsigargin from Sigma Aldrich (St Louis, MO, USA), PD150606, Ru360 and inhibitor of eIF2α

dephosphorylation (Salubrinal) from Calbiochem (San Diego, CA, USA). Calcium chelator BAPTA-AM (1, 2-bis-(o-aminophenoxy) ethane-N,N,N',N'-tetraacetic acid tetra-(acetoxymethyl)ester) and sodium pyruvate were obtained from Invitrogen (Carlsbad, CA, USA).

3.4 Cell cultures

All cell lines were purchased from American Type Culture Collection (Manassas, VA, USA). Cell lines HL60 (human promyelotic leukemia), 4T1 (mouse mammary carcinoma) and MDA-MB-231 (human breast carcinoma) were kept at exponential growth in RPMI 1640 medium supplemented with 10% fetal calf serum. MEFs-wild-type (wt) and p38a-/- (KO), kindly provided by Dr. AR Nebreda, were grown in Dulbecco's modified Eagle's medium with antibiotics and 10% fetal calf serum. MEFs-wild-type (wt) and PERK -/- (KO), a kind gift of Prof. D. Ron, were grown in Dulbecco's modified Eagle's medium supplemented with antibiotics, 10% fetal calf serum, β-mercaptoethanol (55 mM final concentration) and nonessential amino acids.

3.5 Photosensitization and cell death determination

HL60 (human promyelotic leukemia), 4T1 (mouse mammary carcinoma) cells were cultivated overnight at 37˚C and 5% CO_2 in the presence of EG-porphyrin derivatives at a concentration of 0.01-10 μM to result in 60-80% photoinduced mortality. The cells were then washed with PBS, illuminated with filtered light (500-520 nm, 2.5 J/cm^2) and harvested at various time points after irradiation for further analysis. Cell viability was determined 24 h post-PDT by the trypan blue exclusion method. Control dark experiments (without illumination) were performed in parallel.

3.6 Inhibitor and scavenger experiments

Cells loaded with EG-porphyrin derivatives were washed and preincubated for 1 h prior to light exposure with 15-20 μM p38 MAP kinase inhibitor (PD 169316), 5 μM JNK inhibitor II (SP600125), 20 mM $^1O_2$ scavenger L-histidine, 4-5 mM ROS scavenger trolox, 10 mM tiron, 5-15 mM NAC, 1% DMSO, 10 mM sodium pyruvate (Na pyruv), 4-5 μM mitochondrial uniporter inhibitor Ru360 or 20 μM calpain inhibitor PD150606. The preincubation in experiments using calcium chelator 5-10 μM BAPTA-AM, 100 μM caspase inhibitor Z-VAD-FMK and specific inhibitor of eIF2α phosphatase

enzymes salubrinal (20 μM) lasted 2 hours. After irradiation the cells were further incubated up to next day for viability determination by the trypan blue exclusion method.

3.7 DNA analysis

DNA fragmentation was determined in PDT-treated HL60 and 4T1 cells. Cells were harvested by centrifugation (700 g for 5 min), incubated with 0.5 ml extraction buffer (10 mM TRIS, 0.1 mM EDTA, 0.5% SDS) containing RNase (10 μg/ml) at 37°C for 1 h and digested with proteinase K (final concentration 300 μg/ml) for 2 h at 50°C. The DNA was then extracted with phenol/chloroform mixture (1:1), precipitated with ethanol and analyzed by 1.5% agarose gel electrophoresis for 3.5 h (2 V/cm gradient). The 1 kb DNA Ladder (Invitrogen, Carlsbad, CA, USA) was used to size the DNA fragments. After being stained with ethidium bromide, DNA bands were viewed under 312 nm light.

3.8 RT-PCR analysis

RNA was extracted by immediately dissolving the cell pellet in 1 ml Trizol reagent (Invitrogen, Carlsbad, CA, USA) following manufacturer's instructions. Reverse transcription was performed using M-MLV Reverse Transcriptase (Promega, Madison, WI, USA). PCR was performed with GoTaq polymerase (Promega, Madison, WI, USA) and the resulting products were resolved in 1.5% agarose gel. For qPCR, each sample was prepared in triplicate by placing 1 μl of the cDNA template with FastStart SYBR Green Master (Roche Diagnostics, Mannheim, Germany) to a final volume of 10 μl. Samples were amplified by the Light Cycler 480 (Roche Diagnostics, Mannheim, Germany). Oligonucleotide primers are described in Table 3.2. The relative expression levels of each target gene were normalized to the mRNA of the internal standard gene β-actin.

Table 3.2: List of oligonucleotide primers used in the study.

Gene	Primer (forward/reverse)
murine ATF4	ACCAGTCGGGTTTGGGGGCT/TTCCGAGGAGCCCGCCTTGT
murine CHOP	CTGCCTTTCACCTTGGAGAC/CGTTTCCTGGGGATGAGATA
murine β-actin	GATCTGGCACCACACCTTCT/GGGGTGTTGAAGGTCTCAAA
human ATF4	CCACTAGGTACCGCCAGAAG/GCCTTGCGGACCTCTTCTAT
human CHOP	TCGCCGAGCTCTGATTGACC/AAGCCTTCCCCCTGCGTATGT
human β-actin	GAGTCCTGTGGCATCCACGA/AGGAGGAGCAATGATCTTGAT

Abbreviations: ATF4, activating transcription factor 4; CHOP, the proapoptotic protein (C/EBP-homologous protein-10 also known as GADD153

3.9 Preparation of cell extracts and western immunoblot analysis

Cell extracts were prepared at the indicated time points following irradiation. After treatment cells were washed with ice-cold PBS and lysed on ice in 1x SDS sample buffer (62.5 mM TRIS pH 6.8, 1 % SDS, 10% glycerol, 72 mM β-mercaptoethanol, 0.01% bromphenol blue) or RIPA buffer (10 mM TRIS pH7.5, 150 mM NaCl, 5 mM EDTA, 1% Triton X 100 + protease inhibitor cocktail (Roche Diagnostics, Mannheim, Germany) and 1 mM PMSF (phenylmethylsulfonyl fluoride). Proteins were separated by 9-15% SDS-PAGE and transferred to nitrocellulose membrane (Hybond-ECL nitrocellulose membranes, Amersham Biosciences).

The membranes were blocked in 5% nonfat dry milk in TBST buffer (50 mM Tris, 150 mM NaCl, 0.05% Tween 20) for 1 h at room temperature and incubated with primary antibody overnight at 4˚C. The membranes were then washed in TBST and incubated for 1 h at room temperature with horseradish peroxidase-conjugated secondary antibodies. Detection was carried out with the enhanced chemiluminescence (ECL) detection system. Equal protein loading and transfer was verified by Ponceau-S staining of the membrane and actin reprobing.

Cytosolic, mitochondrial and nuclear fractions were prepared using a cell fractionation kit (Abcam Ltd., UK) according to the manufacturer´s instructions. As internal loading controls for fractionation experiments, we used cytosolic GAPDH and nuclear PARP.

3.10 Flow cytometry analysis

3.10.1 Annexin V assay

HL60 cells were treated overnight with EG-porphyrin derivatives and were illuminated as previously described (2.5 J/cm^2). After 4.5-6.5 h the cells were resuspended in 100 μl of binding buffer and incubated with both Annexin V (Roche Diagnostics, Mannheim, Germany) and PI (propidium iodide) (Sigma Aldrich, St Louis, MO, USA) for 10 min in the dark. Then 10^4 cells were analyzed by a flow cytometer (BD LSRII, FlowJo software). The percentage of live, dead, and apoptotic cells was determined. The viable cells (B3) were located in the lower left corner (negative for both Annexin V-FITC and PI). Early apoptotic cells (B4) were in the lower right corner (Annexin V-FITC positive), and late apoptotic cells (B2) were in the upper right corner (positive for both Annexin V-FITC and PI). The total percentage of apoptotic cells was represented as a combination of B2 + B4.

3.10.2 Fluo-4-AM

Cells pre-loaded overnight with EG-porphyrin derivatives were washed and then stained with 4 μM Fluo-4-AM from Molecular Probes (Invitrogen, Carlsbad, CA, USA) for 30 min. During FACS (Fluorescent activated cell sorting) inflow, HL60 cells were exposed for 30 s and 4T1 cells for 1 min to laser beam (424 nm) and then Ca^{2+} efflux was detected by a BD LSRII flow cytometer. Next, the cells were measured using a modified protocol: preincubation for 1 h with ROS scavenger L-histidine (20 mM) or 2 h with calcium chelator BAPTA-AM (5 μM); and continued as described above.

3.11 Microscopic studies

We studied the subcellular localization of EG-porphyrin derivatives in 4T1 tumor cells. Cells were grown on coverslips in 35 mm Petri dishes were incubated with EG-porphyrin derivatives in complete medium for 16 h.

3.11.1 Confocal microscopy - subcellular localization

After incubation, cells were loaded with 75 nM MitoTracker Green, 500 nM LysoTracker Green, or 250 nM ER-Tracker Blue-White (Molecular Probes) (Invitrogen, Carlsbad, CA, USA) for 30 min at 37˚C in the complete medium. Cells were washed

with PBS three times, overlaid with media without phenol red, and examined under a DMI 6000 inverted Leica TCS AOBS SP5 tandem scanning confocal microscope with an AR (488 nm) laser and an x100 oil immersion objective. The emission spectra of derivatives were detected between 640 and 700 nm. In the same cells, the emission spectra of green MitoTracker or LysoTracker were detected in the 500-550 nm range, and emission spectra of blue ER-Tracker were detected in the 420-480 nm range. Experiments were repeated three times in minimal ambient light.

3.11.2 ROS detection

For ROS detection 4T1 cells were seeded on coverslips or on Petri dishes and then incubated with EG-porphyrin derivatives in complete medium for 16 h. After incubation, cells were washed and loaded with 10 μM APF (3′-(p-aminophenyl) fluorescein) from Sigma Aldrich (St Louis, MO, USA) present in phenol red-free culture media for 30 min. Dye-loaded cells were stimulated for 10 s under a DM IRB microscope (Leica) by UV light using Leica filter cube A (excitation filter BP 340–380 nm and long pass filter LP 425 nm for emission) and fluorescence images were acquired by a DFC 480 camera using an x10 or x63 oil immersion objective and Leica filter cube N2.1 (excitation filter BP 515–560 nm and long pass filter LP 590 nm for emission) for EG-porphyrin derivatives and cube I3 (excitation filter BP 450–490 nm and long pass filter LP 515 nm for emission) for APF fluorescence.

3.11.3 Immunofluorescence CHOP detection

Cells grown on coverslips in 35 mm Petri dishes were incubated with EG-porphyrin derivatives in complete medium for 16 h. After incubation, cells were washed and illuminated with filtered light 2.5 J/cm^2. Two hours later the cells were fixed with 3% paraformaldehyde for 30 min, permeabilized with 0.5 % Triton and then blocked with 5% BSA at room temperature. Subsequently, coverslips were incubated with primary antibody against CHOP (diluted 1:1000, Cell Signaling Technology Inc., Beverly, MA, USA) at room temperature for 1 h and with Cy3 anti-mouse secondary antibody for 30 min (Jackson ImmunoResearch Laboratories, Bar Harbor, ME, USA). After being washed, the slides were mounted in 50% glycerol and staining was visualized under a fluorescence microscope DM IRB, Leica microscope equipped with a DFC 480 camera using an x100 oil immersion objective and Leica cube N 2.1 (excitation filter BP 515-

560 nm and long pass filter LP 590 nm for emission). All images were taken under the same settings.

3.11.4 Intracellular uptake of EG-porphyrin derivatives into MEF cells

MEF cells grown on coverslips were incubated with EG-porphyrin derivatives (800 nM mTPP(EG)4, 5 μM pTPP(EG)4, 2 μM pTPPF(EG)4) in complete medium for 16 h. After washing, porphyrin fluorescence was observed under a microscope.

3.12 Transfection

4T1 cells were seeded onto 35 mm dishes and allowed to reach 50% confluence on the day of transfection. The small interfering RNA (siRNA) constructs, the ON-TARGETplus SMART pool PERK (L-044901-00-0010), ON-TARGETplus SMART pool CAPNS1 (L-048840-01-0010) and the non-targeting siRNA control ON-TARGETplus Non-targeting Pool (D-001810-10-05), were used (Dharmacon, Lafayette, CO, USA). Cells were transfected with 50 nM siRNA diluted in RPMI medium using Lipofectamine RNAiMAX reagent (Invitrogen, Carlsbad, CA, USA) according to the manufacturer's transfection protocol. For further analysis the cells were used on the third day after the transfection.

3.13 *In vivo* Experiments

In cooperation with the First Faculty of Medicine, Charles University in Prague, we tested the effect of glycol porphyrin derivatives *in vivo*. Derivatives mTPP(EG)4, pTPP(EG)4, pTPPF(EG)4, mTPP(EG)1, mTPP(EG)2 and mTPP(EG)3 were selected for *in vivo* analysis to define their PDT effectiveness. We used nude mice (NuNu). We made fresh stock solutions of the sensitizers by dissolving the drug in 20 μl of 20% DMSO and adjusting the mixture with water to provide the application dose of 3 mg/kg in a volume of 0.1 ml per 20 g mice. MDA-MB-231cells (1×10^7) that were suspended in 0.1 ml of PBS and 0.1 ml of Matrigel (BD Biosciences, Franklin Lakes, NJ) were injected subcutaneously into hind flanks of the mice. PDT experiments were performed when the tumor mass reached a volume of 100 mm^3 (about 10 days after transplantation). The tumor area (2 cm^2) was irradiated by a 500-700 nm xenon lamp ONL 051 (maximum at 635 nm, Preciosa Crytur, Turnov, Czech Republic) with total impact energy of 100 J/cm^2 and a fluence rate of 200 mW/cm^2. The tested interval

between drug administration and photoirradiation varied from 2 to 72 h. The complete PDT treatment was repeated after 1 week. Tumor dimensions were determined by caliper measurements every third or fourth day after the treatment. The volume of each tumor was calculated as $\pi/6 \times a \times b \times c$ (where a is the longitudinal diameter, b is the short diameter, and c is the thickness). All aspects of the animal experiment and husbandry were carried out in compliance with national and European regulations.

3.14 Statistical analysis

Results are shown as mean values of at least three independent experiments (n) and standard deviation (±SD) represented by bars. The significance of differences was estimated by ANOVA or by t-test. *P<0.050, **P<0.01, ***P<0.001 represent the level of significance (P<0.050 was considered significant). For all statistical analyses, GraphPad Software was used.

4 RESULTS

4.1 Intracellular uptake of EG-porphyrin derivatives in 4T1 cells

The effect of the variation of peripheral glycol chain number, length, and position on the intracellular concentration and distribution was determined by fluorescence of the porphyrin derivatives in 4T1 cells and compared to the parent compounds (pTHPP, mTHPP corresponding to compounds **1a**, **1b** in Scheme 3.1) without glycol chains. The porphyrins (0.5-10 μM) were added to the medium, and cells were analyzed 2 and 16 h later by fluorescence microscopy. No principal temporal redistribution of the fluorescence pattern of any compound was observed. Meta derivatives (compounds mTPP(EG)1-4, corresponding to compounds **2** and **10-12** in Schemes 3.1 and 3.3, respectively) exhibited diffuse fluorescence throughout the cytoplasmic area within 2 h, whereas para derivatives, pTPP(EG)4, pTPPF(EG)4 (corresponding to compounds **4** and **6**, respectively, in Scheme 3.1.), and pTPPF(DEG)4, pTPPF(ETA)4 (corresponding to compounds **8** and **9** in Scheme 3.2.) displayed the characteristic punctuated pattern with increasing intensity after prolonged incubation (exemplified by mTPP(EG)4 and pTPPF(EG)4 in Figure 4.2). The fluorescence of parent compounds mTHPP and pTHPP was weaker, and it showed delayed kinetics in comparison with glycol derivative mTPP(EG)4. In contrast, methoxy-glycol porphyrins mTPP(EGME)4, pTPP(EGME)4, pTPPF(EGME)4 (corresponding to compounds **3, 5** and **7** in Schemes 3.1 and 3.2) did not show any significant intracellular fluorescence (not shown), indicating poor cellular uptake leading to very low biological activity (Table 4.1). Thus, they were excluded from further investigations.

4.2 *In vitro* phototoxicity

To investigate the photodynamic potential of the glycol porphyrin derivatives, we incubated HL60 and 4T1 cells with increasing concentrations of the porphyrins and then illuminated them with filtered light (500-520 nm, 2.5 J/cm^2). Cells that were incubated with the porphyrins without illumination (dark control) were kept in parallel. Following the illumination of the cell lines, the viability of post-PDT cultures was determined the next day by the trypan blue exclusion method, and dose/response curves were obtained. The IC50 values, which represent the concentration of the porphyrins that is required to kill 50 % of cells, were calculated for each curve, and they are summarized in Table 4.1.

Porphyrin mTPP(EG)4 with symmetrical EG substitutions in all four meta phenyl positions was able to evoke IC50 in HL60 and 4T1 cells at 47- and 20-fold lower concentrations, respectively, than the corresponding derivative pTPP(EG)4 with EG chains in para position (Table 4.1). Fluorinated para-substituted porphyrin pTPPF(EG)4 showed an increased biological efficacy in comparison with its unfluorinated analog pTPP(EG)4. However, in the case of fluorinated para-substituted porphyrins, both the elongation of the glycol chains (pTPPF(DEG)4) and the substitution of nitrogen for oxygen (pTPPF(ETA)4) weakened the biological activity of the resulting compound, which thereby indicates a delicate influence of various factors on the biological activity of the synthesized porphyrin derivatives. mTHPC, an active compound of the marketed drug Foscan, was included for comparison with porphyrin derivatives under the same experimental conditions as those for the parent mTHPP and pTHPP (Table 4.1, Figure 4.4). Furthermore, although active concentrations of mTHPC fall within a range that is similar to that of the glycol porphyrins, the used optimal wavelengths filters, 650 and 500 nm, respectively, provided different light intensities (3.7 and 0.7 mW/cm^2, respectively) and resulting light doses (13.3 and 2.5 J/cm^2, respectively). Therefore, the overall photodynamic dose (drug dose × light dose) that is required to reach IC50 was about five times lower for mTPP(EG)4 than for mTHPC, which shows the superior potency of mTPP(EG)4.

We introduced various numbers of ethylene glycol chains to the meta position; the resulting asymmetric mono (mTPP(EG)1), bis (mTPP(EG)2), and tris (mTPP(EG)3) derivatives did not show such a relation. The number of EG chains substantially affected neither the intracellular localization (Figure 4.4) nor the *in vitro* PDT efficacy (Table 4.1). Conversely, the best PDT efficacy was achieved with mTPP(EG)3 derivative. It is generally accepted that peripheral substitutions play an important role in the biological availability and activity of the compound. Our results suggest that porphyrins with EG functionalities in the meta position displayed a 1.4- to 4-fold higher PDT efficacy than did parent tetrahydroxyphenyl porphyrin mTHPP (Table 4.1).

Generally, the porphyrins with rather high cell-penetration efficiency (mTPP(EG)4, pTPP(EG)4, pTPPF)EG)4, pTPPF(DEG)4 and pTPPF(ETA)4) displayed high phototoxic activity, whereas poorly penetrating porphyrins (mTPP(EGME)4, pTPP(EGME)4, and pTPPF(EGME)) were inefficient. Furthermore, very effective derivatives mTPP(EG)4, mTPP(EG)1, mTPP(EG)2 and mTPP(EG)3 mostly

accumulated in the endoplasmic reticulum, whereas the localization in lysosomes, with the exception of pTPPF(EG)4, resulted in a lower photodynamic efficacy (pTPP(EG)4, pTPPF(DEG)4 and pTPPF(ETA)4) (Table 4.1, Figures 4.3 and 4.4). It can be concluded that EG substitution on the porphyrin periphery leads to dramatic enhancement of PDT efficacy.

In addition, a further explanation of the unique photodynamic abilities of EG-porphyrins versus those of parent hydroxyphenyl porphyrin is based on their different aggregation properties, which were affected by the exchange of the phenolic terminal group for the alcoholic terminal group. The parent hydroxy porphyrin mTHPP exhibited a strong tendency to aggregate in the lower pH 6, which was demonstrated by a decrease in absorbance that is obvious from the spectral analysis of its aqueous solutions (Figure 4.1). In contrast, EG derivatives mTPP(EG)2-4 did not show such behavior in response to the relevant physiological pH (Figure 4.1), and they are therefore more favorable PSs. These spectral characteristics correlate with intracellular fluorescence data (Figures 4.2, 4.3 and 4.4) and are consistent with biological performance (Table 4.1) because lower aggregation translates into higher photodynamic efficacy.

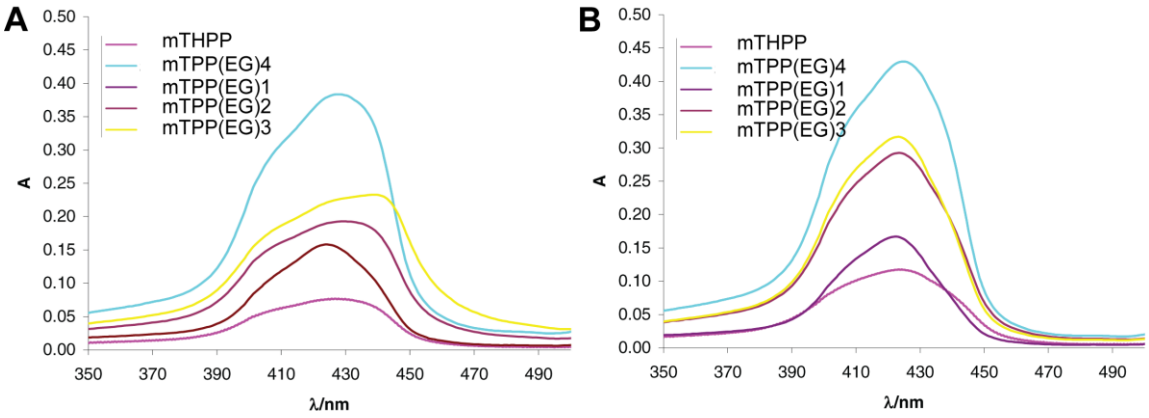

Figure 4.1 Absorption spectra of porphyrin derivatives at pH 6.00 (A) and pH 7.34 (B). The spectra of mTHPP, mTPP(EG)1-4 (c=2.7*10-6) were measured in 0.001M phosphate buffer (pH 6.00 (A) or pH 7.34 (B); 98% water, 2%DMSO) (v/v).

Table 4.1 Concentration of porphyrin derivatives and overall photodynamic dose required for 50% inhibition of the cell viability.

	HL60		4T1	
derivative	**IC_{50} (nM) ± SD**[a]	**OPD**[b]	**IC_{50} (nM) ± SD**	**OPD**
mTHPP[c]	126 ± 5	312	200 ± 40	500
pTHPP[c]	660 ± 30	2500	1050 ± 50	3990
mTPP(EG)4[c]	42 ± 5	105	110 ± 8	275
mTPP(EGME)4[c]	NE[e]	NE		
pTPP(EG)4[c]	2000 ± 130	5000	2200 ± 240	5500
pTPP(EGME)4[c]	NE	NE		
pTPPF(EG)4[c]	150 ± 30	375	200 ± 20	500
pTPPF(EGME)4[c]	NE	NE		
pTPPF(DEG)4[c]	5300 ± 240	13 250	6500 ± 160	16260
pTPPF(ETA)4[c]	2200 ± 160	550	2600 ± 80	6500
mTPP(EG)1[c]	93 ± 10	232	143 ± 6	358
mTPP(EG)2[c]	33 ± 5	83	95 ± 12	238
mTPP(EG)3[c]	31 ± 7	78	93 ± 7	233
mTHPC[d]	42 ± 8	559	117 ± 71	1556

a Values represent the mean ± SD of three to six replicated experiments.
b Overall photodynamic dose (drug dose × light dose).
c Exposed to 500-520 nm light (light dose 2.5 J/cm^2 for porphyrin derivatives but 3.8 J/cm^2 for pTHPP).
d Exposed to 620-660 nm light (light dose 13.3 J/cm^2).
e NE is not effective at concentrations ≤10 μM.

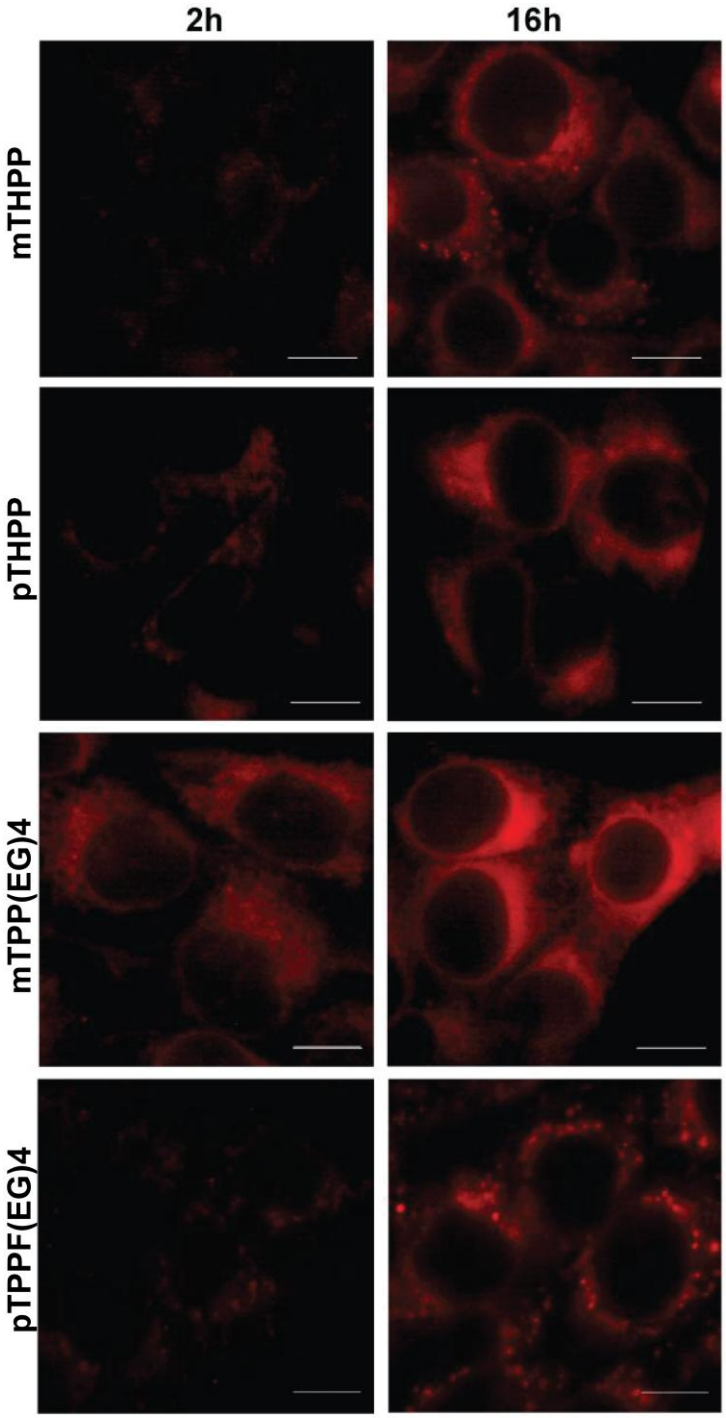

Figure 4.2 Intracellular uptake of porphyrin derivatives. 4T1 cells grown on coverslips were incubated with 1 μM parental mTHPP, 5 μM parental pTHPP or 1 μM EG-porphyrin derivatives (mTPP(EG)4 and pTPPF(EG)4) for indicated time (2, 16 h) and fluorescence was observed with the DM IRB, Leica microscope equipped with the DFC 480 camera using an ×100 oil immersion objective and Leica filter cube N2.1 (excitation filter BP 515–560 nm and long pass filter LP 590 nm for emission). Images were taken under the same settings. Scale bars: 10 μM.

4.3 Subcellular localization of meta and para EG-porphyrin derivatives in 4T1 cells

Not only the cellular uptake, but also selective accumulation of PSs inside the cell is important for the phototoxic activity. To identify the intracellular compartment where the derivatives have accumulated, we co-stained cells with fluorescent LysoTracker Green, MitoTracker Green, and ER Tracker Blue-White probes, and the cells were analyzed by confocal microscopy.

None of the compounds had accumulated in the mitochondria. The co-staining with LysoTracker Green revealed that all para derivatives pTPP(EG)4, pTPPF(EG)4, pTPPF(DEG)4 and pTPPF(ETA)4 accumulated in a subset of LysoTracker-stained structures (Figures 4.3 and 4.4). Fluorination had no observable effect on the localization (Figure 4.3). In contrast, similar to the parental mTHPP, all meta derivatives with one (mTPP(EG)1), two (mTPP(EG)2), three (mTPP(EG)3) and four (mTPP(EG)4) ethylene glycol chains exhibited strong co-localization with the ER Tracker Blue-White probe (Figures 4.3 and 4.4). Importantly, in comparison with ethylene glycol-functionalized porphyrins, mTHPP displayed lower intensity of intracellular fluorescence, which after prolonged incubation, partially affiliated with a subset of LysoTracker stained structures and thereby indicated formation of aggregates that were entrapped in this compartment (Figure 4.4: left column, third panel). Therefore, the localization pattern of the porphyrin derivatives inside the cells seems to be affected mainly by the position of ethylene glycol chains. Similar observations have been published for different glycol-conjugated porphyrins (44).

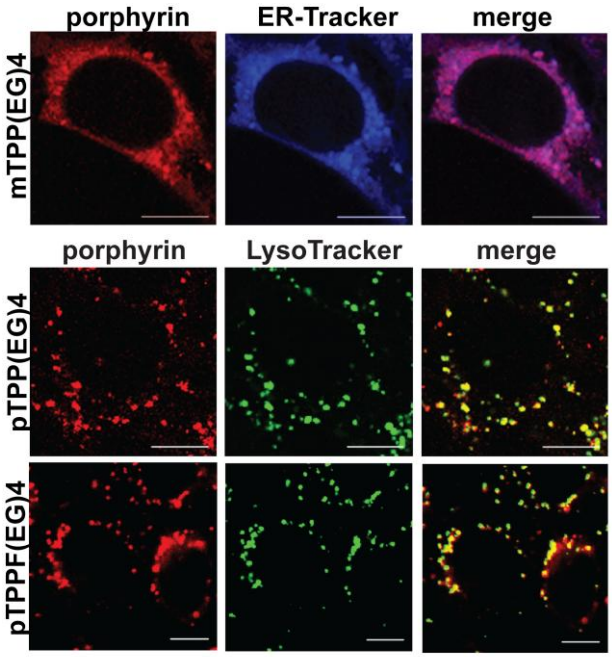

Figure 4.3 Subcellular localization of EG-porphyrin derivatives determined by confocal laser scanning microscopy (CLSM). 4T1 cells were sequentially loaded with porphyrins and specific probes for endoplasmic reticulum and lysosomes. Porphyrin fluorescence (red) is shown in the left panels, ER-Tracker fluorescence (blue) or LysoTracker fluorescence (green) is shown in the middle panels, and an overlay of ER-Tracker or LysoTracker fluorescence with porphyrin fluorescence is shown in the right panels. Co-localization is pink and yellow/orange, respectively. Used concentrations of derivatives are given in the Materials and Methods. Scale bars: 10 μM.

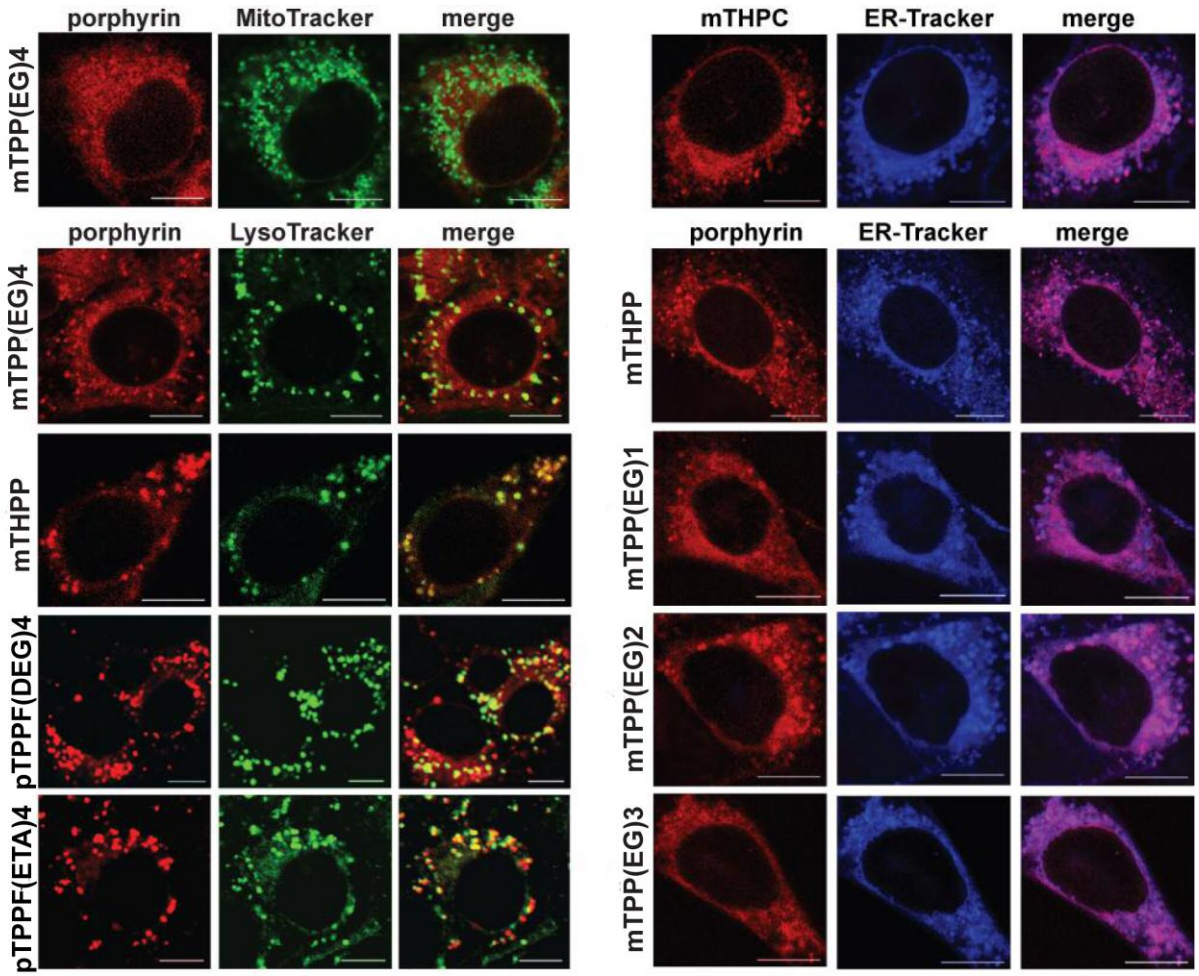

Figure 4.4 Subcellular localization of EG-porphyrin derivatives determined by confocal laser scanning microscopy (CLSM). CMLS images of the glycol-porphyrin derivatives and mitochondria probe (MitoTracker), lysosome probe (LysoTracker), endoplasmic reticulum probe (ER-Tracker) loaded 4T1 cells. The porphyrin fluorescence (red); MitoTracker or LysoTracker probe fluorescence (green); ER-Tracker probe fluorescence (blue); merge images in case of co-localization are orange/yellow or pink colors, respectively. Used concentrations of derivatives are given in Material and Methods. Scale bars: 10 μm.

4.4 Glycol porphyrin derivatives kill cells by apoptosis

There are many reports providing evidence that cells exposed to PDT might die by a regulated process, apoptosis. Here we show that glycol-functionalized porphyrins are potent PSs with the capacity to initiate apoptosis in both suspension and adherent cancer cells. To study the mode of the cell death, we selected the optimal concentration of each derivative to kill 50-80% cells at low light dose (2.5 J/cm^2). One of the hallmarks of apoptosis is the change in membrane permeability demonstrated by phosphatidylserine externalization on the outer leaflet of the plasma membrane, which is an early feature of apoptotic cells. The apoptosis determination was conducted by dual fluorescence of Annexin V-FITC/PI (propidium iodide) and was measured by flow cytometry to distinguish necrotic, apoptotic and live cells. HL60 cells were treated with mTPP(EG)4, pTPP(EG)4, pTPPF(EG)4, pTPPF(DEG)4 and pTPPF(ETA)4 overnight, and 4.5-6.5 h after illumination, they were stained with Annexin V-FITC and PI. As shown in Figure 4.5, the percentage of the Annexin positive cells slightly varied depending on the derivative. Kinetic studies showed that in an early stage after PDT treatment only a few cells were positive for either Annexin or PI. However, with time progression (4-6 h), a large portion of cells that were stained with Annexin (early apoptotic cells) later (>5 h) also became PI-positive (late apoptotic cells). Therefore, the total percentage of apoptotic cells is considered to be the sum of early apoptotic cells (B4) and late apoptotic cells (B2), that is, B2+B4. Photoactivation seems to be an ultimate requirement for the induction of apoptosis because control cells without illumination (Figure 4.5) did not show significant cell death. From these results it could be concluded that all of the derivatives induced apoptosis extensively at the selected concentrations.

To further confirm the apoptotic phenotype of HL60 and 4T1 cells, we examined another biochemical hallmark of apoptosis. The integrity of DNA that was isolated from the cells exposed to photosensitization was studied by gel electrophoresis. In both cell types that were exposed to mTPP(EG)4-, pTPP(EG)4-, pTPPF(EG)4-, pTPPF(DEG)-, and pTPPF(ETA)4-mediated PDT, pronounced DNA fragmentation was detectable within 3 to 4 h after illumination (Figure 4.6). In contrast, DNA of the control cells that were incubated with PS without illumination remained intact.

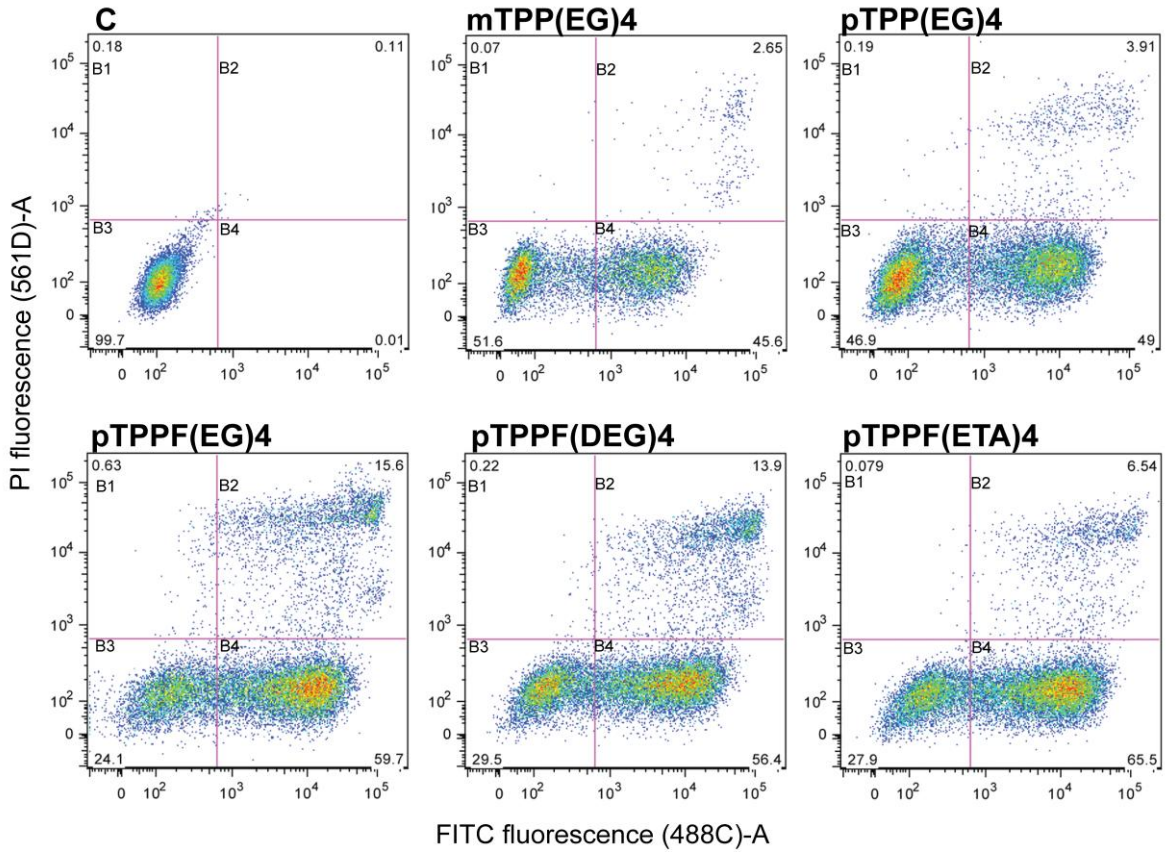

Figure 4.5 Apoptosis detection in HL60 cells by use of the Annexin V assay. Cells were treated with glycol porphyrin derivatives mTPP(EG)4 (180) nM), pTPP(EG)4 (3 μM), pTPPF(EG)4 (300 nM), pTPPF(DEG)4 (6.5 μM), and pTPPF(ETA)4 (2.2 μM) overnight and illuminated with 500-520 nm light (2.5 J/cm^2, 0.7 mW/ cm^2). Following incubation in the dark (mTPP(EG)4 for 4.5; pTPP(EG)4 for 6.5; and pTPPF(EG)4, 8, and 9 for 5.5 h), cells were stained with Annexin V and propidium iodide (PI) and analyzed by flow cytometry. The total percentage of apoptotic cells is the sum of early apoptotic cells that were positive for Annexin V-FITC (B4) and late apoptotic cells that were stained with Annexin and PI (B2). Control cells (C) were treated with porphyrin without illumination.

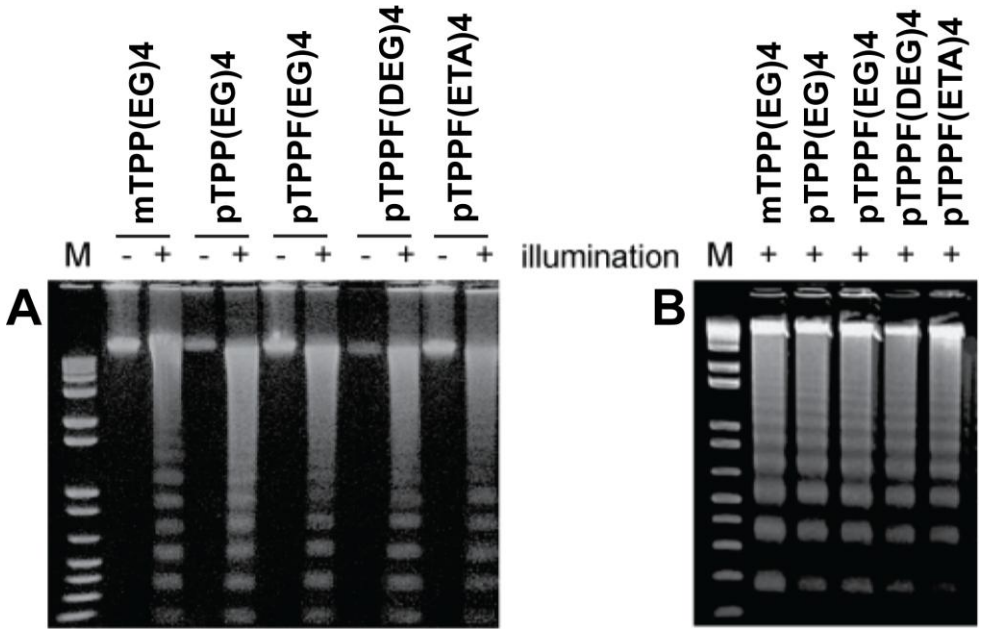

Figure 4.6 DNA fragmentation in 4T1 (A) and HL60 cells (B) that were exposed to PDT with glycol porphyrin derivatives. Cells were treated with mTPP(EG)4 (300-350 nM), pTPP(EG)4 (3-4 μM), pTPPF(EG)4 (500-600 nM), pTPPF(DEG)4 (5-6 μM), and pTPPF(ETA)4 (2-2.5 μM) for 16 h, illuminated (2.5 J/cm^2), and subsequently cultured in fresh medium for 3 to 4 h. In control cells, the illumination step was omitted (-). After harvesting, the DNA fragmentation was analyzed by 1.5% agarose gel electrophoresis. M is the DNA marker.

4.5 Effects of EG-porphyrin derivatives-mediated PDT on tumor growth *in vivo*

The anticancer effects of PDT are thought to occur at two different levels: (1) direct lethal effects on tumor cells and (2) vascular impairment that limits blood supply to the region (22).

Derivatives mTPP(EG)4, pTPP(EG)4, pTPPF(EG)4, mTPP(EG)1, mTPP(EG)2 and mTPP(EG)3 were selected for *in vivo* analysis to define their PDT effectiveness. Here we present results for the 2- or 6- day interval in which the maximal tumor growth reduction was recorded (Figure 4.7). Animals that were treated with para derivatives pTPP(EG)4, pTPPF(EG)4 (Figure 4.7A) and meta derivative with one EG chain mTPP(EG)1 (Figure 4.7B) exhibited only transient tumor regression, and from day 10, primary tumors started to regrow gradually. Tumor relapse likely originated from a small population of tumor cells that survived PDT. Only in mice that were treated with meta derivatives of porphyrins with two and more EG chains (mTPP(EG)2, mTPP(EG)3 and mTPP(EG)4), all tumors were completely eliminated with no

detectable relapse of primary tumor (Figure 4.7). This result confirms the superior PDT efficacy of meta derivatives with two, three and four EG chains.

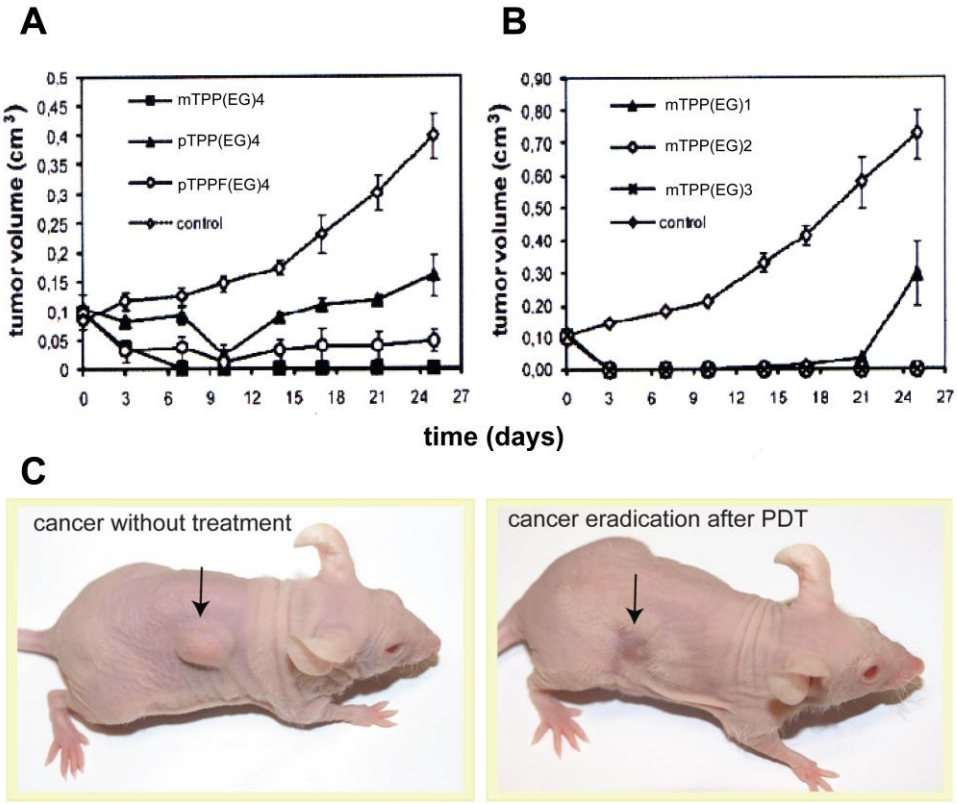

Figure 4.7 Effects of glycol-porphyrin-mediated PDT on tumor growth. Nude mice (NuNu) bearing subcutaneously growing human breast carcinoma MDA-MB-231 (*n*) 5 per each group) received an iv. dose of the drug (3 mg/kg), and after 2 h for mTPP(EG)4, pTPP(EG)4, pTPPF(EG)4, mTPP(EG)1, mTPP(EG)2 and 6 h for mTPP(EG)3, tumor areas were illuminated with light (100 J/cm^2). After one week, the PDT treatment was repeated. The control group consisted of mice that were exposed to illumination without PS application. The tumor size was measured repeatedly and the tumor volume was determined. Graphs summarize the results from two different experiments.

4.6 EG-porphyrin derivatives interact with sialic acid

The high effectiveness of glycol porphyrin derivatives toward cancer cells led us to speculate that one of the key properties of these compounds might be the preferential association with biomolecules that are characteristic of cancer cells. We selected sialic acid as a well known example of a tumor marker that is localized on the cell surface, and we examined the selectivity of its binding with mTPP(EG)4, pTPP(EG)4 and pTPPF(EG)4. A strong interaction for mTPP(EG)4, pTPP(EG)4 and pTPPF(EG)4 was demonstrated by titration experiments. The interaction of sialic acid and representative

porphyrin derivative pTPPF(EG)4 is described in Figure 4.8. The calculated binding constant pKa (for 2:1 complex) is 7.4, 8.2, and 10.1 for mTPP(EG)4, pTPP(EG)4 and pTPPF(EG)4, respectively. Such strong interaction with sialic acid might have some biological relevance by playing a role in cancer-cell recognition. This ability, together with the induction of apoptosis, suggests that a proper design of chemical structure (choice of substituents and their positions) might result in tailored substances that are able to target a specific cell type (cancer cells, in particular). The strong interaction of EG-porphyrin derivatives with the tumor marker (sialic acid) indicates the preferential association of these compounds with tumor cells.

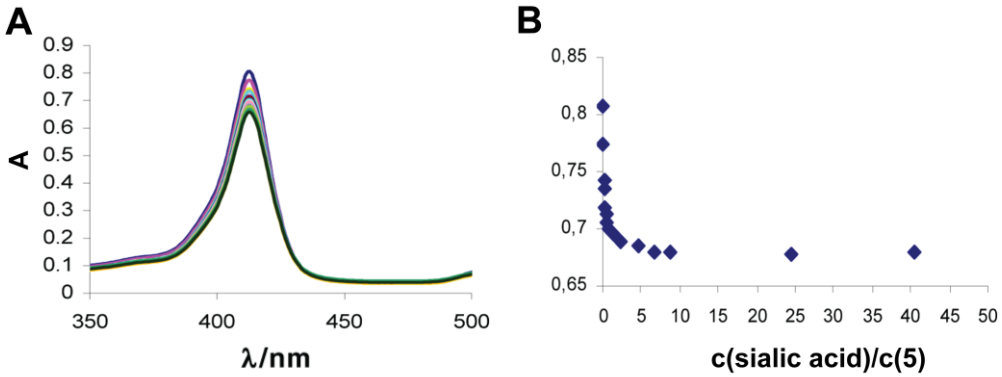

Figure 4.8 EG-porphyrin derivatives interact with tumor marker – sialic acid.
(A) Absorbance changes during the titration of pTPPF(EG)4 (c =2 × 10^{-6} mol/L) with sialic acid at pH 5.5 (0.01 M phosphate buffer) in the presence of 15% PEG 400.
(B) Titration curve of pTPPF(EG)4 with sialic acid at the maximum of absorbance (413 nm). Calculated pKas are 10.1. Stoichiometry of the complex (sialic acid/pTPPF(EG)4) is 2:1.

4.7 ROS as primary triggers of cell death signals in EG-porphyrin-mediated cell death

In numerous PDT studies it has been demonstrated that generation of ROS is responsible for the initiation of cell death. To analyze the contribution of particular oxygen species we implemented various scavengers and antioxidants and monitored their impact on EG-porphyrin-mediated cell death. HL60 and 4T1 cells loaded with EG-porphyrins were pre-incubated for 1 h with singlet oxygen and ROS scavengers and then exposed to light. The cell viability evaluated next day was dependent on the used porphyrin derivative, scavenger, and partly on the cell type. Generally, in both cell types

the most dramatic reduction of the cell death was caused by singlet oxygen ($^1O_2$) quencher L-histidine, by trolox and by NAC, known as radical scavengers and antioxidants (Figure 4.9). Tiron, claimed to be a superoxide anion ($^{\bullet}O_2^-$) scavenger, was effective mainly in the context of mTPP(EG)4 in HL60 cells, and DMSO as hydroxyl radical ($^{\bullet}OH$) scavenger was moderately effective and reached a significant level only in the case of pTPP(EG)4. PEG-catalase and sodium pyruvate as hydrogen peroxide (H_2O_2) scavengers slightly attenuated the demise of cells treated with para derivatives, but not with the meta derivative. To dissect the role of ROS species triggering apoptotic cell death, we used a 3'-p-(aminophenyl) fluorescein (APF) probe, which was successfully used to monitor the formation of both $^1O_2$ and $^{\bullet}OH$ in L1210 cells subjected to benzoporphyrin-mediated PDT according to Price et al. (102). APF, unlike 2',7'-dichlorodihydrofluorescein, was found resistant to light-induced autoxidation, and it is therefore more appropriate for monitoring formation of both ROS in the context of PDT (111). Cells loaded with EG-porphyrins were incubated with the APF probe as described in Materials and Methods in the presence or absence of L-histidine or DMSO. Immediately after incubation the cells were exposed to UV light for 10 s and pictures of APF fluorescence activated by ROS were collected by a camera under identical settings using an x10 objective (Figure 4.10). Control cells without porphyrins, when incubated with the APF probe after UV exposure, did not show any fluorescence (data not shown). L-histidine treatment in accordance with phototoxicity data dramatically reduced APF fluorescence and reflects the major role of $^1O_2$ formation in all three EG porphyrin derivatives. According to Price (102), the portion of the fluorescence quenched by DMSO represents the contribution of $^{\bullet}OH$. The significant reduction of toxicity and APF fluorescence in the case of pTPP(EG)4 photooxidation therefore indicated important participation of $^{\bullet}OH$.

The photogenerated singlet oxygen has a short lifetime and a limited diffusion path in biological systems, indicating that primary molecular targets of the photodynamic process must reside within a few nanometers of the photosensitizer. As shown in Figures 4.3 and 4.4, para derivatives preferentially accumulate in the lysosomes and the meta derivative localizes in ER; hence the immediate generation of ROS should occur in the lysosomes and ER, respectively. We therefore used the APF probe to monitor the ROS generation induced by exposure to UV light as described above. APF and porphyrin fluorescence was visualized under a fluorescence microscope using an x63

objective. As shown in Figure 4.11, APF fluorescence was generated rapidly within seconds after UV light exposure and mostly overlapped with porphyrin location. Thus, the immediate ROS generation corresponds to primary porphyrin compartmentalization.

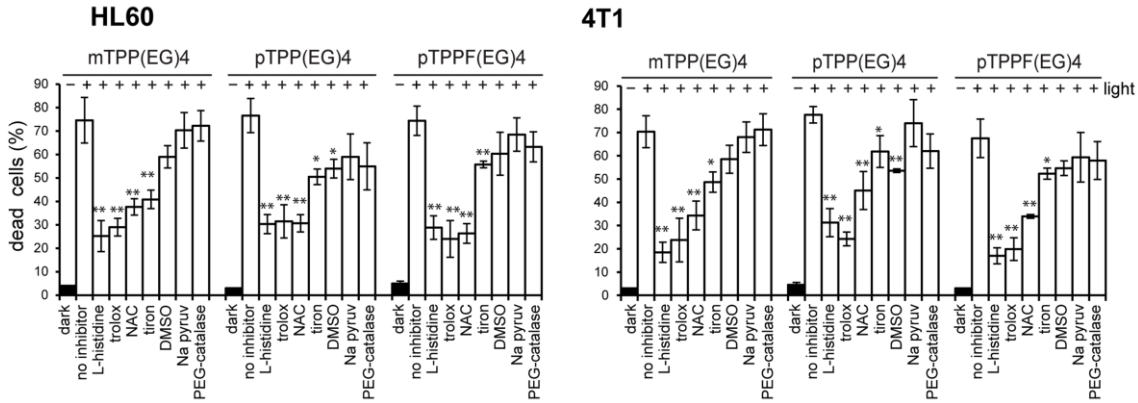

Figure 4.9 Effect of ROS scavengers on cell viability after PDT. 4T1 cells were loaded with EG-porphyrin derivatives for 16 h, washed and then pre-incubated for 1 h with L-histidine (20 mM), trolox (5 mM), NAC (15 mM), tiron (10 mM), DMSO (1%), PEG-catalase (300 U/ml) and sodium pyruvate (Na pyruv) (10 mM) before light exposure. Similarly, HL60 cells were pre-incubated with L-histidine (20 mM), trolox (4 mM), NAC (5 mM), tiron (10 mM), DMSO (1%), PEG-catalase (300 U/ml) and sodium pyruvate (Na pyruv) (10 mM). After irradiation the cells were further cultivated and cell viability was determined 24 h post-PDT by the trypan blue exclusion method. Cells treated with EG-porphyrin derivatives without irradiation were used as controls (dark). The percentage of dead cells was expressed as the mean ± SD (n=3). *P<0.050, ** P<0.01 represents statistical differences between PDT-treated cells vs. PDT-treated cells in the presence of L-histidine, trolox, NAC, tiron and DMSO.

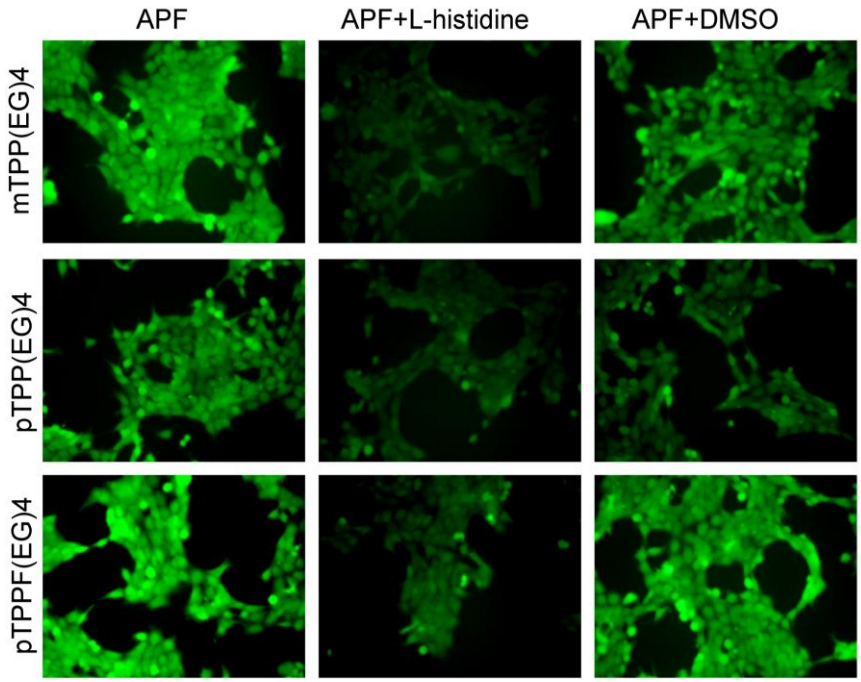

Figure 4.10 ROS detection. 4T1 cells incubated with EG-porphyrin derivatives were washed and loaded with 10 μM APF(3′-(p-aminophenyl) fluorescein) in the presence or absence of L-histidine (20 mM) or DMSO (1%) for 30 min. Dye-loaded cells were then stimulated with UV light for 10 s under a DM IRB microscope (Leica) and fluorescence images were acquired immediately using an x10 objective.

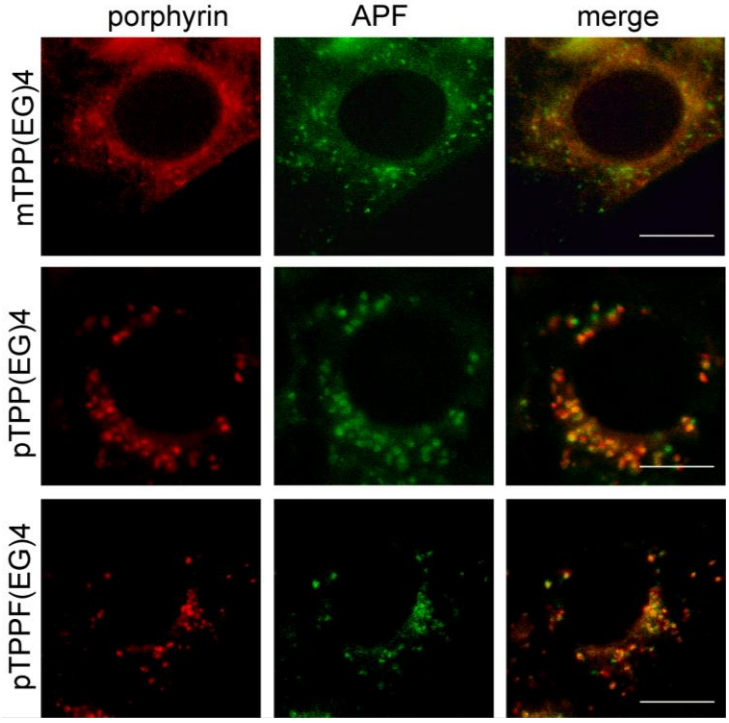

Figure 4.11 *In situ* detection of ROS generation. 4T1 cells grown on coverslips were sequentially loaded with porphyrin derivatives and APF probe. After 30 min incubation with the APF probe cells were exposed to UV light for 10 s and fluorescence images were acquired immediately using an x63 objective. Fluorescent images of EG-porphyrin derivatives (left panels), APF probe (middle panels) and their overlay (right panels). Scale bars: 10 μm.

4.8 MAP kinases (MAPK) and their role in EG-porphyrin-mediated apoptosis

Apoptosis is characterized as an ordered process in which multiple events take place including post-translation modifications of key regulatory molecules such as protein kinases, Bcl-2 family members, and caspases. To investigate the intracellular signaling events that are set in motion in cells photosensitized with various glycol porphyrin derivatives, we analyzed the protein profile of several important players by Western blot analysis (Figure 4.12).

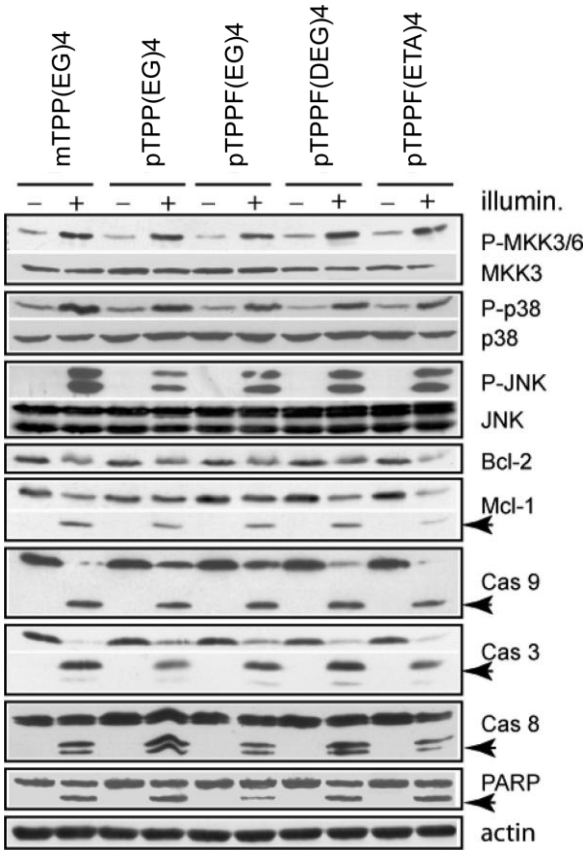

Figure 4.12 Induction of apoptosis in HL60 cells by glycol porphyrin derivatives demonstrated by the activation of MAP kinases, caspases, and changes in the Bcl-2 family. Cells that were treated with derivatives were exposed to light (2.5 J/cm^2) (+), and they were harvested 2 h post-PDT. Whole cell lysates were analyzed by Western blot analysis. Control samples that run in parallel represent lysates from cells in which the illumination step was omitted (-). The kinase activity was determined by phospho-specific antibodies (P-) that were used at first (upper panel), and then the membrane was reprobed with antibodies to total MAPK (lower panel). The activated forms of caspases, cleaved Mcl-1 and PARP proteins, are labeled by arrows. Equal protein loading is demonstrated by actin reprobing.

We wanted to find out whether there is a correlation among the chemical structures of the PSs, their intracellular localization and the activation of signaling pathways following light exposure. As shown in Figure 4.12, in spite of the differences in the structure of glycol-porphyrin derivatives and their PDT efficacy (Table 4.1), very similar pathways leading to apoptosis were activated (Figure 4.12). The activation of the p38 MAP kinase pathway, including that of upstream kinases MKK3/6, which was demonstrated by their phosphorylation (P-MKK3/6, P-p38), was found to be much higher in the cells that were exposed to photosensitization than in nonilluminated controls. Surprisingly, in cells that underwent photoinduced apoptosis, the levels of antiapoptotic Bcl-2 and Mcl-1 proteins were reduced, and caspases-3, -8, and -9 were activated (which was demonstrated by their proteolytic cleavage, indicated by an arrow), including cleavage of the caspase-3 target, PARP. Although mTPP(EG)4 localized mostly in the endoplasmic reticulum, similar molecular events were activated as in the case of predominantly lysosomally localized pTPP(EG)4, pTPPF(EG)4, pTPPF(DEG)4, and pTPPF(ETA)4. It is generally accepted that there is a strong correlation between the cell-death mechanism and primary photodamage sites, which are determined by the intracellular localization of the PS (26).

The importance of the p38 MAP kinase signaling mechanism for the induction of apoptosis in various tumor cell lines by pTPPF(EG)4 was described in recent publication coming from our laboratory (69). Therefore, the next step was to examine whether MAPK activation is required for the apoptotic process mediated by mTPP(EG)4 and pTPP(EG)4 as well. For this purpose, we used pharmacological JNK kinase inhibitor (SP600125) and p38-specific inhibitor (PD169316). For comparison we included the previously studied pTPPF(EG)4. The inhibition of JNK and p38 activity by these compounds in HL60 and 4T1 cells was verified by Western blot analysis showing reduction of p38 phosphorylation (P-p38) and c-Jun phosphorylation (P-c-Jun, the target of JNK kinase) following treatment (Figures 4.13A and 4.13B-lower panels). Importantly, the inhibition of JNK kinase did not influence EG-porphyrin-mediated cell death, thereby excluding JNK involvement in this process. On the other hand, the effects of p38 pharmacological inhibitor (PD169316) had a different impact on the demise of cells treated with various EG-porphyrin derivatives. The inhibition of p38 kinase activation resulted in reduction of apoptotic cell death induced by both para

derivatives (pTPP(EG)4, pTPPF(EG)4), but no effect was observed for meta derivative mTPP(EG)4 (Figures 4.13A and 4.13B - upper panels).

To confirm the necessity of p38 MAPK activation for the onset of apoptosis, MEFs with inactivated *p38α* -/- (KO) gene were implemented in PDT experiments (Adams, Porras et al. 2000). Primarily, it was shown that MEFs-KO exposed to para derivative pTPPF(EG)4)-mediated PDT did not die by apoptosis. The cells remained mostly attached to the dish and displayed normal morphology and much lower induction of cell death (69). Therefore, we examined the effect of pTPP(EG)4 and mTPP(EG)4 porphyrin derivatives using the same experimental model. Consistently, MEFs KO cells were remarkably resistant to pTPP(EG)4-mediated PDT (Figure 4.13C). In contrast, no obvious decrease of cell mortality was observed employing the meta derivative (Figure 4.13C). These results confirm that p38 MAPK activation plays a substantial role in the induction of apoptosis for both pTPP(EG)4 and pTPPF(EG)4 derivatives localized to lysosomes, but not for ER-localized mTPP(EG)4.

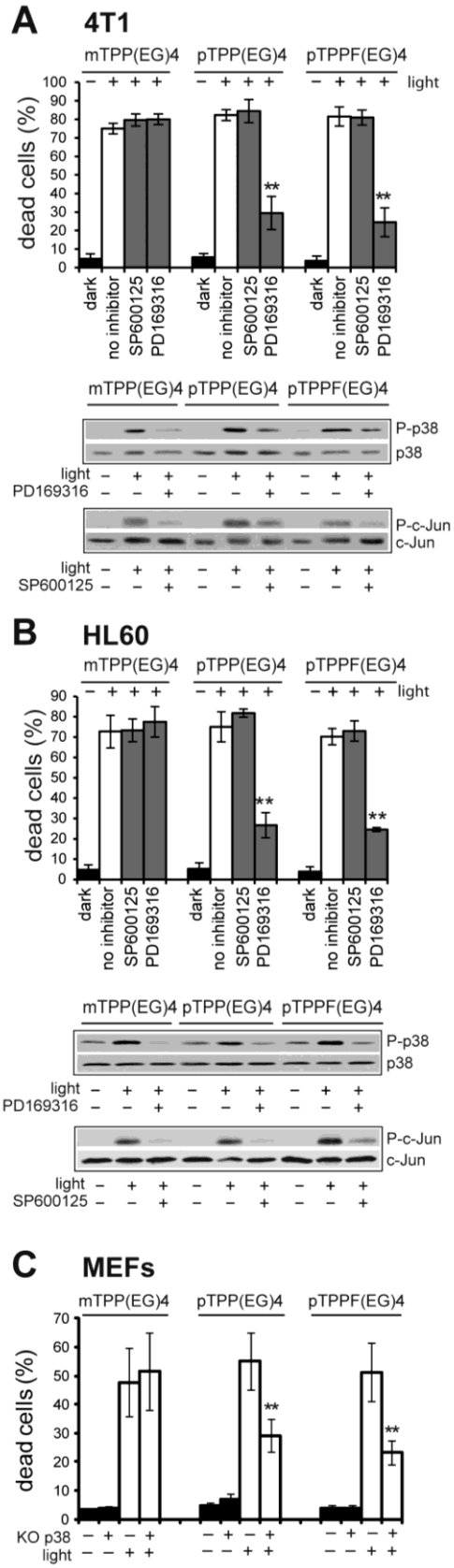
A
4T1
mTPP(EG)4
pTPP(EG)4
pTPPF(EG)4
light
dead cells (%)
dark
no inhibitor
SP600125
PD169316
**
P-p38
p38
PD169316
P-c-Jun
c-Jun
SP600125
B
HL60
C
MEFs
KO p38

Figure 4.13 Effect of kinase inhibitors on EG-porphyrin-mediated phototoxicity in 4T1 and HL60 cells. 4T1 cells (**A**) or HL60 cells (**B**) were loaded with EG-porphyrin derivatives for 16 h, washed and then preincubated for 1 h with JNKII inhibitor (5 μM) and PD169316 (10-20 μM) before light exposure. After irradiation the cells were further cultivated and cell viability was determined 24 h post-PDT by the trypan blue exclusion method. Cells treated with EG-porphyrin derivatives without irradiation were used as controls (dark). The percentage of dead cells was expressed as the mean ± SD (n=4) ** P<0.01 represents statistical differences between PDT-treated cells vs. PDT-treated cells in the presence of JNKII or PD169316.
For Western blot analysis cells were preincubated for 1 h with JNKII inhibitor (SP600125) or p38 inhibitor (PD169316) and 2 h post-irradiation analyzed with specific antibodies recognizing the phosphorylated forms of p38 and c-Jun by Western blot (P-p38 and P-c-Jun, respectively). Equal loading is demonstrated by total c-Jun and p38 protein.
(**C**) Effect of p38 deletion on apoptotic cell death. Mouse embryo fibroblasts (MEFs) with intact (wt) and inactivated *p38*α−/− (KO) gene were exposed to EG-porphyrin-mediated PDT. Cell viability was evaluated 24 h post-PDT by the trypan blue exclusion method. **P<0.01 represents statistical differences between wt MEF vs. KO MEF exposed to PDT.

4.9 Photoactivation of EG-porphyrin derivatives induces various levels of ER stress implementing Ca^{2+}

mTPP(EG)4 photo-induced apoptosis seems to be ruled by some other mechanism(s) than that induced by the para derivatives. In order to find out the responsible signaling pathways we focused on ER, the main store of Ca^{2+}, where mTPP(EG)4 is prevalently localized. The impact of changes in Ca^{2+} homeostasis on the cell death was evaluated. Firstly, cytosolic Ca^{2+} levels in cells loaded with EG-porphyrin derivatives were monitored by flow cytometry using fluorescent Ca^{2+} indicator Fluo-4-AM. A major rise of (Ca^{2+})cyt was observed within one minute after the cells were exposed to the laser beam. Our experiments indicate that the cytosolic levels of Ca^{2+} are increased in the presence mTPP(EG)4 and to a lower extent in the presence of pTPP(EG)4 or pTPPF(EG)4 (Figure 4.14).

When the cells were pre-treated with a calcium-inhibiting agent, BAPTA-AM (Molecular Probes), which diminishes intracellular Ca^{2+} concentration, Fluo-4 signal was completely abrogated in HL60 cells loaded with all three porphyrin derivatives (Figure 4.15). A similar inhibitory effect was observed when the cells were pre-treated with $^1O_2$ scavenger L-histidine (Figure 4.15). This observation proves that ROS generation is a primary event leading to a (Ca^{2+})cyt rise. Moreover, cells pre-loaded with membrane-permeable intracellular Ca^{2+} chelator BAPTA-AM exhibited a significantly reduced level of mTPP(EG)4-mediated apoptosis (Figure 4.16). Thus, the phototoxicity of mTPP(EG)4 is at least partly dependent on the rise of (Ca^{2+})cyt in 4T1 and HL60 cells, but other cell death mechanism(s) not mediated by Ca^{2+} may also be

implicated. In contrast, pTPP(EG)4- and pTPPF(EG)4-induced cell death was not affected by BAPTA-AM preincubation. It indicates that ER stress demonstrated by a moderate (Ca^{2+})cyt efflux in para derivatives does not play a critical role in the initiation of apoptosis. Cell death is mediated by another mechanism allowing full development of apoptosis in the presence of BAPTA. Furthermore, we were not able to detect any contribution of extracellular Ca^{2+} influxes on the phototoxicity of either meta or para porphyrin derivatives using calcium-free medium or pretreatment with extracellular chelator EDTA (Figure 4.17).

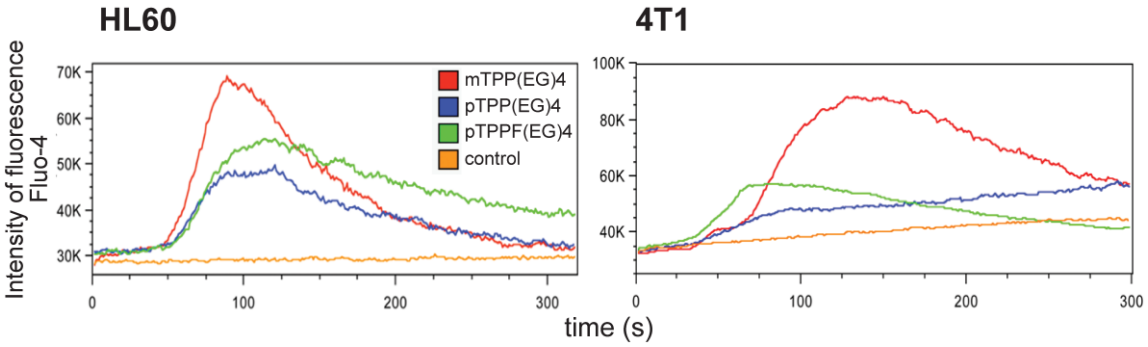

Figure 4.14 Intracellular calcium levels in HL60 and 4T1 cells. The effect of EG-porphyrin derivatives on cytosolic Ca^{2+} levels was monitored by flow cytometry of laser-illuminated cells containing fluorescent Ca^{2+} indicator Fluo-4-AM (4 μM) (Molecular Probes). Cells treated in the same way but without porphyrin were used as controls.

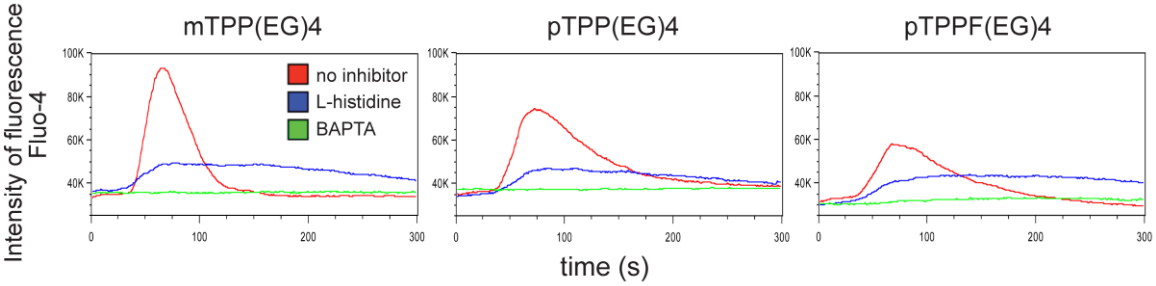

Figure 4.15 Effect of BAPTA and L-histidine on the intracellular Ca^{2+} level. HL60 cells were loaded with EG-porphyrin derivatives for 16 h, washed and then preincubated for 1 h with ROS scavenger L-histidine (20 mM) or 2 h with calcium chelator BAPTA-AM (5 μM). The cytosolic Ca^{2+} level was monitored by flow cytometry using fluorescent Ca^{2+} indicator Fluo-4-AM (4 μM).

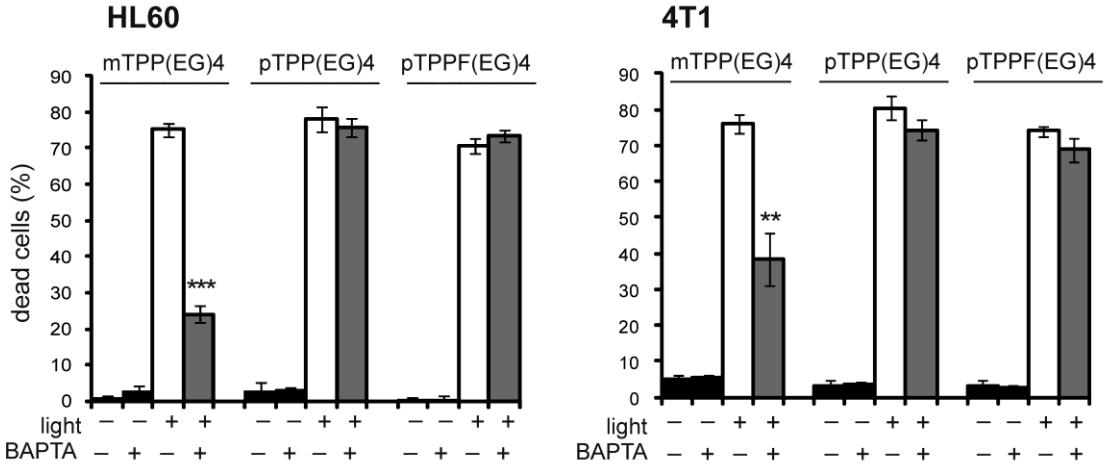

Figure 4.16 Effect of BAPTA-AM preincubation on photoinduced apoptosis. Cells loaded with EG-porphyrin derivatives were pre-incubated with the membrane-permeable intracellular Ca^{2+} chelator BAPTA-AM (5 μM HL60, 10 μM 4T1) for 2 h to inactivate the released Ca^{2+} and then irradiated with 2.5 J/cm^2 of light at 500±20 nm. This corresponds to an LD_{70} PDT dose. Cell viability was determined 24 h post-photodynamic therapy by the trypan blue exclusion method. The percentage of dead cells was expressed as the mean ± SD (n=4). **P<0.01, ***P<0.001 represents statistical differences between PDT-treated cells vs. PDT-treated cells in the presence of BAPTA-AM.

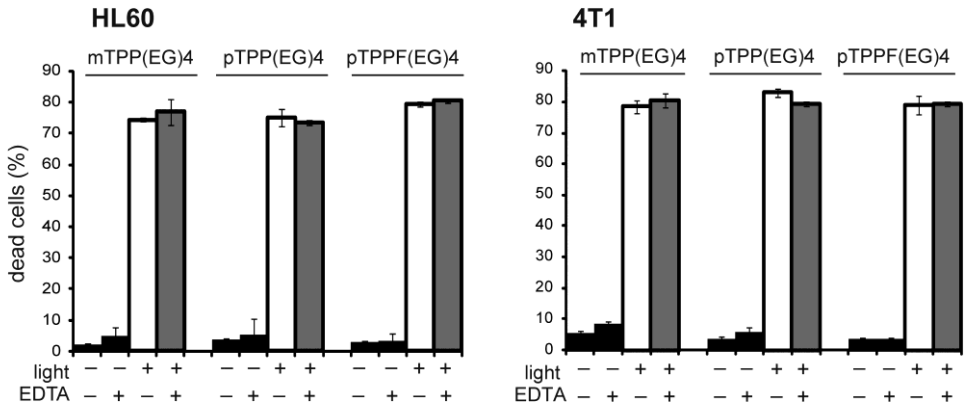

Figure 4.17 Effect of EDTA preincubation on photoinduced apoptosis. Cells loaded with EG-porphyrin derivatives were preincubated with the extracellular Ca^{2+} chelator EDTA (100 μM) for 2 h and then irradiated with 2.5 J/cm^2 of light at 500±20 nm. This corresponds to an LD_{70} PDT dose. Cell viability was determined 24 h post-photodynamic therapy by the trypan blue exclusion method. The percentage of dead cells was expressed as the mean ± SD (n=4).

4.10 Efflux of Ca^{2+} from stressed-ER and uptake of the released Ca^{2+} by mitochondria

Efflux of Ca^{2+} from the stressed ER and uptake of the released Ca^{2+} by mitochondria have been reported to activate/potentiate the intrinsic apoptotic pathway (75). Therefore, we examined the effect of blocking mitochondrial Ca^{2+} uptake by Ru360, a specific uniporter inhibitor of the mitochondrial Ca^{2+}. Data collected from these experiments displayed a reduced level of mTPP(EG)4-mediated phototoxicity (Figure 4.18A). Moreover, the cytosolic rise of cytochrome c induced by EG-porphyrin photoactivation was prevented by Ru360 pretreatment in mTPP(EG)4 but not in pTPP(EG)4- or pTPPF(EG)4-loaded cells (Figure 4.18B). Correspondingly, cytosolic reduction of the cytochrome c level was accompanied by its higher content in mitochondrial extract. In summary, our findings demonstrate that mTPP(EG)4-mediated apoptosis is inhibited either by calcium chelator BAPTA-AM or by mitochondrial uniporter inhibitor Ru360.

Hence, the flux of ER-derived Ca^{2+} into the mitochondria is likely involved in the initiation and development of apoptosis in the mTPP(EG)4 PDT model.

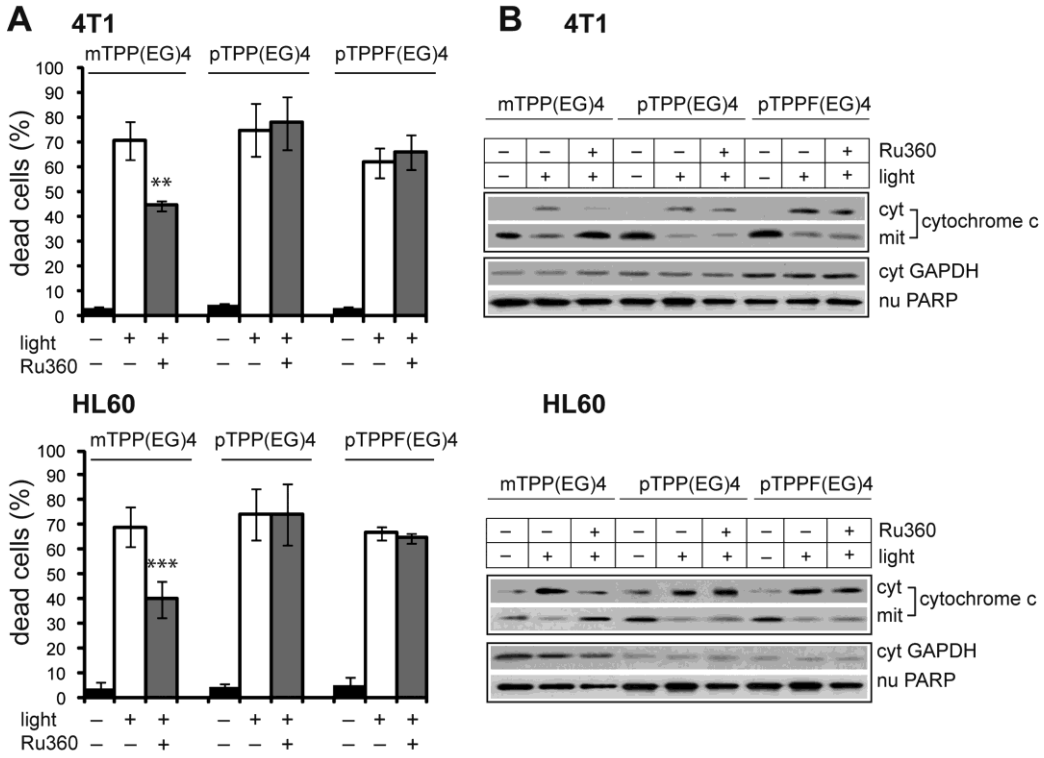

Figure 4.18 Effect of Ru360.
(**A**) Cells loaded with EG-porphyrin derivatives were pre-treated with Ru360 (5 μM 4T1, 4 μM HL60) for 1 h to inhibit Ca^{2+} mitochondrial uptake. After irradiation the cells were further incubated in medium and their viability was determined 24 h later by the trypan blue exclusion method. The percentage of dead cells was expressed as the mean ± SD (n=3-6). **P<0.01, ***P<0.001 represents statistical differences between PDT-treated cells vs. PDT-treated cells in the presence of Ru360.
(**B**) Cells were preincubated for 1 h with Ru360 (4-5 μM), and 2 h post-irradiation the cytosolic, mitochondrial and nuclear extracts were prepared and analyzed by Western blotting with specific antibody recognizing cytochrome c, GAPDH and PARP. Results are representatives of at least three experiments.

4.11 The effect of EG-porphyrin derivatives on the activation of calpain and relevant caspases

Next, we determined the effect of EG-porphyrins on the activation of calpain and relevant caspases. The activation of calpain was monitored by cleavage of fodrin (Figure 4.19), a marker of calpain action (20). Fodrin is known to be cleaved by both calpains and caspase-3, resulting in a calpain-specific 150 kD fragment and a 120 kD fragment generated by caspase-3. In 4T1 cells subjected to mTPP(EG)4-PDT, fodrin cleavage appeared 0.5 h post irradiation and correlated with caspase-12 activation (Figure 4.19, top panels). In contrast, lower activation with delayed kinetics of fodrin and caspase-12 was determined in cultures treated with para derivatives. Similar results

with slightly delayed kinetics were obtained in human cells (HL60) when tested for caspase-4, human homolog of caspase-12 (Fig. 4.19, lower panels).

In addition, EG-porphyrin-induced activation of fodrin, caspase-9 and caspase-3 was attenuated by BAPTA-AM pre-treatment in the case of meta but not of para derivatives (Figure 4.20).

Further, we tested the influence of calpain inhibitor PD150606 on the viability of 4T1 and HL60 cells exposed to PDT. Pre-treatment with calpain inhibitor reduced mTPP(EG)4-mediated phototoxicity, thereby bringing an additional proof for the engagement of the Ca^{2+} pathway in the mechanism of cell death (Figure 4.21).

We also investigated the effect of calpain inhibitor PD150606, ROS scavengers (L-histidine and trolox) and caspase inhibitor Z-VAD-FMK on the fodrin cleavage and phototoxicity in parallel experiments. ROS inhibitors suppressed fodrin cleavage and phototoxicity of all three photosensitizers. In contrast, calpain inhibitor reduced fodrin cleavage in all of them but attenuated cell death only for the meta derivative, by 21%. The caspase inhibitor reduced the level of caspase-specific 120 kD fodrin fragment and attenuated PDT-induced cell death mediated by both meta and para derivatives (Figure 4.22).

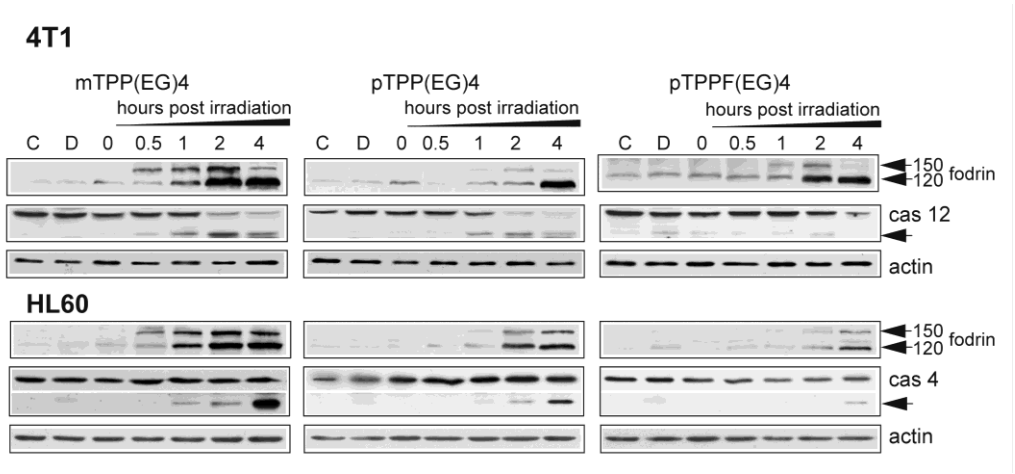

Figure 4.19 Effect of EG-porphyrin derivatives on the Ca^{2+} signaling pathway.
Western blot analysis of fodrin, caspase-12 (4T1 cells) and caspase-4 (HL60 cells). Cells treated with EG-porphyrin derivatives were harvested at various times after irradiation and subjected to Western blot analysis with antibodies recognizing fodrin and caspase-12. Reprobing with β-actin antibody was used to confirm equal loading.

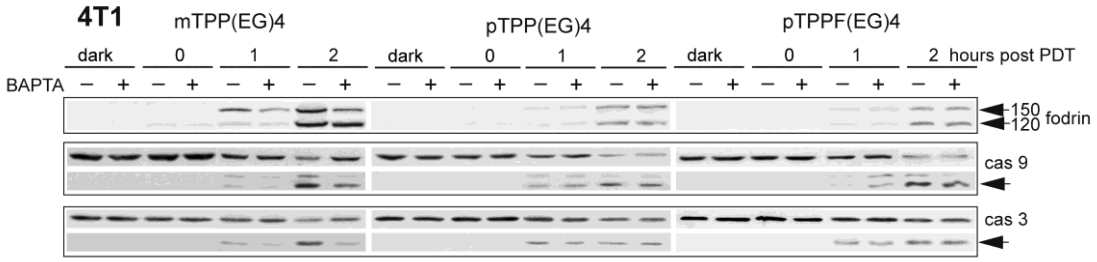

Figure 4.20 Effect of EG-porphyrin derivatives on the Ca^{2+} signaling pathway. Pretreatment of 4T1 cells with BAPTA-AM (10 μM) resulted in the inhibition of fodrin, caspase-9 and caspase-3 activation caused by mTPP(EG)4-PDT. 4T1 cells loaded with porphyrin derivatives were preincubated for 2 h with BAPTA-AM and then exposed to light (2.5 J/cm^2). At various time after irradiation the cells were lysed and analyzed with antibody recognizing fodrin, full-length and cleaved p39 form of caspase-9, and full-length and cleaved p17 form of caspase-3 on Western blots.

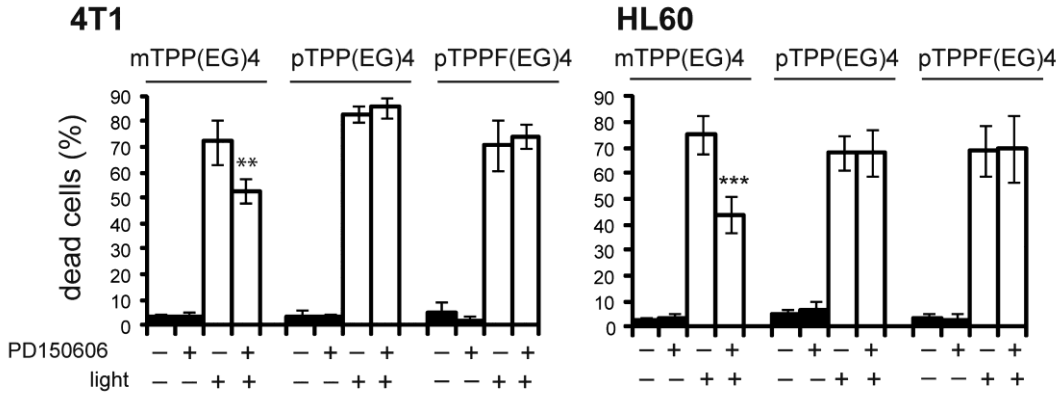

Figure 4.21 Effect of calpain inhibitor PD150606 on viability of 4T1 and HL60 cells. Cells were incubated with PD150606 (20 μM) for 1 h and then irradiated. Cell viability was estimated after 24 h by the trypan blue exclusion method. The percentage of dead cells was expressed as the mean ± SD (n=4-5). **P<0.01, ***P<0.001 represents statistical differences between PDT-treated cells vs. PDT-treated cells in the presence of PD150606.

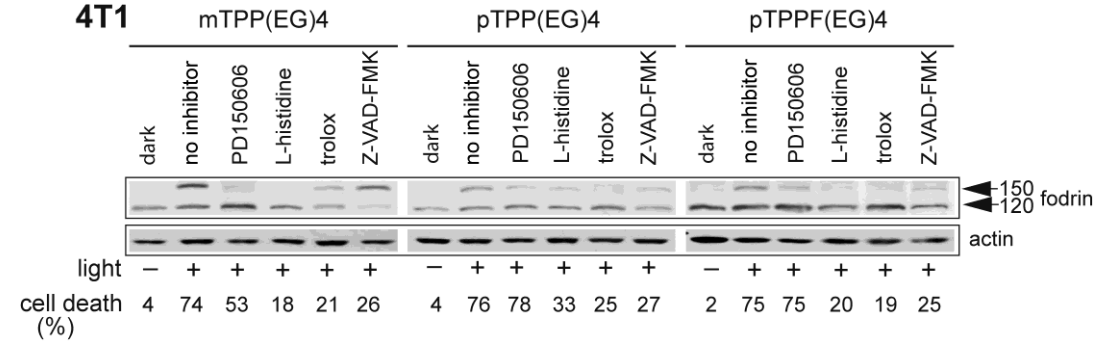

Figure 4.22 Effect of calpain inhibitor, ROS scavengers (L-histidine and trolox), and caspase inhibitor (Z-VAD-FMK) on the activation of fodrin. Cells were treated as described in Materials and Methods and analyzed by Western blot. Equal protein loading is demonstrated by actin reprobing. The viability of cells subjected to simultaneous treatment done in parallel is presented under the Western panel.

To elucidate the importance of the calpain activation in EG porphyrin-mediated phototoxicity, we knocked down the expression of Capn4 using specific siRNA.

Transfection of Capn4 siRNA, but not control siRNA (NC), decreased the level of endogenous Capn4/Capns1 protein and reduced fodrin cleavage (Figure 4.23A). Moreover, Capn4 siRNA significantly reduced the amount of dead cells in mTPP(EG)4-treated cells (Figure 4.23B). Despite that knockdown of Capn4 decreased fodrin cleavage also in para derivatives, no effect on cell viability was observed (Figure 4.23B). In summary, all these experiments confirm an important role of calpain activation in mTPP(EG)4- but not pTPP(EG)4- and pTPPF(EG)4-induced cell death.

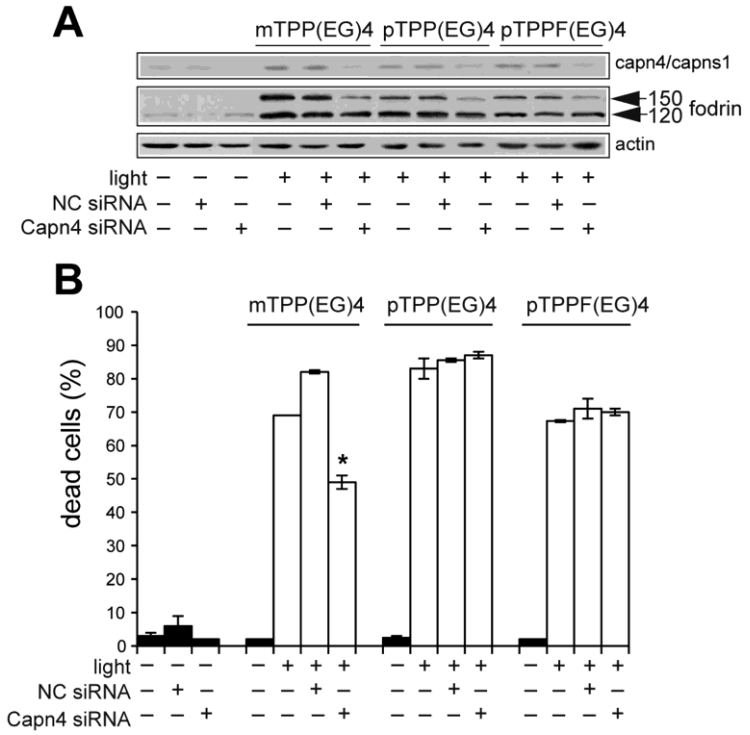

Figure 4.23 Effect of Capn4 siRNA on the demise of PDT-treated cells.
(**A**) Western blot analysis of fodrin in 4T1 cells after Capn4 siRNA transfection. Transfected cells were subjected to EG-porphyrin-mediated PDT, harvested and resolved by Western blot analysis. Equal protein loading is demonstrated by actin reprobing.
(**B**) Viability of cells transfected with Capn4 siRNA. Transfected and control cells were subjected to EG-porphyrin-mediated PDT and cell viability was monitored 24 h later. The percentage of dead cells was expressed as the mean ± SD (n=3). *P<0.05 represents the statistical difference between transfected PDT-treated cells vs. non-transfected or control siRNA-transfected PDT-treated cells.

4.12 mTPP(EG)4 localized in ER causes severe ER stress and subsequent activation of several UPR target genes

Any insult that disturbs ER homeostasis ultimately results in ER stress due to the accumulation of misfolded proteins (UPR response) (119). To analyze whether EG-porphyrins trigger UPR, we first assayed stress sensor PERK. The PERK pathway is activated through phosphorylation of PERK and of its substrate eIF2α. Indeed, immediately after irradiation (time 0) of mTPP(EG)4-loaded cells an evident increase of PERK phosphorylation and phosphorylation of its substrate eIF2α was observed. No such response was detected using para derivatives pTPP(EG)4 and pTPPF(EG)4 (Figure 4.24A). Accordingly, the expression of ATF4 and CHOP/GADD153 transcription factors was dramatically increased following irradiation (time 0 and 0.5, respectively). A similar pattern of the PERK pathway activation was detected in human HL60 cells (Figure 4.24A, lower panel). ATF4 and CHOP mRNA expression was markedly increased by mTPP(EG)4-PDT, but only modestly by pTPP(EG)4-PDT in both cell types (Figure 4.24B). This is in agreement with the results obtained at the protein level. The role of ER stress in mTPP(EG)4-mediated phototoxicity was further accentuated by experiments using salubrinal. Salubrinal inhibits eIF2α dephosphorylation and is known to protect cells from ER stress by reducing translational activity and lowering protein load (8). Accordingly, salubrinal significantly protected cells against mTPP(EG)4-mediated apoptosis (Figure 4.25).

In summary, our results indicate that the PERK signaling pathway plays a crucial role in the mTPP(EG)4-mediated apoptosis.

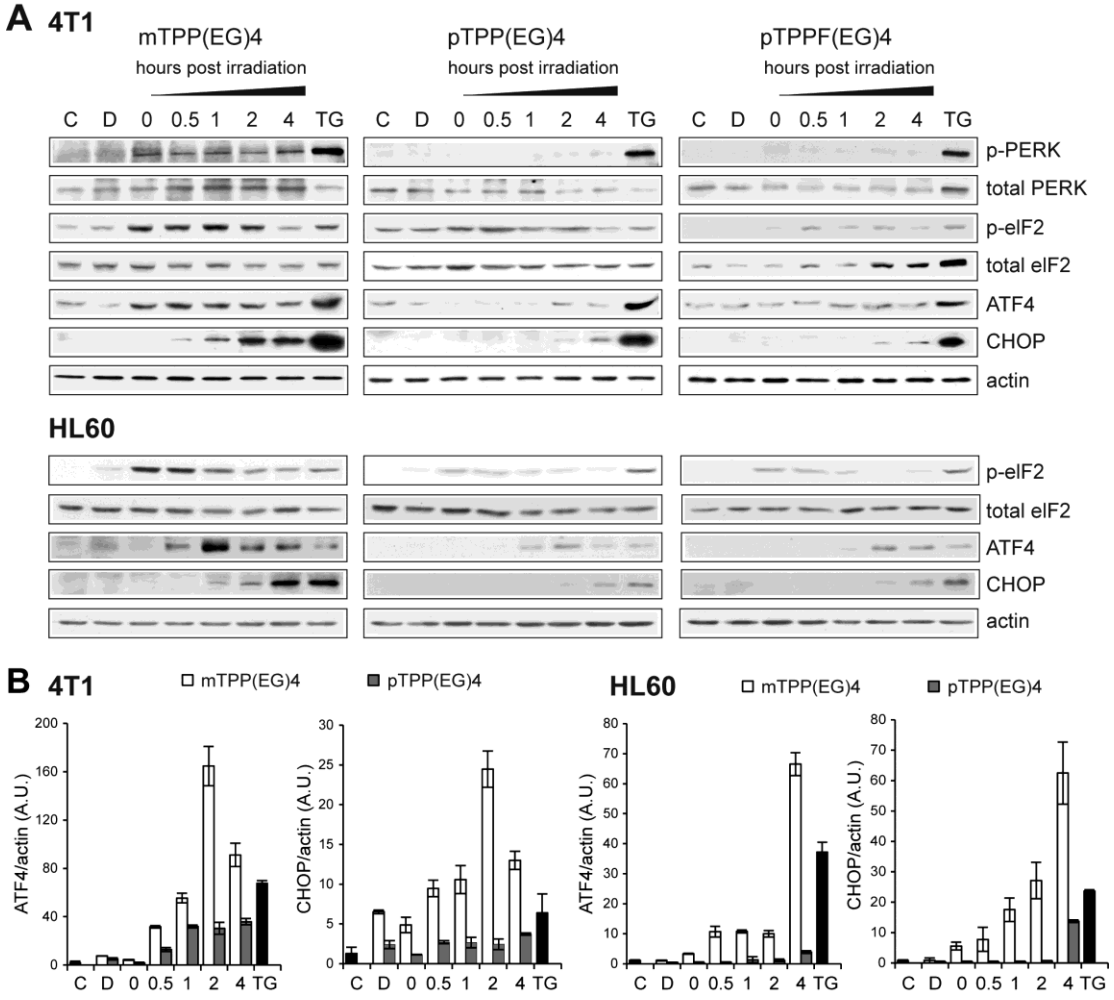

Figure 4.24 Kinetics of PERK pathway activation by EG-porphyrin-mediated PDT.
(**A**) Induction of ER stress proteins (P-PERK, P-eIF2α, ATF4, CHOP) detected by Western blot analysis. The activity of PERK and eIF2α was determined by phospho-specific antibodies (p-) and then the membranes were reprobed with antibodies to total PERK and eIF2α. Equal protein loading is demonstrated by actin reprobing. As a positive control we used cells treated with 1 μM thapsigargin (TG) for 6 h.
(**B**) qRT-PCR analysis of total mRNA isolated from PDT-treated 4T1 and HL60 cells. cDNA was prepared from total mRNA and quantitative real-time RT-PCR for ATF4, CHOP and β-actin mRNA was performed. mRNA fold induction values were calculated from ATF4/actin and CHOP/actin ratios as described in Materials and Methods. Experiments were performed in triplicate.

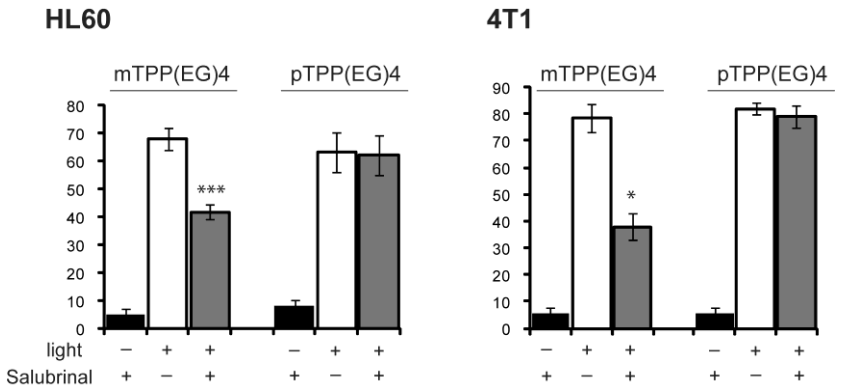

Figure 4.25 Salubrinal pretreatment increases cell viability after mTPP(EG)4-mediated PDT. HL60 and 4T1 cells were pretreated for 2 h with 10 and 20 μM salubrinal, respectively, or with DMSO. The numbers of apoptotic cells were determined by the trypan blue exclusion method 24 h post PDT. The percentage of apoptotic cells was expressed as the mean ± SD (n=3). *P<0.05, ***P<0.001 represents statistical differences between PDT-treated cells vs. PDT-treated cells in the presence of salubrinal.

4.13 PERK knockdown and deficiency partly protects against mTPP(EG)4-mediated apoptosis

To elucidate the role of the PERK pathway in ER stress evoked by EG-porphyrin PDT, we first knocked down the expression of PERK using specific siRNA. Transfection of PERK siRNA, but not control siRNA (NC), significantly reduced the amount of endogenous PERK protein (Figure 4.26A). Moreover, knockdown of PERK abolished induction of ATF4 and CHOP following mTPP(EG)4-PDT (Figure 4.26A). A consistent result was obtained using *in situ* immunostaining of CHOP (Figure 4.26C). Next we tested the influence of PERK silencing on the viability of 4T1 cells exposed to EG-porphyrin-mediated PDT. Figure 4.26B shows that PERK knockdown attenuated cell death induced by mTPP(EG)4, whereas it had no impact on the outcome of para derivatives (pTPP(EG)4 and pTPPF(EG)4) (Figure 4.26B).

Secondly, for PDT experiments we used MEFs with the intact (wt) and inactivated PERK -/- (KO) gene. The loss of PERK was verified by Western blot analysis (Figure 4.27A). Although the intracellular uptake of EG-porphyrin derivatives determined by porphyrin fluorescence was similar in both cell lines (Figure 4.27B), MEFs-KO were remarkably resistant to mTPP(EG)4-PDT. In contrast, no obvious decrease of cell mortality was observed employing para derivatives, thus indicating that PERK activation is not required for cell death mediated by para derivatives (Figure 4.27A).

In summary, both lines of evidences consistently demonstrate the significance of the PERK pathway in mTPP(EG)4-mediated cell death.

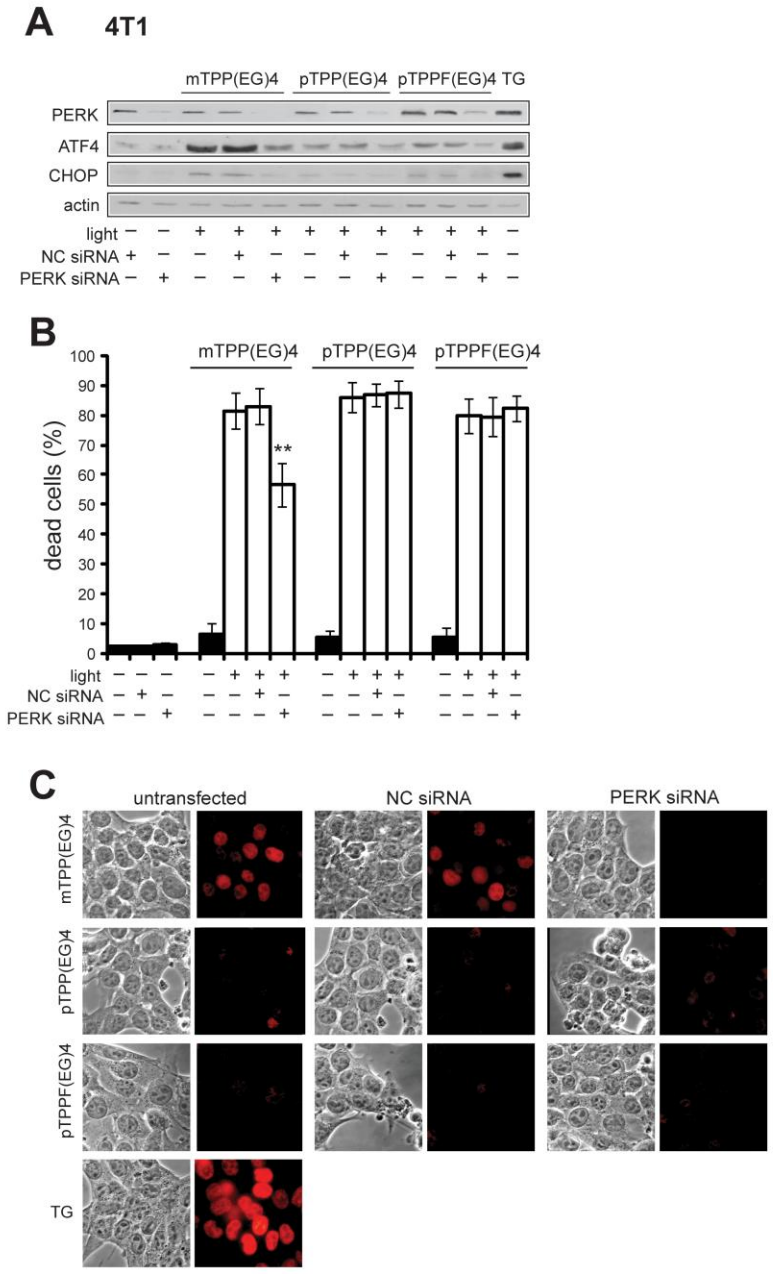

Figure 4.26 Effect of PERK siRNA on the demise of PDT-treated cells. PERK deficiency protects against mTPP(EG)4-mediated cell death.

(**A**) Western blot analysis of PERK, ATF4 and CHOP in 4T1 cells after PERK siRNA transfection. Transfected cells were subjected to EG-porphyrin-mediated PDT, harvested and resolved by Western blot analysis. Equal protein loading is demonstrated by actin reprobing. As a positive control we used cells treated with 1 μM thapsigargin (TG) for 6 h.

(**B**) Viability of cells transfected with PERK siRNA. Transfected and control cells were subjected to EG-porphyrin-mediated PDT and cell viability was monitored 24 h later. The percentage of dead cells was expressed as the mean ± SD (n=7-14). **P<0.01 represents the statistical difference between transfected PDT-treated cells vs. non-transfected or control siRNA-transfected PDT-treated cells.

(**C**) Immunostaining of CHOP after EG-porphyrin derivative-mediated PDT in PERK knockdown cells. Cells were fixed 2 h post PDT, immunostained and observed with a fluorescence microscope. The left panel includes untransfected cells, the middle panel cells transfected with control siRNA and the right panel cells transfected with PERK siRNA.

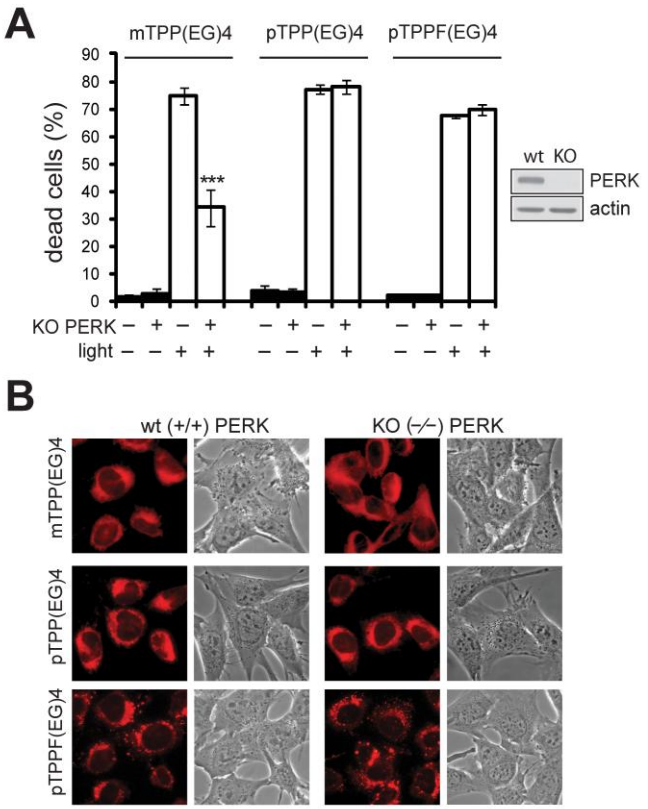

Figure 4.27 PERK deficiency protects against mTPP(EG)4-mediated cell death.
(**A**) Cell viability of MEF-wt and MEF-KO evaluated 24 h post-EG-porphyrin-PDT (350 nM mTPP(EG)4, 3.5 μM pTPP(EG)4, 700 nM pTPPF(EG)4). Verification of the PERK-/- phenotype in MEFs-KO cells by Western blot. The percentage of apoptotic cells was expressed as the mean ± SD (n=6). ***P<0.001 represents statistical differences between PDT-treated MEF-wt cells vs. PDT-treated MEF-KO cells.
(**B**) Fluorescence microscopy demonstrates similar cellular uptake of EG-porphyrin derivatives in MEFs-wt and MEF-KO (800 nM mTPP(EG)4, 5 μM pTPP(EG)4, and 2 μM pTPPF(EG)4).

5 DISCUSSION

The aim of this work was to dissect the molecular events associated with apoptotic cell death induced by photodynamic activation of a group of structurally very similar porphyrin derivatives. Extensive research over the past years demonstrated that photosensitizers used in PDT vary widely in their activity depending on their chemical structure. Differences were even found within a series of molecules with similar basic structural and physicochemical characteristics. It is generally accepted that peripheral substitutions play an important role in the biological availability and activity of the compound. Our results suggest that porphyrins with EG functionalities in the meta position displayed better PDT efficacy than their parent tetrahydroxyphenyl porphyrin mTHPP. The correlation between the cellular uptake of the porphyrins and their photobiological efficacy is evident. Generally, the porphyrins with rather high cell-penetration efficacy (mTPP(EG)4, pTPP(EG)4, pTPPF(EG)4, pTPPF(DEG)4 and pTPPF(ETA)4) displayed high phototoxic activity, whereas poorly penetrating porphyrins (mTPP(EGME)4, pTPP(EGME)4 and pTPPF(EGME)4) were inefficient. Lower photodynamic activities have also been reported for methoxysubstituted arylporphyrins with respect to hydroxyl derivatives (6) but the difference was not as striking as the one we found for glycol porphyrins.

We used porphyrin derivative substituted with EG chains in para-phenyl position that exhibited lower biological efficacy (11–13 fold) than the corresponding fluorinated analog (Table 4.1). The enhancement of the biological activity by fluorination indicates better molecular targeting caused by the presence of fluorine atoms on the phenyl ring leading to altered affinities for specific or nonspecific binding sites (68). Interestingly, in spite of the differences in biological activity, both derivatives target the same organelle (lysosomes) and their photoactivation results in the activation of the p38 MAP kinase cascade, which is critical for caspase-dependent mitochondrially driven apoptosis (Figure 4.13). In contrast, alteration of the glycol chain being in the meta-phenyl position resulted in a different intracellular localization. Such subtle changes in the structure of porphyrins resulting in different intracellular localization were also observed in the case of porphyrin with EG chain at para position (p-TPP(EG)4) localized mainly in the lysosomes, whereas porphyrin with EG chain at meta position (m-TPP(EG)4) was found in the endoplasmic reticulum (ER) (Figure 4.3). It is known

that subcellular localization of the drugs is one of the crucial parameters influencing the efficiency and extent of cell damage, as well as the cell response and the mechanism of the resultant cell death. Thus, position of glycol chains seems to modulate the localization pattern of derivatives inside the cells. Similar observations were made for different glycoconjugated porphyrins (44). Accordingly, this study brings evidence that photoexcitation of mTPP(EG)4 triggers proapoptotic signaling involving pathways different from those for the para derivatives.

Concerning the correlation between photobiological efficacy and cellular uptake, mTPP(EG)4 with symmetrical ethylene glycol substitutions in all four meta-phenyl positions was able to evoke IC50 in HL60 and 4T1 cells at 47- and 20-fold lower concentrations, respectively, than the corresponding derivative pTPP(EG)4 with glycol chains in the para position (Table 4.1). A similar impact of position on activity has been described for chlorins (6). Fluorinated para-substituted porphyrin pTPPF(EG)4 showed an increased biological efficacy in comparison with its unfluorinated analog pTPP(EG)4. Under the same experimental conditions we obtained data for ER-localized tetrahydroxyphenyl chlorine (mTHPC), an active compound of the marketed drug Foscan (110). Therefore, the overall photodynamic dose (drug x light dose) that is required to reach IC50 was about five times lower for meta-EG-functionalized porphyrin mTPP(EG)4 than for mTHPC (Table 4.1). This demonstrates superior potency of mTPP(EG)4. Furthermore, the ethylene glycol chain at the meta position exhibits a superior efficacy that leads to the permanent ablation of human breast carcinoma (MDA-MB-231) in nude mice (Figure 4.7) (68).

As already mentioned, an alteration of glycol chain being in the meta-phenyl position resulted in a different intracellular localization. Accordingly, this study brings evidence that proapoptotic signaling triggered by photoexcitation of mTPP(EG)4 involves different pathways than those induced by para derivatives. Nevertheless, some similarities such as immediate p38 and JNK MAPK activation were found. However, the inhibition of p38 activation via pharmacological inhibitors or gene deletion did not interfere with the cell death in contrast to para derivatives. Such observation indicates that p38 kinase does not play a significant role in mTPP(EG)4-mediated apoptosis (Figure 4.13). Results of other reports using various photosensitizers, clearly show that the role of p38 activation in PDT response is ambiguous. Initiation of apoptosis via activation of the stress-activated p38 MAPK signal pathway was reported for ALA

(137), Rose Bengal (147) and Pc4 (140). On the other hand, p38 phosphorylation has been shown to protect cells from Hypericin- and Zn-BC-AM-mediated PDT (5, 66) but had no influence on the Photofrin-PDT outcome (123). An adaptive mechanism against oxidative stress was attributed to p38 stress-activated kinase as its inhibition blocked autonomous regrowth and migration of cancer cells escaping PDT-induced cell death (12). Recently, p38 activation as a death signal has been described for the endocytically located photosensitizer TPPS2a (meso-tetraphenyl-porphine) suitable for photochemical internalization, a method used for release of endosomally/lysosomally trapped macromolecular drugs into the cell cytosol, to enhance their biological effect *in vitro* (133). We can relate our results with these data because para EG-porphyrins exhibit similar intracellular localization and mechanism involving p38 MAPK activation in the cell death induction. Even though our results seem to further support the concept that the activation patterns and functions of MAPK after photochemical treatment are strongly dependent on the photosensitizer, targeted cell type, cellular localization and PDT regimes, certain common features seem to emerge. The remaining question, however, is why the evident strong p38 MAPK activation in mTPP(EG)4-mediated PDT does not play a role in cell death like in para derivatives. The answer might reside in the intracellular location of ROS production and/or the nature of their prevailing species.

The photoactivation of both types of derivatives resulted in the formation of $^1O_2$ and other ROS species as primary messengers triggering other signaling pathways. Dougherty's group established that $^1O_2$ was involved in the phototoxicity of PDT (22). A very short half-life is a critical aspect of $^1O_2$, which disables migration from the site of formation, with resulting immediate oxidation of any nearby biological molecules. Therefore, photodamage is generally confined to a very limited region, i.e. the region of photosensitizer's localization illuminated by the exciting light source. When the cells were preincubated with $^1O_2$ and ROS scavengers, their sensitivity to photodynamic insults dramatically decreased. Several other ROS can be formed from singlet oxygen or via other excited-state pathways. These include the superoxide anion radical ($^{\bullet}O_2^-$), hydrogen peroxide (H_2O_2) and the hydroxyl radical ($^{\bullet}OH$).

The application of various ROS scavengers suggested that the major species generated by photoactivation of EG-porphyrins is singlet oxygen (Figures 4.9-4.11). However, participation of other species depending on the used derivative was indicated by the

example of significant formation of hydroxyl radicals in pTPP(EG)4-mediated PDT. The site of ROS generation, including their half-life, might also have a strong impact on the molecular targets and activation of signaling cascades. The APF fluorescent probe revealed compartments overlapping with porphyrin localization as primary sites of ROS induction, that is ER for mTPP(EG)4 and lysosomes for p(TPP(EG)4 and pTPPF(EG)4. We must take into account that the demonstrated localization of porphyrin derivatives is not absolute and is also dependent on the used concentration, thus affecting ROS site production. A precise dissection of individual ROS species and their involvement in triggering specific signals remains to be defined. Further investigation is needed to specify the role of ROS generation sites and re-localization of longer-lasting species such as hydrogen peroxide (H_2O_2), whose involvement might be indicated by the moderate inhibitory effect of PEG-catalase on cell death induced by the para derivatives. These questions still remain not fully answered due to the limitation of recent techniques and lack of more specific probes usable for in situ detection.

Crosstalk between ER and mitochondria may be facilitated via the release of Ca^{2+} ions from the ER into the cytosol, in response to ER stress. Mitochondrial uptake of Ca^{2+} initiates membrane fission and caspase activation via an uncertain mechanism. A close physical contact of mitochondria and ER enables Ca^{2+} fluxes between these organelles and determines the mitochondrial Ca^{2+} responses (106). When mitochondrial Ca^{2+} uptake is inhibited, the propagation of Ca^{2+} signal into the mitochondria and translation into the mitochondrial cell death machinery is abrogated.

The inhibition of mitochondrial Ca^{2+} uptake by Ru360 corresponded with the reduction of the cytoplasmic cytochrome c level and significant attenuation of apoptosis (Figure 4.18). It substantiates a causative role of intracellular Ca^{2+} rise in mTPP(EG)4-mediated apoptosis, similarly as described in some models (19, 42, 51, 78, 94, 112, 143, 146), and supports the notion that in response to ER stress, the ER-mitochondria cross talk is facilitated via the release of Ca^{2+} ions from the ER into the cytosol. A close physical contact of mitochondria and ER enables Ca^{2+} fluxes between these organelles and determines the mitochondrial Ca^{2+} response (106). When mitochondrial Ca^{2+} uptake is inhibited, the propagation of Ca^{2+} signal into the mitochondria and translation into the mitochondrial cell death machinery is abrogated.

In other models demonstrating the $[Ca^{2+}]$cyt increase, however, different functional outcomes were reported, as having no role (9, 59) or even a protective role (49, 100).

Such discrepancies can be related to the source mediating the rise of the $[Ca^{2+}]$cyt (both influx of extracellular Ca^{2+} and release of Ca^{2+} from different intracellular stores, e.g. ER, mitochondria) and to the specificity of the sensitizers, and particularly of their targets within the cells (reviewed in (3, 11)).

In some PDT cases, the increase in $[Ca^{2+}]$cyt was associated with immediate $^1O_2$-mediated damage to the sarco/endoplasmic reticulum Ca^{2+}-ATPase-2 (SERCA2) pump (34, 113, 116). A decreased level of SERCA2 was evident for photosensitizers (Hypericin, Verteporfin) immediately after light irradiation (12, 29). Our attempts to define the role of SERCA2, however, did not prove SERCA2 to be a molecular target in mTPP(EG)4-mediated PDT. In contrast to the above-mentioned paradigms, in EG porphyrin-treated cells the SERCA2 protein level diminished with slower kinetics, i.e. 1-2 h post irradiation (data not shown) regardless of the sensitizer (similar for both meta and para derivatives). Therefore, the SERCA2 drop in our model rather reflects general protein degradation occurring during the apoptotic process.

The signaling mechanisms transducing the primary photodamage to the ER into cell death pathways in PDT-treated cells have not been completely solved, but a role for the activation of calpains, Ca^{2+}- dependent cysteine proteases, has been proposed in recent studies. Calpains were found to be activated either as an alternative mechanism of caspase-independent apoptosis (131) or in parallel to the canonical caspase-dependent pathways (2, 31, 55).

However, an engagement of calpains in PDT models is questionable (2, 74). The conflicting data can be explained by the differences between the models employed. In addition, some studies suggest that the involvement of calpain in apoptosis seems to be more prominent in certain cell types, e.g. thymocytes, monocytes, cardiomyocytes, and neurons (128). In our model, calpain activity demonstrated by fodrin cleavage was significant in mTPP(EG)4-treated cells. It was inhibited by calpain inhibitor PD150606 and ROS scavengers (L-histidine and trolox), but only partly attenuated by BAPTA. Therefore, it is possible that a portion of the calpain activity might not be Ca^{2+}-dependent.

Importantly, calpain inhibition correlated with suppression of mTPP(EG)4-mediated cell death in both HL60 and 4T1 cells lines. However, neither BAPTA nor the calpain inhibitor protected cells from the death completely. This strongly indicates that Ca^{2+}, besides activating calpain and the Ca^{2+} uptake by mitochondria, has other pro-death

roles. A rather unclear role of calpain activation is emerging in the context of para derivatives. The lately discovered cross-talk between the caspase and calpain proteolytic systems brings another level of complexity (91, 96). It was shown that caspases, including caspase-3, can promote calpain activity through cleavage of calpastatin, the endogenous protein inhibitor of calpains (101), and thus regulate calpain activity during apoptotic cell death. In our setting the calpain activity monitored by fodrin cleavage exhibited slower kinetics with para derivatives than with mTPP(EG)4 (1-2 h versus 0.5 h post PDT) (Figure 4.19) and occurred simultaneously with caspase activation. This could indicate that the major part of calpain activity in para derivatives is not dependent on Ca^{2+} but rather results from caspase activation. In favor of this interpretation is the insensitivity to BAPTA treatment (Figure 4.20) and reduction of so-called "calpain-specific" 150 kD fodrin fragment by broad-spectrum caspase inhibitor Z-VAD-FMK (Figure 4.22). In addition, both the calpain inhibitor and BAPTA did not show any impact on cell death in the context of para derivatives. Similar results were obtained with bisulfonated aluminum phthalocyanine (AlPcS2) in lymphoblastoid CCRF-CEM cells (2), which together with pTPP(EG)4 and pTPPF(EG)4 represent photosensitizers without significant role of calpains in PDT.

In agreement with data obtained using the inhibitors, knockdown of calpain with specific Capn4 siRNA brought another line of evidence confirming significant reduction of mTPP(EG)4-mediated cell death in 4T1 cells but no effect in combination with para porphyrins (Figures 4.23). Taken together, activation of calpains is an essential step in the mTPP(EG)4- but not in the pTPP(EG)4-and pTPPF(EG)4-mediated apoptosis. Preliminary experiments implementing capn4 KO MEFs support such conclusion.

In rodent cells, prolonged ER stress stimulates the activation of pro-caspase-12 (89). This ER membrane-localized enzyme is cleaved and activated by calpain during ER stress, or in response to the mobilization of intracellular Ca^{2+} stores (145). In mTPP(EG)4-treated cells the activation of caspase-12 and human caspase-4 appeared simultaneously with the cleavage of fodrin, which is a substrate of calpain action (20). However, we were not able to effectively block caspase-12 and -4 activation by calpain inhibitor to confirm a direct link between calpain and caspase activity (preliminary data). There are at least two possible explanations: either the activation of stress-related caspases is not mediated by calpains but by some other mechanism in our model, or the

calpain inhibitor affects some caspase-independent pathway(s) participating in mTPP(EG)4-mediated cell death. A novel function of Ca^{2+} calpain in the processing of mitochondrial apoptosis-inducing factor (AIF), which mediates caspase-independent apoptotic cell death, has been reported recently (92) and seems to be an appropriate candidate to explore in the context of mTPP(EG)4-mediated apoptosis.

In addition, the study shows that the unfolded protein response (UPR) participates in the initiation of apoptosis mediated by mTPP(EG)4-PDT. The PERK pathway is activated through phosphorylation of PERK and phosphorylation of its substrate eIF2α immediately after irradiation. This is followed by full induction of transcription factors ATF4 and CHOP (Figure 4.24), which are relevant for the regulation of stress response genes (i.e. genes involved in metabolism, the redox status of cells, and regulation of apoptosis). It has been reported that under conditions of persistent ER stress, CHOP induction is an important element of the switch from pro-survival to pro-death signaling (119). Moreover, PDT-mediated apoptosis with a mitochondrial and ER-localizing porphyrin was reduced in chop-deficient cells, thereby confirming CHOP contribution to the induction of apoptosis in photosensitized cells (135). In our experiments using cells transfected with PERK siRNA, no detectable CHOP expression was detected in contrast to control siRNA after PDT. In addition, PERK knockdown and PERK deficiency (Figures 4.26 and 4.27) protected cells against mTPP(EG)4-mediated apoptosis. Further, in PERK-KO MEFs we observed an increased resistance to ROS-mediated mitochondrial apoptosis, but sensitization against thapsigargin (130). Although several previous reports based on expression profiling indicated activation of the PERK-eIF2a-ATF4 branch of the UPR (12, 109) and were validated at the protein level (56, 93), to our best knowledge this study for the first time brings evidence that PERK pathway actually plays a causative role in PDT-induced apoptosis. Interestingly, we were not able to detect activation of other two UPR sensors, IRE1 and ATF6 (data not shown), which were described in other ER stress models (reviewed by (119)).

So far only two reports describe the possible involvement of the IRE1-XBP1 arm of the UPR in ADPM06- and Hypericin- PDT (12, 93) but no report about ATF6 engagement. It could mean that activation of this UPR sensor is not of use in the PDT context.

6 CONCLUSIONS

1. The structure/activity relationship and the biological efficacy of porphyrin-based PSs were demonstrated on a series of low molecular weight glycol-functionalized meso-tetraphenylporphyrins. The design and synthesis of glycol-functionalized porphyrins that contain one to four low molecular weight glycol chains linked via ether bonds to the meta-phenyl positions of meso-tetraphenylporphyrin were described. In addition, the fluorinated and nonfluorinated para derivatives were compared and the presence of fluorine atoms was associated with better biological virtue. Various glycol chain substitutions on the phenyl ring of porphyrin derivatives exhibited dramatically different effects on the cellular uptake, intracellular localization and PDT efficacy.

The superior potency of mTPP(EG)4 was demonstrated by a five times lower photodynamic dose (drug dose x light dose) required for 50% inhibition of the tumor cell viability than for clinically used Foscan.

2. The cellular uptake of the derivatives significantly depends on the terminal groups of the glycol substituent; only hydroxy glycol porphyrins (mTPP(EG)1-4, pTPP(EG)4, pTPPF(EG)4, pTPPF(DEG)4 and pTPPF(ETA)4), in contrast with methoxy glycol porphyrins (mTPP(EGME)4, pTPP(EGME)4 and pTPPF(EGME)4), exhibit intracellular uptake and phototoxicity.

Meta derivatives (compounds mTPP(EG)1-4) exhibited diffuse fluorescence throughout the cytoplasmic area within 2 h, whereas para derivatives, pTPP(EG)4 and pTPPF(EG)4, displayed the characteristic punctuated pattern with increasing intensity after prolonged incubation.

3. The localization pattern of the porphyrin derivatives inside the cells seems to be affected mainly by the position of ethylene glycol chains. Similar to the parental tetrahydroxyphenyl porphyrin (mTHPP), all derivatives with ethylene glycol in meta position (mTPP(EG)1-4) exhibited better intracellular uptake with predominant endoplasmic reticulum localization. In contrast, para position (pTPP(EG)4, pTPPF(EG)4, pTPPF(DEG)4 and pTPPF(ETA)4) led to the

localization in lysosome-like structures. Fluorination had no observable effect on the localization.

4. Glycol porphyrin derivatives are very potent inducers of apoptosis in tumor cells that assert tumor-marker recognition. Hydroxy glycol porphyrins, in contrast with methoxy glycol porphyrins, show high induction of apoptosis in tumor cell lines *in vitro*. The strong interaction EG-porphyrin derivatives with a tumor marker (sialic acid) indicates the preferential association of these compounds with tumor cells.

5. We have analyzed the molecular mechanisms of photoinduced cell death using porphyrins with EG chain at meta (mTPP(EG)4) or para position (pTPP(EG)4 and pTPPF(EG)4). Both types of derivatives induced death of tumor cells via reactive oxygen species (ROS).

Para derivatives activated the p38 MAP kinase cascade, which in turn induced the mitochondrial apoptotic pathway. Inhibition of p38 MAPK or knockout of the p38a gene resulted in reduction of the apoptotic cell death induced by both para derivatives (p-TPP(EG)4 and p-TPPF(EG)4).

In contrast, meta derivative mTPP(EG)4 induced dramatic changes in Ca^{2+} homeostasis manifested by Ca^{2+} rise in the cytoplasm, activation of calpains and stress caspases-12/-4. ER stress developed into unfolded protein response. Immediately after irradiation the PERK pathway was activated through phosphorylation of PERK, eIF2α and induction of transcription factors ATF4 and CHOP, which regulate stress response genes. PERK knockdown and PERK deficiency protected cells against mTPP(EG)4-mediated apoptosis. These results indicate that the PERK signaling pathway plays a crucial role in the mTPP(EG)4-mediated apoptosis.

6. In mice that were treated with mTPP(EG)2-4-mediated PDT all tumors were completely eliminated with no detectable relapse of primary tumor. Such superior PDT efficacy, leading to permanent ablation of human mammary carcinoma (MDA-MB-231) in immunodeficient mice, was not found in animals treated with mTPP(EG)1, pTPP(EG)4 or pTPPF(EG)4.

In summary, the results presented here demonstrate preferential characteristics of novel meta-ethylene glycol derivatives as photosensitizers and also reveal the molecular mechanism of their action together with their high potential for *in vivo* PDT applications.

7 LIST OF PAPERS

Kralova J, Briza T, **Moserova I**, Dolensky B, Vasek P, Pouckova P, Kejik Z. Glycol porphyrin derivatives as potent photodynamic inducers of apoptosis in tumor cells. *J. Med. Chem.* 2008**,** *51*, 5964–5973 (IF=5.207)

Moserova I, Kralova J. Role of ER stress response in photodynamic therapy: ROS generated in different subcellular compartments trigger diverse cell death pathways. *PLoS ONE*, 2012, *7*(3):e32972 (IF=4.411)

Briza T, Kralova J, Ciegler P, Kejik Z, Pouckova P, Vasek P, **Moserova I**, Martasek P, Kral V. Combination of two chromophores: Synthesis and PDT application of porphyrin–pentamethinium conjugate. *Bioorg Med Chem Lett.* 2012, 22(1):82-4 (IF=2.661)

8 REFERENCES

1. Agostinis P, Berg K, Cengel KA, Foster TH, Girotti AW, Gollnick SO, Hahn SM, Hamblin MR, Juzeniene A, Kessel D, Korbelik M, Moan J, Mroz P, Nowis D, Piette J, Wilson BC, and Golab J. Photodynamic therapy of cancer: an update. *CA: a cancer journal for clinicians* 61: 250-281, 2011.

2. Almeida RD, Gomes ER, Carvalho AP, and Duarte CB. Calpains are activated by photodynamic therapy but do not contribute to apoptotic tumor cell death. *Cancer Lett* 216: 183-189, 2004.

3. Almeida RD, Manadas BJ, Carvalho AP, and Duarte CB. Intracellular signaling mechanisms in photodynamic therapy. *Biochim Biophys Acta* 1704: 59-86, 2004.

4. Antignani A, and Youle RJ. How do Bax and Bak lead to permeabilization of the outer mitochondrial membrane? *Current opinion in cell biology* 18: 685-689, 2006.

5. Assefa Z, Vantieghem A, Declercq W, Vandenabeele P, Vandenheede JR, Merlevede W, de Witte P, and Agostinis P. The activation of the c-Jun N-terminal kinase and p38 mitogen-activated protein kinase signaling pathways protects HeLa cells from apoptosis following photodynamic therapy with hypericin. *J Biol Chem* 274: 8788-8796, 1999.

6. Banfi S, Caruso E, Buccafurni L, Murano R, Monti E, Gariboldi M, Papa E, and Gramatica P. Comparison between 5,10,15,20-tetraaryl- and 5,15-diarylporphyrins as photosensitizers: synthesis, photodynamic activity, and quantitative structure-activity relationship modeling. *J Med Chem* 49: 3293-3304, 2006.

7. Belzacq AS, El Hamel C, Vieira HL, Cohen I, Haouzi D, Metivier D, Marchetti P, Brenner C, and Kroemer G. Adenine nucleotide translocator mediates the mitochondrial membrane permeabilization induced by lonidamine, arsenite and CD437. *Oncogene* 20: 7579-7587, 2001.

8. Boyce M, Bryant KF, Jousse C, Long K, Harding HP, Scheuner D, Kaufman RJ, Ma D, Coen DM, Ron D, and Yuan J. A selective inhibitor of eIF2alpha dephosphorylation protects cells from ER stress. *Science* 307: 935-939, 2005.

9. Buytaert E, Callewaert G, Hendrickx N, Scorrano L, Hartmann D, Missiaen L, Vandenheede JR, Heirman I, Grooten J, and Agostinis P. Role of endoplasmic reticulum depletion and multidomain proapoptotic BAX and BAK proteins in shaping cell death after hypericin-mediated photodynamic therapy. *FASEB J* 20: 756-758, 2006.

10. Buytaert E, Callewaert G, Vandenheede JR, and Agostinis P. Deficiency in apoptotic effectors Bax and Bak reveals an autophagic cell death pathway initiated by photodamage to the endoplasmic reticulum. *Autophagy* 2: 238-240, 2006.

11. Buytaert E, Dewaele M, and Agostinis P. Molecular effectors of multiple cell death pathways initiated by photodynamic therapy. *Biochim Biophys Acta* 1776: 86-107, 2007.

12. Buytaert E, Matroule JY, Durinck S, Close P, Kocanova S, Vandenheede JR, de Witte PA, Piette J, and Agostinis P. Molecular effectors and modulators of hypericin-mediated cell death in bladder cancer cells. *Oncogene* 27: 1916-1929, 2008.

13. Calfon M, Zeng H, Urano F, Till JH, Hubbard SR, Harding HP, Clark SG, and Ron D. IRE1 couples endoplasmic reticulum load to secretory capacity by processing the XBP-1 mRNA. *Nature* 415: 92-96, 2002.

14. Callsen D, and Brune B. Role of mitogen-activated protein kinases in S-nitrosoglutathione-induced macrophage apoptosis. *Biochemistry* 38: 2279-2286, 1999.

15. Cecconi F, Alvarez-Bolado G, Meyer BI, Roth KA, and Gruss P. Apaf1 (CED-4 homolog) regulates programmed cell death in mammalian development. *Cell* 94: 727-737, 1998.

16. Cory S, and Adams JM. The Bcl2 family: regulators of the cellular life-or-death switch. *Nat Rev Cancer* 2: 647-656, 2002.

17. Crupi V, Giordano R, Majolino D, Migliardo P, Venuti V, Micali N, Villari V, Mineo P, Vitalini D, and Scamporrino E. Spectroscopic evidence of aggregation processes in porphyrin-based star-polymers in aqueous solutions. *Molecular Physics* 101: 1517-1526, 2003.

18. Dewaele M, Maes H, and Agostinis P. ROS-mediated mechanisms of autophagy stimulation and their relevance in cancer therapy. *Autophagy* 6: 838-854, 2010.

19. Ding X, Xu Q, Liu F, Zhou P, Gu Y, Zeng J, An J, Dai W, and Li X. Hematoporphyrin monomethyl ether photodynamic damage on HeLa cells by means of reactive oxygen species production and cytosolic free calcium concentration elevation. *Cancer Lett* 216: 43-54, 2004.

20. Diwakarla S, Nagley P, Hughes ML, Chen B, and Beart PM. Differential insult-dependent recruitment of the intrinsic mitochondrial pathway during neuronal programmed cell death. *Cell Mol Life Sci* 66: 156-172, 2009.

21. Dolmans DE, Fukumura D, and Jain RK. Photodynamic therapy for cancer. *Nat Rev Cancer* 3: 380-387, 2003.

22. Dougherty TJ, Gomer CJ, Henderson BW, Jori G, Kessel D, Korbelik M, Moan J, and Peng Q. Photodynamic therapy. *J Natl Cancer Inst* 90: 889-905, 1998.

23. Dougherty TJ, Kaufman JE, Goldfarb A, Weishaupt KR, Boyle D, and Mittleman A. Photoradiation therapy for the treatment of malignant tumors. *Cancer Res* 38: 2628-2635, 1978.

24. Du C, Fang M, Li Y, Li L, and Wang X. Smac, a mitochondrial protein that promotes cytochrome c-dependent caspase activation by eliminating IAP inhibition. *Cell* 102: 33-42, 2000.

25. Edinger AL, and Thompson CB. Death by design: apoptosis, necrosis and autophagy. *Current opinion in cell biology* 16: 663-669, 2004.

26. Fabris C, Valduga G, Miotto G, Borsetto L, Jori G, Garbisa S, and Reddi E. Photosensitization with zinc (II) phthalocyanine as a switch in the decision between apoptosis and necrosis. *Cancer Res* 61: 7495-7500, 2001.

27. Festjens N, Vanden Berghe T, Cornelis S, and Vandenabeele P. RIP1, a kinase on the crossroads of a cell's decision to live or die. *Cell Death Differ* 14: 400-410, 2007.

28. Finsen NR. *Phototherapy*. Arnold, 1901.

29. Granville DJ, Ruehlmann DO, Choy JC, Cassidy BA, Hunt DW, van Breemen C, and McManus BM. Bcl-2 increases emptying of endoplasmic reticulum Ca2+ stores during photodynamic therapy-induced apoptosis. *Cell Calcium* 30: 343-350, 2001.

30. Granville DJ, Shaw JR, Leong S, Carthy CM, Margaron P, Hunt DW, and McManus BM. Release of cytochrome c, Bax migration, Bid cleavage, and activation of caspases 2, 3, 6, 7, 8, and 9 during endothelial cell apoptosis. *Am J Pathol* 155: 1021-1025, 1999.

31. Grebenova D, Kuzelova K, Smetana K, Pluskalova M, Cajthamlova H, Marinov I, Fuchs O, Soucek J, Jarolim P, and Hrkal Z. Mitochondrial and endoplasmic reticulum stress-induced apoptotic pathways are activated by 5-aminolevulinic acid-based photodynamic therapy in HL60 leukemia cells. *J Photochem Photobiol B* 69: 71-85, 2003.

32. Griffiths GJ, Dubrez L, Morgan CP, Jones NA, Whitehouse J, Corfe BM, Dive C, and Hickman JA. Cell damage-induced conformational changes of the pro-apoptotic protein Bak in vivo precede the onset of apoptosis. *J Cell Biol* 144: 903-914, 1999.

33. Gross A, Jockel J, Wei MC, and Korsmeyer SJ. Enforced dimerization of BAX results in its translocation, mitochondrial dysfunction and apoptosis. *EMBO J* 17: 3878-3885, 1998.

34. Grover AK, Samson SE, and Misquitta CM. Sarco(endo)plasmic reticulum Ca2+ pump isoform SERCA3 is more resistant than SERCA2b to peroxide. *Am J Physiol* 273: C420-425, 1997.

35. Hahn SM, Fraker DL, Mick R, Metz J, Busch TM, Smith D, Zhu T, Rodriguez C, Dimofte A, Spitz F, Putt M, Rubin SC, Menon C, Wang HW, Shin D, Yodh A, and Glatstein E. A phase II trial of intraperitoneal photodynamic therapy for patients with peritoneal carcinomatosis and sarcomatosis. *Clin Cancer Res* 12: 2517-2525, 2006.

36. Hahn SM, Smith RP, and Friedberg J. Photodynamic therapy for mesothelioma. *Curr Treat Options Oncol* 2: 375-383, 2001.

37. Hajnoczky G, Davies E, and Madesh M. Calcium signaling and apoptosis. *Biochem Biophys Res Commun* 304: 445-454, 2003.

38. Harding HP, Novoa I, Zhang Y, Zeng H, Wek R, Schapira M, and Ron D. Regulated translation initiation controls stress-induced gene expression in mammalian cells. *Mol Cell* 6: 1099-1108, 2000.

39. Hegde R, Srinivasula SM, Zhang Z, Wassell R, Mukattash R, Cilenti L, DuBois G, Lazebnik Y, Zervos AS, Fernandes-Alnemri T, and Alnemri ES. Identification of Omi/HtrA2 as a mitochondrial apoptotic serine protease that disrupts inhibitor of apoptosis protein-caspase interaction. *J Biol Chem* 277: 432-438, 2002.

40. Hendren SK, Hahn SM, Spitz FR, Bauer TW, Rubin SC, Zhu T, Glatstein E, and Fraker DL. Phase II trial of debulking surgery and photodynamic therapy for disseminated intraperitoneal tumors. *Ann Surg Oncol* 8: 65-71, 2001.

41. Hendrickx N, Dewaele M, Buytaert E, Marsboom G, Janssens S, Van Boven M, Vandenheede JR, de Witte P, and Agostinis P. Targeted inhibition of p38alpha MAPK suppresses tumor-associated endothelial cell migration in response to hypericin-based photodynamic therapy. *Biochem Biophys Res Commun* 337: 928-935, 2005.

42. Hermes-Lima M. How do Ca2+ and 5-aminolevulinic acid-derived oxyradicals promote injury to isolated mitochondria? *Free Radic Biol Med* 19: 381-390, 1995.

43. Hibi M, Lin A, Smeal T, Minden A, and Karin M. Identification of an oncoprotein- and UV-responsive protein kinase that binds and potentiates the c-Jun activation domain. *Genes Dev* 7: 2135-2148, 1993.

44. Hirohara S, Obata M, Saito A, Ogata S, Ohtsuki C, Higashida S, Ogura S, Okura I, Sugai Y, Mikata Y, Tanihara M, and Yano S. Cellular uptake and photocytotoxicity of glycoconjugated porphyrins in HeLa cells. *Photochem Photobiol* 80: 301-308, 2004.

45. Hitomi J, Katayama T, Eguchi Y, Kudo T, Taniguchi M, Koyama Y, Manabe T, Yamagishi S, Bando Y, Imaizumi K, Tsujimoto Y, and Tohyama M. Involvement of caspase-4 in endoplasmic reticulum stress-induced apoptosis and Abeta-induced cell death. *J Cell Biol* 165: 347-356, 2004.

46. Holler N, Zaru R, Micheau O, Thome M, Attinger A, Valitutti S, Bodmer JL, Schneider P, Seed B, and Tschopp J. Fas triggers an alternative, caspase-8-independent cell death pathway using the kinase RIP as effector molecule. *Nature immunology* 1: 489-495, 2000.

47. Hoppe V, and Hoppe J. Mutations dislocate caspase-12 from the endoplasmatic reticulum to the cytosol. *FEBS Lett* 576: 277-283, 2004.

48. Hsieh YJ, Wu CC, Chang CJ, and Yu JS. Subcellular localization of Photofrin determines the death phenotype of human epidermoid carcinoma A431 cells triggered by

photodynamic therapy: when plasma membranes are the main targets. *J Cell Physiol* 194: 363-375, 2003.

49. Hubmer A, Hermann A, Uberriegler K, and Krammer B. Role of calcium in photodynamically induced cell damage of human fibroblasts. *Photochem Photobiol* 64: 211-215, 1996.

50. Ichinose S, Usuda J, Hirata T, Inoue T, Ohtani K, Maehara S, Kubota M, Imai K, Tsunoda Y, Kuroiwa Y, Yamada K, Tsutsui H, Furukawa K, Okunaka T, Oleinick NL, and Kato H. Lysosomal cathepsin initiates apoptosis, which is regulated by photodamage to Bcl-2 at mitochondria in photodynamic therapy using a novel photosensitizer, ATX-s10 (Na). *Int J Oncol* 29: 349-355, 2006.

51. Inanami O, Yoshito A, Takahashi K, Hiraoka W, and Kuwabara M. Effects of BAPTA-AM and forskolin on apoptosis and cytochrome c release in photosensitized Chinese hamster V79 cells. *Photochem Photobiol* 70: 650-655, 1999.

52. Iyer AK, Greish K, Seki T, Okazaki S, Fang J, Takeshita K, and Maeda H. Polymeric micelles of zinc protoporphyrin for tumor targeted delivery based on EPR effect and singlet oxygen generation. *Journal of drug targeting* 15: 496-506, 2007.

53. Josefsen LB, and Boyle RW. Photodynamic therapy and the development of metal-based photosensitisers. *Metal-based drugs* 2008: 276109, 2008.

54. Jung CH, Jun CB, Ro SH, Kim YM, Otto NM, Cao J, Kundu M, and Kim DH. ULK-Atg13-FIP200 complexes mediate mTOR signaling to the autophagy machinery. *Molecular biology of the cell* 20: 1992-2003, 2009.

55. Karmakar S, Banik NL, Patel SJ, and Ray SK. 5-Aminolevulinic acid-based photodynamic therapy suppressed survival factors and activated proteases for apoptosis in human glioblastoma U87MG cells. *Neurosci Lett* 415: 242-247, 2007.

56. Kaul A, and Maltese WA. Killing of cancer cells by the photoactivatable protein kinase C inhibitor, calphostin C, involves induction of endoplasmic reticulum stress. *Neoplasia* 11: 823-834, 2009.

57. Kessel D. The role of low-density lipoprotein in the biodistribution of photosensitizing agents. *J Photochem Photobiol B* 14: 261-262, 1992.

58. Kessel D, and Castelli M. Evidence that bcl-2 is the target of three photosensitizers that induce a rapid apoptotic response. *Photochem Photobiol* 74: 318-322, 2001.

59. Kessel D, Castelli M, and Reiners JJ. Ruthenium red-mediated suppression of Bcl-2 loss and Ca(2+) release initiated by photodamage to the endoplasmic reticulum: scavenging of reactive oxygen species. *Cell Death Differ* 12: 502-511, 2005.

60. Kessel D, Luo Y, Deng Y, and Chang CK. The role of subcellular localization in initiation of apoptosis by photodynamic therapy. *Photochem Photobiol* 65: 422-426, 1997.

61. Kessel D, Luo Y, Mathieu P, and Reiners JJ, Jr. Determinants of the apoptotic response to lysosomal photodamage. *Photochem Photobiol* 71: 196-200, 2000.

62. Kessel D, Vicente MG, and Reiners JJ, Jr. Initiation of apoptosis and autophagy by photodynamic therapy. *Lasers Surg Med* 38: 482-488, 2006.

63. Kim HR, Luo Y, Li G, and Kessel D. Enhanced apoptotic response to photodynamic therapy after bcl-2 transfection. *Cancer Res* 59: 3429-3432, 1999.

64. Klotz LO, Fritsch C, Briviba K, Tsacmacidis N, Schliess F, and Sies H. Activation of JNK and p38 but not ERK MAP kinases in human skin cells by 5-aminolevulinate-photodynamic therapy. *Cancer Res* 58: 4297-4300, 1998.

65. Kobayashi N, and Nakai K. Applications of magnetic circular dichroism spectroscopy to porphyrins and phthalocyanines. *Chemical Communications* 2007.

66. Koon HK, Chan PS, Wu ZG, Wong RN, Lung ML, Chang CK, and Mak NK. Role of mitogen-activated protein kinase in Zn-BC-AM PDT-induced apoptosis in nasopharyngeal carcinoma cells. *Cell Biochem Funct* 28: 239-248, 2010.

67. Kral V, Kralova J, Kaplanek R, Briza T, and Martasek P. Quo vadis porphyrin chemistry? *Physiological research / Academia Scientiarum Bohemoslovaca* 55 Suppl 2: S3-26, 2006.

68. Kralova J, Briza T, Moserova I, Dolensky B, Vasek P, Pouckova P, Kejik Z, Kaplanek R, Martasek P, Dvorak M, and Kral V. Glycol porphyrin derivatives as potent photodynamic inducers of apoptosis in tumor cells. *J Med Chem* 51: 5964-5973, 2008.

69. Kralova J, Dvorak M, Koc M, and Kral V. p38 MAPK plays an essential role in apoptosis induced by photoactivation of a novel ethylene glycol porphyrin derivative. *Oncogene* 27: 3010-3020, 2008.

70. Kroemer G, Galluzzi L, and Brenner C. Mitochondrial membrane permeabilization in cell death. *Physiol Rev* 87: 99-163, 2007.

71. Lamkanfi M, Kalai M, and Vandenabeele P. Caspase-12: an overview. *Cell Death Differ* 11: 365-368, 2004.

72. Lee JB, Choi JY, Chun JS, Yun SJ, Lee SC, Oh J, and Park HR. Relationship of protoporphyrin IX synthesis to photodynamic effects by 5-aminolaevulinic acid and its esters on various cell lines derived from the skin. *The British journal of dermatology* 159: 61-67, 2008.

73. Li LY, Luo X, and Wang X. Endonuclease G is an apoptotic DNase when released from mitochondria. *Nature* 412: 95-99, 2001.

74. Lien YC, Kung HN, Lu KS, Jeng CJ, and Chau YP. Involvement of endoplasmic reticulum stress and activation of MAP kinases in beta-lapachone-induced human prostate cancer cell apoptosis. *Histol Histopathol* 23: 1299-1308, 2008.

75. Liu H, Bowes RC, 3rd, van de Water B, Sillence C, Nagelkerke JF, and Stevens JL. Endoplasmic reticulum chaperones GRP78 and calreticulin prevent oxidative stress, Ca2+ disturbances, and cell death in renal epithelial cells. *J Biol Chem* 272: 21751-21759, 1997.

76. Lu PD, Harding HP, and Ron D. Translation reinitiation at alternative open reading frames regulates gene expression in an integrated stress response. *J Cell Biol* 167: 27-33, 2004.

77. Ma Y, Brewer JW, Diehl JA, and Hendershot LM. Two distinct stress signaling pathways converge upon the CHOP promoter during the mammalian unfolded protein response. *J Mol Biol* 318: 1351-1365, 2002.

78. Mak NK, Li KM, Leung WN, Wong RN, Huang DP, Lung ML, Lau YK, and Chang CK. Involvement of both endoplasmic reticulum and mitochondria in photokilling of nasopharyngeal carcinoma cells by the photosensitizer Zn-BC-AM. *Biochem Pharmacol* 68: 2387-2396, 2004.

79. Marchal S, Francois A, Dumas D, Guillemin F, and Bezdetnaya L. Relationship between subcellular localisation of Foscan and caspase activation in photosensitised MCF-7 cells. *Br J Cancer* 96: 944-951, 2007.

80. Matroule JY, Carthy CM, Granville DJ, Jolois O, Hunt DW, and Piette J. Mechanism of colon cancer cell apoptosis mediated by pyropheophorbide-a methylester photosensitization. *Oncogene* 20: 4070-4084, 2001.

81. Miller JD, Baron ED, Scull H, Hsia A, Berlin JC, McCormick T, Colussi V, Kenney ME, Cooper KD, and Oleinick NL. Photodynamic therapy with the phthalocyanine

photosensitizer Pc 4: the case experience with preclinical mechanistic and early clinical-translational studies. *Toxicol Appl Pharmacol* 224: 290-299, 2007.

82. Minamikawa T, Sriratana A, Williams DA, Bowser DN, Hill JS, and Nagley P. Chloromethyl-X-rosamine (MitoTracker Red) photosensitises mitochondria and induces apoptosis in intact human cells. *J Cell Sci* 112 (Pt 14): 2419-2430, 1999.

83. Mizushima N, Kuma A, Kobayashi Y, Yamamoto A, Matsubae M, Takao T, Natsume T, Ohsumi Y, and Yoshimori T. Mouse Apg16L, a novel WD-repeat protein, targets to the autophagic isolation membrane with the Apg12-Apg5 conjugate. *J Cell Sci* 116: 1679-1688, 2003.

84. Moan J, and Berg K. The photodegradation of porphyrins in cells can be used to estimate the lifetime of singlet oxygen. *Photochem Photobiol* 53: 549-553, 1991.

85. Moan J, and Berg K. Photochemotherapy of cancer: experimental research. *Photochem Photobiol* 55: 931-948, 1992.

86. Momoi T. Caspases involved in ER stress-mediated cell death. *J Chem Neuroanat* 28: 101-105, 2004.

87. Nadanaka S, Okada T, Yoshida H, and Mori K. Role of disulfide bridges formed in the luminal domain of ATF6 in sensing endoplasmic reticulum stress. *Mol Cell Biol* 27: 1027-1043, 2007.

88. Nakagawa T, and Yuan J. Cross-talk between two cysteine protease families. Activation of caspase-12 by calpain in apoptosis. *J Cell Biol* 150: 887-894, 2000.

89. Nakagawa T, Zhu H, Morishima N, Li E, Xu J, Yankner BA, and Yuan J. Caspase-12 mediates endoplasmic-reticulum-specific apoptosis and cytotoxicity by amyloid-beta. *Nature* 403: 98-103, 2000.

90. Nakamura K, Bossy-Wetzel E, Burns K, Fadel MP, Lozyk M, Goping IS, Opas M, Bleackley RC, Green DR, and Michalak M. Changes in endoplasmic reticulum luminal environment affect cell sensitivity to apoptosis. *J Cell Biol* 150: 731-740, 2000.

91. Neumar RW, Xu YA, Gada H, Guttmann RP, and Siman R. Cross-talk between calpain and caspase proteolytic systems during neuronal apoptosis. *J Biol Chem* 278: 14162-14167, 2003.

92. Norberg E, Gogvadze V, Ott M, Horn M, Uhlen P, Orrenius S, and Zhivotovsky B. An increase in intracellular Ca2+ is required for the activation of mitochondrial calpain to release AIF during cell death. *Cell Death Differ* 15: 1857-1864, 2008.

93. O'Connor AE, Mc Gee MM, Likar Y, Ponomarev V, Callanan JJ, O'Shea D F, Byrne AT, and Gallagher WM. Mechanism of cell death mediated by a BF2-chelated tetraaryl-azadipyrromethene photodynamic therapeutic: dissection of the apoptotic pathway in vitro and in vivo. *Int J Cancer* 130: 705-715, 2012.

94. Ogata M, Inanami O, Nakajima M, Nakajima T, Hiraoka W, and Kuwabara M. Ca(2+)-dependent and caspase-3-independent apoptosis caused by damage in Golgi apparatus due to 2,4,5,7-tetrabromorhodamine 123 bromide-induced photodynamic effects. *Photochem Photobiol* 78: 241-247, 2003.

95. Oleinick NL, Morris RL, and Belichenko I. The role of apoptosis in response to photodynamic therapy: what, where, why, and how. *Photochem Photobiol Sci* 1: 1-21, 2002.

96. Orrenius S, Zhivotovsky B, and Nicotera P. Regulation of cell death: the calcium-apoptosis link. *Nat Rev Mol Cell Biol* 4: 552-565, 2003.

97. Ortel B, Shea CR, and Calzavara-Pinton P. Molecular mechanisms of photodynamic therapy. *Frontiers in bioscience : a journal and virtual library* 14: 4157-4172, 2009.

98. Pattingre S, Espert L, Biard-Piechaczyk M, and Codogno P. Regulation of macroautophagy by mTOR and Beclin 1 complexes. *Biochimie* 90: 313-323, 2008.

99. Pattingre S, Tassa A, Qu X, Garuti R, Liang XH, Mizushima N, Packer M, Schneider MD, and Levine B. Bcl-2 antiapoptotic proteins inhibit Beclin 1-dependent autophagy. *Cell* 122: 927-939, 2005.

100. Penning LC, Rasch MH, Ben-Hur E, Dubbelman TM, Havelaar AC, Van der Zee J, and Van Steveninck J. A role for the transient increase of cytoplasmic free calcium in cell rescue after photodynamic treatment. *Biochim Biophys Acta* 1107: 255-260, 1992.

101. Porn-Ares MI, Samali A, and Orrenius S. Cleavage of the calpain inhibitor, calpastatin, during apoptosis. *Cell Death Differ* 5: 1028-1033, 1998.

102. Price M, Reiners JJ, Santiago AM, and Kessel D. Monitoring singlet oxygen and hydroxyl radical formation with fluorescent probes during photodynamic therapy. *Photochem Photobiol* 85: 1177-1181, 2009.

103. Rao RV, Ellerby HM, and Bredesen DE. Coupling endoplasmic reticulum stress to the cell death program. *Cell Death Differ* 11: 372-380, 2004.

104. Reiners JJ, Jr., Agostinis P, Berg K, Oleinick NL, and Kessel D. Assessing autophagy in the context of photodynamic therapy. *Autophagy* 6: 7-18, 2010.

105. Reiners JJ, Jr., Caruso JA, Mathieu P, Chelladurai B, Yin XM, and Kessel D. Release of cytochrome c and activation of pro-caspase-9 following lysosomal photodamage involves Bid cleavage. *Cell Death Differ* 9: 934-944, 2002.

106. Rizzuto R, Pinton P, Carrington W, Fay FS, Fogarty KE, Lifshitz LM, Tuft RA, and Pozzan T. Close contacts with the endoplasmic reticulum as determinants of mitochondrial Ca2+ responses. *Science* 280: 1763-1766, 1998.

107. Rutkowski DT, and Kaufman RJ. A trip to the ER: coping with stress. *Trends Cell Biol* 14: 20-28, 2004.

108. Samis JA, Back DW, Graham EJ, DeLuca CI, and Elce JS. Constitutive expression of calpain II in the rat uterus during pregnancy and involution. *Biochem J* 276 (Pt 2): 293-299, 1991.

109. Sanovic R, Krammer B, Grumboeck S, and Verwanger T. Time-resolved gene expression profiling of human squamous cell carcinoma cells during the apoptosis process induced by photodynamic treatment with hypericin. *Int J Oncol* 35: 921-939, 2009.

110. Senge MO, and Brandt JC. Temoporfin (Foscan(R), 5,10,15,20-tetra(m-hydroxyphenyl)chlorin)--a second-generation photosensitizer. *Photochem Photobiol* 87: 1240-1296, 2011.

111. Setsukinai K, Urano Y, Kakinuma K, Majima HJ, and Nagano T. Development of novel fluorescence probes that can reliably detect reactive oxygen species and distinguish specific species. *J Biol Chem* 278: 3170-3175, 2003.

112. Shahzidi S, Cunderlikova B, Wiedlocha A, Zhen Y, Vasovic V, Nesland JM, and Peng Q. Simultaneously targeting mitochondria and endoplasmic reticulum by photodynamic therapy induces apoptosis in human lymphoma cells. *Photochem Photobiol Sci* 10: 1773-1782, 2011.

113. Scherer NM, and Deamer DW. Oxidative stress impairs the function of sarcoplasmic reticulum by oxidation of sulfhydryl groups in the Ca2+-ATPase. *Arch Biochem Biophys* 246: 589-601, 1986.

114. Srinivasula SM, Hegde R, Saleh A, Datta P, Shiozaki E, Chai J, Lee RA, Robbins PD, Fernandes-Alnemri T, Shi Y, and Alnemri ES. A conserved XIAP-interaction motif in caspase-9 and Smac/DIABLO regulates caspase activity and apoptosis. *Nature* 410: 112-116, 2001.

115. Susin SA, Zamzami N, Castedo M, Hirsch T, Marchetti P, Macho A, Daugas E, Geuskens M, and Kroemer G. Bcl-2 inhibits the mitochondrial release of an apoptogenic protease. *J Exp Med* 184: 1331-1341, 1996.

116. Suzuki YJ, and Ford GD. Inhibition of Ca(2+)-ATPase of vascular smooth muscle sarcoplasmic reticulum by reactive oxygen intermediates. *Am J Physiol* 261: H568-574, 1991.

117. Swamy N, Purohit A, Fernandez-Gacio A, Jones GB, and Ray R. Nuclear estrogen receptor targeted photodynamic therapy: selective uptake and killing of MCF-7 breast cancer cells by a C17alpha-alkynylestradiol-porphyrin conjugate. *J Cell Biochem* 99: 966-977, 2006.

118. Synytsya A, Kral V, Volka K, and Sessler JL. In vitro interaction of macrocyclic photosensitizers with intact mitochondria: a spectroscopic study. *Biochim Biophys Acta* 1620: 85-96, 2003.

119. Szegezdi E, Logue SE, Gorman AM, and Samali A. Mediators of endoplasmic reticulum stress-induced apoptosis. *EMBO Rep* 7: 880-885, 2006.

120. Tao J, Sanghera JS, Pelech SL, Wong G, and Levy JG. Stimulation of stress-activated protein kinase and p38 HOG1 kinase in murine keratinocytes following photodynamic therapy with benzoporphyrin derivative. *J Biol Chem* 271: 27107-27115, 1996.

121. Teiten MH, Marchal S, D'Hallewin MA, Guillemin F, and Bezdetnaya L. Primary photodamage sites and mitochondrial events after Foscan photosensitization of MCF-7 human breast cancer cells. *Photochem Photobiol* 78: 9-14, 2003.

122. Tkadlecová M, Foltýnová J, Valík M, and Král V. Spectroscopic binding studies of novel fluorescent distamycin derivatives. *Tetrahedron Letters* 49: 323-326, 2008.

123. Tong Z, Singh G, Valerie K, and Rainbow AJ. Activation of the stress-activated JNK and p38 MAP kinases in human cells by Photofrin-mediated photodynamic therapy. *J Photochem Photobiol B* 71: 77-85, 2003.

124. Usuda J, Azizuddin K, Chiu SM, and Oleinick NL. Association between the photodynamic loss of Bcl-2 and the sensitivity to apoptosis caused by phthalocyanine photodynamic therapy. *Photochem Photobiol* 78: 1-8, 2003.

125. Usuda J, Chiu SM, Murphy ES, Lam M, Nieminen AL, and Oleinick NL. Domain-dependent photodamage to Bcl-2. A membrane anchorage region is needed to form the target of phthalocyanine photosensitization. *J Biol Chem* 278: 2021-2029, 2003.

126. Van Cruchten S, and Van Den Broeck W. Morphological and biochemical aspects of apoptosis, oncosis and necrosis. *Anatomia, histologia, embryologia* 31: 214-223, 2002.

127. van Loo G, Saelens X, van Gurp M, MacFarlane M, Martin SJ, and Vandenabeele P. The role of mitochondrial factors in apoptosis: a Russian roulette with more than one bullet. *Cell Death Differ* 9: 1031-1042, 2002.

128. Vanags DM, Porn-Ares MI, Coppola S, Burgess DH, and Orrenius S. Protease involvement in fodrin cleavage and phosphatidylserine exposure in apoptosis. *J Biol Chem* 271: 31075-31085, 1996.

129. Vanden Berghe T, Kalai M, van Loo G, Declercq W, and Vandenabeele P. Disruption of HSP90 function reverts tumor necrosis factor-induced necrosis to apoptosis. *J Biol Chem* 278: 5622-5629, 2003.

130. Verfaillie T, Rubio N, Dewaele M, Bultynck G, Decuypere JP, Martinet W, Gupta S, Samali A, and Agostinis P. PERK deficiency distorts the ER – mitochondrial

interface and protects against ROS-induced intrinsic apoptosis. In: *18th Euroconference on Apoptosis*,Ghent, Belgium: 2010, p. P-138.

131. Vittar NB, Awruch J, Azizuddin K, and Rivarola V. Caspase-independent apoptosis, in human MCF-7c3 breast cancer cells, following photodynamic therapy, with a novel water-soluble phthalocyanine. *Int J Biochem Cell Biol* 42: 1123-1131, 2010.

132. Wei Y, Pattingre S, Sinha S, Bassik M, and Levine B. JNK1-mediated phosphorylation of Bcl-2 regulates starvation-induced autophagy. *Mol Cell* 30: 678-688, 2008.

133. Weyergang A, Kaalhus O, and Berg K. Photodynamic therapy with an endocytically located photosensitizer cause a rapid activation of the mitogen-activated protein kinases extracellular signal-regulated kinase, p38, and c-Jun NH2 terminal kinase with opposing effects on cell survival. *Mol Cancer Ther* 7: 1740-1750, 2008.

134. Witold K S. Electron spin resonance study on the mechanism of polyethylene glycol—membrane interaction. *FEBS Letters* 151: 228-232, 1983.

135. Wong S, Luna M, Ferrario A, and Gomer CJ. CHOP activation by photodynamic therapy increases treatment induced photosensitization. *Lasers Surg Med* 35: 336-341, 2004.

136. Woodburn KW, Fan Q, Miles DR, Kessel D, Luo Y, and Young SW. Localization and efficacy analysis of the phototherapeutic lutetium texaphyrin (PCI-0123) in the murine EMT6 sarcoma model. *Photochem Photobiol* 65: 410-415, 1997.

137. Wu RW, Yow CM, Wong CK, and Lam YH. Photodynamic therapy (PDT) - Initiation of apoptosis via activation of stress-activated p38 MAPK and JNK signal pathway in H460 cell lines. *Photodiagnosis Photodyn Ther* 8: 254-263, 2011.

138. Xie Z, and Klionsky DJ. Autophagosome formation: core machinery and adaptations. *Nature cell biology* 9: 1102-1109, 2007.

139. Xu Y, Huang S, Liu ZG, and Han J. Poly(ADP-ribose) polymerase-1 signaling to mitochondria in necrotic cell death requires RIP1/TRAF2-mediated JNK1 activation. *J Biol Chem* 281: 8788-8795, 2006.

140. Xue L, He J, and Oleinick NL. Promotion of photodynamic therapy-induced apoptosis by stress kinases. *Cell Death Differ* 6: 855-864, 1999.

141. Xue LY, Chiu SM, Fiebig A, Andrews DW, and Oleinick NL. Photodamage to multiple Bcl-xL isoforms by photodynamic therapy with the phthalocyanine photosensitizer Pc 4. *Oncogene* 22: 9197-9204, 2003.

142. Xue LY, Chiu SM, and Oleinick NL. Photochemical destruction of the Bcl-2 oncoprotein during photodynamic therapy with the phthalocyanine photosensitizer Pc 4. *Oncogene* 20: 3420-3427, 2001.

143. Yoo JO, Lim YC, Kim YM, and Ha KS. Differential cytotoxic responses to low- and high-dose photodynamic therapy in human gastric and bladder cancer cells. *J Cell Biochem* 112: 3061-3071, 2011.

144. Yoshida H, Matsui T, Yamamoto A, Okada T, and Mori K. XBP1 mRNA is induced by ATF6 and spliced by IRE1 in response to ER stress to produce a highly active transcription factor. *Cell* 107: 881-891, 2001.

145. Zhivotovsky B, and Orrenius S. Calcium and cell death mechanisms: a perspective from the cell death community. *Cell Calcium* 50: 211-221, 2011.

146. Zhou Z, Yang H, and Zhang Z. Role of calcium in phototoxicity of 2-butylamino-2-demethoxy-hypocrellin A to human gastric cancer MGC-803 cells. *Biochim Biophys Acta* 1593: 191-200, 2003.

147. Zhuang S, Demirs JT, and Kochevar IE. p38 mitogen-activated protein kinase mediates bid cleavage, mitochondrial dysfunction, and caspase-3 activation during apoptosis induced by singlet oxygen but not by hydrogen peroxide. *J Biol Chem* 275: 25939-25948, 2000.

9 PUBLICATIONS ENCLOSED IN FULL